UNIVERSITY OF LIÈGE

AEROSPACE AND MECHANICAL ENGINEERING DEPARTMENT

THERMODYNAMICS LABORATORY

About the Use of Radiant Ceiling Simulation Models as Commissioning Tools

by

Néstor FONSECA DÍAZ

A thesis submitted to the requirement

for the degree of

Doctor of Applied Sciences

Liège, Belgium, December 15th, 2009.

In memory of my parents Gloria and José

“We have a method, and that method helps us to reach not absolute truth, only asymptotic approaches to the truth — never there, just closer and closer, always finding vast new oceans of undiscovered possibilities”

Carl Sagan.
"Wonder and Skepticism", Skeptical Enquirer, 1995.

Summary

This study focuses on the experimental and theoretical analyses of radiant ceiling performance and on the use of their simulation models as commissioning tools.

A *steady state* model of such system appears to be an appropriate tool for preliminary calculation, design and diagnosis in commissioning processes. Therefore, the main objective is to support a Functional Performance Test of the system in order to verify the radiant ceiling performance in cooling and/or heating modes. A series of experimental results obtained for seven types of cooling ceilings are used in order to validate this model.

A *dynamic* model is also proposed to interpret the interactions of the radiant ceiling system with its environment (walls, facade, internal loads and ventilation system). This dynamic model is used to support a global commissioning procedure, to verify the radiant ceiling behavior and to evaluate the comfort conditions of the occupants. In this modeling the resultant temperature is calculated as a comfort indicator, as it depends strongly on the transient variation of the surface temperatures in the room. Dynamic tests in heating and cooling mode are used to validate the model.

As an example of model application, the cooling ceiling system of a commercial building in Brussels is experimentally evaluated. Commissioning test results show that the influence of surfaces temperatures inside the room, especially the facade and ventilation are significant and that the radiant ceiling system must be evaluated together with its designed environment and not as a separate HVAC equipment.

Keywords: *Radiant Ceiling, Heating, Cooling, Experimental, Commissioning, Modeling, Validation*

Acknowledgements

I would not have been able to complete this work without the aid and support of countless people over the past few years.

First of all I would like to express my sincere gratitude to Professor Jean Lebrun from the University of Liège who has been my supervisor since the beginning of my study. I am very grateful for his supervision, knowledge and critical comments but especially for the opportunity to work with him.

I also wish to express my gratitude to Professors Philippe André from the University of Liège for providing valuable suggestions and his unconditional support.

Special gratitude goes to Jules Hannay and Cleide Aparecida Silva from JCJ Energetics Innovations Consulting for sharing their time and experience in the experimental and commissioning work and especially for their friendship and encouragement throughout the development of this work.

Sincere thanks are extended to Professors Cristian Cuevas and Adelqui Fissore from the University of Concepción, Chile and Professor Wei Qingpeng from Tsinghua University, Department of Building Science, China for their valuable instructions and suggestions during the preparation of this work.

My special appreciation goes to Kevin Sartor, Bernard Georges, Stéphane Bertagnolio, Sylvain Quoilin and Professors Vincent Lermort and Philippe Ngendakumana for their continuous support and valuable ideas.

This study would not have been possible without the help of Technicians Jean-Marie Ralet, Richard Labenda, Bernard Loly and José Concha who assisted me during the test bench preparation. I enjoyed the atmosphere, their friendship and support.

Additionally, I would like to thank several people who helped me with the manuscript preparation and correction. In this context I would like to thank Magdalena Calusinska, Danielle Makaire and David Valentiny.

I would also like to express special gratitude to the Leonard family, my Belgian family, for their unconditional support and friendship.

Nomenclature

A	Area, [m^2]
A.U	Global heat transfer coefficient, [W K^{-1}]
C	Thermal mass, [J K^{-1}] or empirical convection coefficient, [-]
$\dot{C}$	Capacity flow rate, [W K^{-1}]
c	Specific heat, [J kg^{-1} K^{-1}]
D	Diameter, [m]
E	Emissive power, [W m^{-2}]
F	View factor, [-]
g	gravity acceleration, [m^2 s^{-1}]
H	Height, [m]
h	Convection (radiation) heat transfer coefficient, [W m^{-2} K^{-1}]
J	Radiosity, [W m^{-2}]
k	Thermal conductivity or coverage factor, [W m^{-1} K^{-1}] or [-]
L	Length, [m]
m	Mass, [kg]
$\dot{M}$	Mass flow rate, [kg s^{-1}]
MRT	Mean radiant temperature, [℃]
N	Number, [-]
NTU	Number of transfer units, [-]
P	Pressure [Pa] or Perimeter, [m]
PMV	Predicted mean vote index, [-]
PPD	Predicted percent dissatisfied, [%]
$\dot{Q}$	Heat flow, [W]
$\dot{Q}'$	Heat flow per unit length, [W m^{-1}]
$\dot{q}$	Heat flux, [W m^{-2}]

R'	Thermal resistance per unit length, [K m W^{-1}]
t	Temperature, [℃]
U	Overall heat transfer coefficient, [W m^{-2} K^{-1}]
u	Velocity, [m s^{-1}]
W	Width, [m]
w	Distance between tubes, [m]

Dimensionless numbers

Gr	Grashoff number $(g\beta(t_s-t_\infty)L^3/v^2)$
Nu	Nusselt Number (hL_c/k)
Pr	Prandtl number (v/α)
Ra	Rayleigh number (G*r Pr*)
Re	Reynolds number (CD/ *v*)

Greek symbols

α	Thermal diffusivity, [m^2 s^{-1}]
ε	Effectiveness [-] or emissivity [-]
η	Efficiency [-]
β	Expansion coefficient, [K^{-1}]
δ	Thickness, [m]
ρ	Density or Ceiling panel porosity factor, [kg m^{-3}] or [-]
Δ_T	Temperature difference, [K]
μ	Dynamic viscosity, [Pa s]
γ	Kinematics viscosity or freedom degree, [m^2 s^{-1}] or [-]

Subscripts

a	Air
ave	Average
b	Black body
conv	Convective
comb	Combined
CC	Cooling ceiling

e	External
effec	Effective
ex	Exhaust
exp	Experimental
f	Floor or fictitious
fac	Facade (windows and external wall)
FC	Forced convection
HC	Heating ceiling
i	Internal
ins	Insulation
int	Interior
meas	Measured
min	Minimum
mix	mixed
mr	Mean radiant
NC	Natural convection
occ	Occupants
p	Panels blocks connected in parallel
rad	Radiative
RC	Radiant ceiling
res	Resultant
su	Supply
s	Panels connected in series, side or surface
t	Tube
vent	Ventilation
w	Water or wall
win	Window
x	Fin distance
0	Fin base

Contents

Introduction 0.1

Aim of the thesis 0.2

Outline of the thesis 0.3

Contributions of the thesis 0.4

Chapter 1: Fundamentals

1.1 Introduction 1.1

1.2 Commissioning context. 1.2

1.2.1 Commissioning process 1.2

1.2.2 Commissioning types 1.3

1.2.3 Functional Performance Testing (FPT) 1.4

1.3 General description of radiant ceiling systems 1.5

1.4 Working conditions (Heating, Cooling , ventilation, control) 1.10

1.5 Radiant ceiling heat exchange 1.13

1.5.1 Heat transfer coefficient for internal flow in circular tubes 1.14

1.5.2 Heat transfer from extended surfaces 1.14

1.5.3 Radiant ceiling heat transfer coefficient definitions 1.16

1.5.4 Room-resultant temperature 1.25

1.5.5 Bi-dimensional Conduction 1.26

1.6 Conclusions 1.28

Chapter 2: Experimental analysis in laboratory

2.1 Introduction 2.1

2.2 Measurement systems and uncertainty analysis 2.2

2.3 Test benches description and experimental results 2.7

2.3.1 Test bench type 1 2.7
2.3.1.1 General description 2.7
2.3.1.2 Experimental results 2.12
2.3.2 Test bench type 2 2.21
2.3.2.1 General description 2.21
2.3.2.2 Experimental results 2.26
2.3.3 Test bench type standard DIN 4715-1 2.36
2.3.3.1 General description 2.36
2.3.3.2 Experimental results 2.39
2.4 Conclusions of the experimental analysis 2.42

Chapter 3: Static modeling of the radiant ceiling systems

3.1 Introduction 3.1
3.2 Copper tube radiant ceiling modeling 3.2
3.2.1 Model description 3.3
3.2.2 Validation of the copper tube radiant ceiling model 3.11
3.2.3 Sensitivity analysis 3.13
3.3 Synthetic capillary tube mats radiant ceiling modeling 3.15
3.3.1 Model description 3.16
3.3.2 Validation of the capillary tube mats ceiling model 3.16
3.4 Conclusions 3.19

Chapter 4: Dynamic thermal modeling of radiant ceiling systems and its environment

4.1 Introduction 4.1
4.2 Dynamic modeling 4.3
4.2.1 Radiant ceiling system model 4.4
4.2.2 Thermal zone model 4.5
4.2.3 Walls ceiling model 4.7
4.2.4 Solar gains and infrared losses 4.9

4.2.5 Resultant temperature 4.11

4.3 Dynamic model validation 4.12

4.3.1 Heating mode validation 4.12

4.3.2 Cooling mode validation 4.18

4.4 Conclusions 4.22

Chapter 5: Model assisted commissioning of radiant ceiling systems

5.1Introduction 5.1

5.2 Functional Performance Test procedure. 5.2

5.3 Building and radiant ceiling description 5.5

5.4 Commissioning results: Radiant ceiling (performance test) 5.8

5.4.1 Measurements 5.8

5.4.2 Cooling ceiling performance test results 5.11

5.5 Commissioning results: radiant ceiling coupled to the building (test of global functioning) 5.13

5.5.1 Measurements 5.13

5.5.2 Global functioning commissioning test results 5.14

5.5.3 Sensitive analysis 5.16

5.6 Conclusions 5.18

Chapter 6: General conclusion and recommendations 6.1

References R.1

Annex 1

A.1 Radiant Ceiling Functional Performance Testing Guide FPT A.1

A.2 Functional Performance Test presentation A.2

A.3 Test specifications A.6

Introduction

The demands of building users regarding the environment are growing around the world. In general, they expect a comfortable and healthy indoor environment without an excessive use of natural resources and pollution of outdoor environment. Many new products and systems are developed, such as high efficiency generation systems using renewable, low energy cooling or heating systems, natural ventilation and fenestration systems and integrated control systems.

Cooling ceiling systems are more and more used in non-residential applications, with a high percentage of sensible heat removed and low energy consumption. While the primary air distribution is used to fulfill the ventilation requirements, the secondary water distribution system provides thermal conditioning to the building. According to Conroy *et al.,* (2005), cooling ceiling systems significantly reduce the amount of air transported through the building (often only about 20 % of the normal all-air system air flow rates). This results in the reduction of the fan size, energy consumption and ductwork cross-sectional dimensions (Feustel and Stetiu, 1995).

Due to the large surface available for heat exchange, the water temperature is only slightly lower than the room temperature. This small difference allows for the use of either heat pump with very high coefficient of performance, or alternative cooling sources. Thanks to the new technologies, the original misgivings towards water piping in ceiling directly above the workplace, with attendant fears of possible leakage, condensation, unpleasant radiant asymmetry, etc. have generally given way to a high level of acceptance.

Today, there is an increasing interest in extending its range of application to heating, in order to save on investment costs on one hand and on the other one, to avoid the use of static heaters under or in front of glass facades, which are often undesirable for architectural reasons. However, it is important to note that the commissioning process is especially important in this system, due to the fact that the system performance depends not only on the individual but also on the global operation of the system coupled to the ventilation, fenestration, walls and internal thermal loads distribution. The management of this complexity requires new approaches, new skills and new tools.

Aim of the thesis

This study focuses on the experimental and theoretical analysis and modeling of the radiant ceiling systems as commissioning tool. The objective is to present the results of the experimental analysis and its discussion and give some suggestions on the development of individual and global models of the system and its environment, in order to verify its performance and the comfort level achieved by the global system during a commissioning procedure. Regarding these issues, there remain a certain number of incompletely solved questions, which this work tries to answer:

- What is the influence of variables such as water mass flow rate and log mean temperature difference between the water and the room air temperatures on the (functioning) system?
- How do the ventilation, fenestration, ceiling perforations and thermal load distribution affect the radiant ceiling performance and thermal comfort?
- How much can radiation and convection heat exchange models be simplified and still remain accurate enough as a commissioning tool?
- How far can be used a steady state model in commissioning?

The first question has been already tackled before (Fonseca *et al.,* 2003). Complementary information is provided in chapters 1 and 2.

To answer the second question, an experimental study on the influence of these factors on thermal comfort and ceiling performance is carried out in chapter 2. A sensitivity analysis concerning these variables is presented in chapter 3. Experimental analysis and results were already presented in two publications (Fonseca *et al.,* 2009a and Fonseca *et al., 2009b*).

The third question is answered in chapters 2 and 5, on the basis of the experimental results obtained in Fonseca *et al.,* (2003).

The fourth question is answered in chapters 3 and 4, on the basis of results already presented in the publication Fonseca *et al.* (2009c)

A synthesis of the answers to all these questions is presented in the last part of this work (chapters 5 and 6), where a global model of the radiative and convective exchanges inside the enclosure is proposed as a commissioning tool.

Outline of the thesis

Chapter 1 gives a general description of the components considered in this study as well as the equations used for their sizing. Most appropriate correlations, methodologies and orders of magnitude are identified.

Chapter 2 presents the experimental study. The test benches used for the different components are described. The experimental results are analyzed. The basic information required for the modeling is also presented.

Chapter 3 describes the steady state radiant ceiling model and the main hypothesis supporting it.
The definition of the radiant ceiling geometry and ventilation parameters allows for use of the manufacturer data in order to simplify the commissioning process. On the other hand the choice of resultant temperature as a comfort indicator allows for a relatively easy verification of this parameter in the room.

Chapter 4 gives a detailed description of the dynamic model, which can be used to support a global procedure, to verify the radiant ceiling behavior associated to building, thermal loads, fenestration and ventilation systems and comfort conditions of the occupants. In this model the resultant temperature is calculated as a comfort indicator, as it strongly depends on the transient variation of the surface temperatures in the room.

Chapter 5 presents the application of the models, during a commissioning process. The cooling ceiling system of a commercial building in Brussels is submitted to a functional performance testing procedure. Both detailed static and dynamic models are used.

Chapter 6 proposes some general conclusions and recommendations to improve the models.

Contributions of the thesis

The contributions of this thesis can be divided into three parts:

- one related to the experimental results and methodology.
- another one related to the modeling.
- and a last one focusing on the model application during the commissioning process.

For the experimental analysis, the contribution includes the study of the system in cooling and heating mode, for seven different configurations of the system. Fifty-six tests are analyzed in which the main objective is to observe the influence of parameters such as the mass flow rate, supply water temperature, ceiling perforations, thermal load distribution, fenestration and ventilation system effects on the radiant ceiling capacity and room comfort conditions.

For the modeling, the main contributions are the development and validation of the radiant ceiling models and its environment for two systems and seven different configurations, using steady state and dynamic analysis of the system in cooling and heating mode.

For the model application during the commissioning procedure, the main contributions are the model theoretical approach used (parameter and geometry definition) to allow and simplifies a Functional Performance Test of the system in a commissioning process. Additionally, two commissioning study cases of the system are analyzed as examples of the models application during a commissioning procedure.

1. Fundamentals

1.1 INTRODUCTION

The system studied here consists of an air distribution system coupled to a cooled or heated ceiling surface. It takes profit of convection and long-wave radiation to supply or remove heat from a space. It maintains also acceptable indoor air quality and humidity. In its operation, as an air-conditioning system, a radiant ceiling system thus separates the task of sensible cooling or heating from those of air quality and humidity control.

Radiant heating and cooling systems supply or extract heat from a room through the action of convective and radiative heat exchange between the room environment and heated or cooled panels situated in the ceiling. The radiation heat exchange can be calculated as function of the room geometry and surface characteristics. The convective heat transfer is a function of air velocity and direction at the ceiling level (related to the position of the air inlet), which in turn depends on the room and diffusers geometry, the location and power of the internal heat sources and interaction with the heated or cooled facade.

This chapter summarizes the basic aspects related to these issues, always limited to the system configurations used in this study. The objective of this chapter is to give the following information:

- The main parameters used to describe and specify the commissioning context of this study.
- A brief description of the radiant ceiling concept. These components have been widely studied in laboratory and this study considers also the test standard performed according to DIN 4715-1.
- Some practical aspects related to working conditions (heating, cooling, ventilation, control), information issued from the literature and manufacturers data.
- A detailed analysis of heat exchange and some correlations used to size and to simulate the thermo-hydraulic performance of radiant ceiling systems.

1.2 COMMISSIONING CONTEXT

Commissioning is one of the new tools to manage the complexity of today's HVAC systems. It is actually a quality-oriented process for achieving, verifying and documenting that the performance of facility systems and assemblies meet defined objectives and criteria (IEA Annex 40, 2003).

The definition in ASHRAE Guideline 1, (1996) is probably close to a standard or consensus definition: "Commissioning is the process of ensuring systems are designed, installed, functionally tested and operated in conformance with the design intent. Commissioning begins with planning and includes design, construction star-up, acceptance, training and is applied throughout the life of the building. Furthermore, the commissioning process encompasses and coordinates the traditionally separated functions of systems documentation, equipment start-up, control system calibration, testing, balancing and performance testing"

Possibly the major reason that commissioning is needed is precisely that in many projects "commissioning" the project simply consists of turning everything on and verifying that all motors, chillers and boilers run. The problem becomes serious considering that the most of the global systems are usually not commissioned. Currently the practice is that each contractor (usually manufacturer is not the installer) does (for economical reasons) the strictly necessary for its product to be operational. Therefore despite of the sophisticated BEMS and measurements system provided in the buildings, an inadequate installation, verification and management of the individual and global system performance (according to the AS-BUILT files), produce usually the deterioration of components and global system conditions which implies an increase of the energy consumption and sub-utilization of the expensive monitoring system (Fonseca *et al.,* 2009 b).

1.2.1 Commissioning process

Commissioning has hierarchically five phases and nine steps:

- Pre-Design Phase: program and planning steps
- Design Phase: preliminary Design and working design steps
- Elaboration Phase (Elaboration Step)
- Construction Phase: construction and acceptance steps

- Occupancy and Operation Phase: post-Acceptance and ordinary operation steps

1.2.2 Commissioning types

There are four representative types:

Initial Commissioning: a type of commissioning applied to a construction of a new building and/or an installation of new systems, which is defined as a systematic process beginning with Program Step and ending with Post-Acceptance Step

Retro-Commissioning: first commissioning implemented in an existing building in which a documented commissioning was not implemented before. In many cases, the design documentation of the existing building was lost or unmatched with the current situation. Therefore, the Retro-commissioning would include verification process on the design such as shown in parts of the initial commissioning. It intends to identify any unsolved problems that occurred during construction, just as commissioning does in a new building and to go beyond this point to identify and correct problems that were developed during subsequent operation of the building.

Re-Commissioning: a commissioning implemented after the initial commissioning or the Retro-commissioning when the owner intends to verify, improve and document the performance of the building systems. Reasons to re-commission a building are diverse. It could be a modification in the user requirements, the discovery of underperformance of the systems, the necessity to fix faults found during the initial commissioning, etc. Periodic Re- commission ensures that the original performance persists. The Re- commission is the event that reapplies the original commission in order to keep the building systems performance

On-Going Commissioning: a commissioning conducted continuously in order to maintain, improve and optimize the performance of building systems after the initial commissioning or the Retro-commissioning. The difference between On-Going commissioning and periodic Re- commissioning is the fact that the Re- commissioning refers to the original building systems performance, whereas the On-Going commissioning emphasizes on the performance optimization. The On-Going commissioning is a successive commissioning procedure during Operation & Maintenance Stage to resolve operational problems, improve comfort, optimize energy use and if necessary to recommend retrofits.

1.2.3 Functional Performance Testing (FPT)

The FPT is just one part of the whole commissioning process. It has only to be started on the basis of strict specification, given in the design documentation. The test results and interpretation have to be incorporated into the AS-BUILT records. Information and testing procedures are viewed from a system perspective, rather than a component perspective. This is especially critical for functional performance testing and for the overall success of the system. The FPT of HVAC system means to verify that the equipment, subsystem and total system work with in harmony (including the stability and durability) to show the final function of the building air-conditioning.

The functional performance testing as a commissioning tool is devoted to the detection of a possible malfunction and its diagnosis. The test can be "active" or "passive", according to the way of analyzing the component behavior, with or without artificial perturbation. Active tests are mostly applied in initial commissioning, i.e. at the end of the building construction phase. Later in the building life cycle, i.e. in re-, retro- and on-going commissioning, a “passive” approach is usually preferred, in order to preserve health and comfort conditions inside the building occupancy zones (IEA Annex 40, 2003).

In the frame of the program “Commissioning of Building and HVAC systems to improve energy performance Annex 40” of the International Energy Agency, some FPTs are presented. However there is no specific information about radiant ceiling systems.

Looking at the related literature, some case studies about this system are presented (AuditAC, 2006; EIA, 2003) in which the influence of radiant ceiling on building commissioning is usually simplified. Therefore a FPT for radiant ceiling systems is proposed as a tool for diagnosis in commissioning processes (Annex 1).

1.3 GENERAL DESCRIPTION OR THE RADIANT CEILING SYSTEMS

The radiant ceiling system may be heated electrically or by means of water circulating in metal or plastic pipes embedded in the ceiling. In many instances, insulation is placed behind the heat source to minimize back-loss and also as sound insulation.

Control of the heat output is achieved, in electrical system, by varying the current and in piped systems, by varying the water temperature or flow rate. The control may be linked to a room thermostat or to an external temperature sensor.

Three major types of radiant ceiling systems can be distinguished:

- The metallic ceiling panels, which are incorporated into the false ceilings. The parallel water – pipe circuits are distributed on the upper side of the panels, which form the room false ceiling. The whole system presents a low thermal inertia and the metal panel is used as a decorative element.
- The active slab made of concrete is relatively similar to heating floor. The propylene tubes are embedded in the lower portion of a concrete slab. The cost is low however, due to the high thermal inertia, it is difficult to control the risk of condensation.
- Another technique, similar to the previous one, uses parallel capillary tube mats made of polyethylene (inside diameter is about 2.5 mm). The cost is low and the thermal inertia is reduced (Miriel J. *et al.,* 2002).

The metallic ceiling panels can also be used with capillary tube mats placed directly on top of the ceiling panels. Depending on the application, both copper and capillary tube mats are usually used with glass-wool (thermal and sound) insulation above the pipes.

The system is studied here in two constructive versions, used in three and four configurations respectively: copper tube and synthetic capillary tube mats.

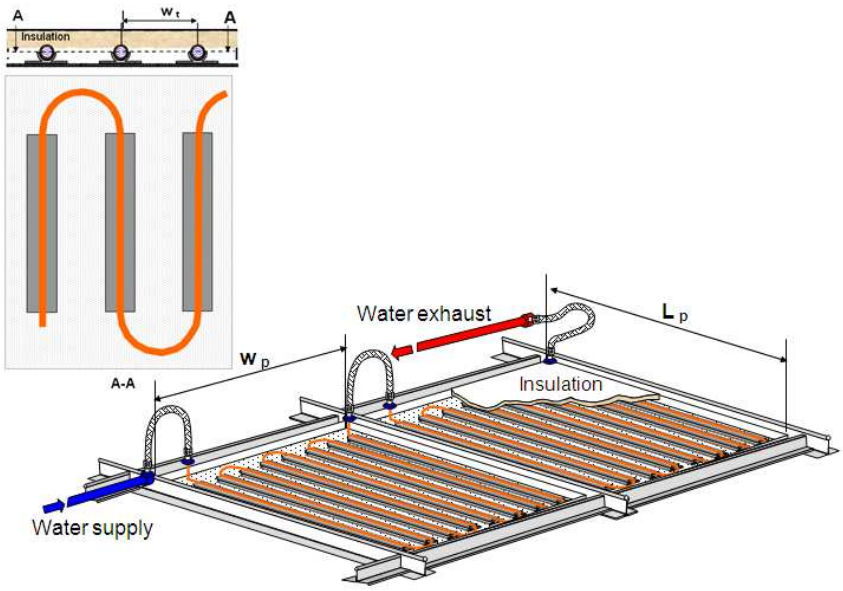

Figure 1.1: **T1**: View of a copper tube secured to steel sheet radiant ceiling

The first constructive version consists of a ceiling in which the copper coils are in direct contact with a smooth perforated metallic surface. The pipe-radiant panel contact must be established in such a way to get a minimum thermal contact resistance. Therefore an aluminum extrusion profile is used. A perforated plate insures suitable convective flow to improve its performance (Figure 1.1).

Figure 1.2: **T2**: Type 2 Cooper tube radiant ceiling

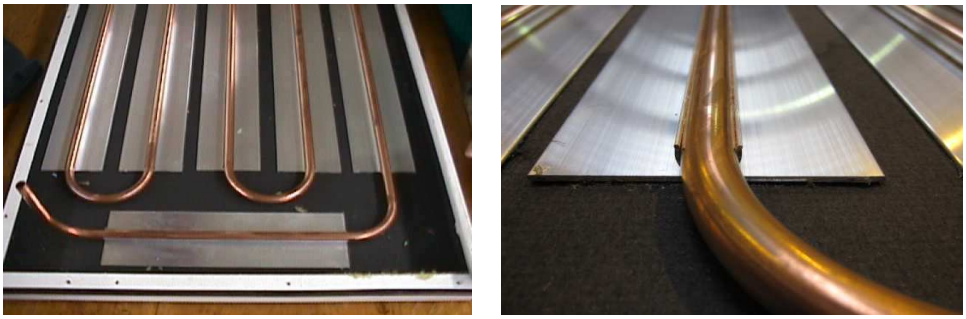

Figure 1.3:**T3**: Type 3 Cooper tube radiant ceiling

For the three types of copper tube ceilings studied here, the system design is almost the same. The differences are only that the type one (**T1**) (Figure 1.1) considers two synthetic glue layers, one between the tubes and the aluminum extrusion profile and another between this one and the metallic plate. Whereas the type two (**T2**) considers only one layer between the plate and the aluminum profile ensuring that the tubes are secured to the profile by pressure during its manufacturing process (Figure 1.2). Type 3 (**T3**) is similar to **T2**. The only difference is an additional layer of paper between the plate and the profile used as sound insulation (Figure 1.3).

The main characteristics of the copper tube radiant ceilings tested are presented in Table 1.1.

Table 1.1: Main characteristic of the tested copper tube radiant ceilings

Characteristic	**T1**	**T2**	**T3**
Radiant surface	On top of a steel plate Thickness:0.8mm	On top of a steel plate. Thickness:1.1mm	On top of a steel plate. Thickness 1 mm
L_p: Panel length	1.15 m	1.8 m.	1.78 m
W_p: Panel width	1.25 m.	0.6 m.	0.52 m
w_t: Tube separation	100 mm.	145 mm.	100 mm
Panel surface:	1.44 m^2	1.08 m^2	3.06 m^2
Perforated area (***ρ***)	21 %	25%	13.6%
N_s: Panels in series	4	6	2 or 4
N_p: Panels in parallel	2 (Cooling)	1 or 3 (Heating or Cooling)	1 , 2 or 3 (Heating or Cooling)
Upward insulation:	30 mm mineral wool.	20 mm mineral wool.	40 mm mineral wool.
Tube-radiant surface union system	Aluminum interconnection profile	Aluminum interconnection profile	Aluminum interconnection profile
D_e	13 mm	12.5 mm	12 mm
D_i	12.5 mm	10.8 mm	10 mm

The second constructive version uses radiant mats consisting of numerous thin capillary tubes (D_i = 2.3 mm) made of polyethylene and mounted in parallel (Figure 1.4). The distance between the individual small tubes is small enough to ensure that a homogeneous temperature is produced on the bottom side of the ceiling.

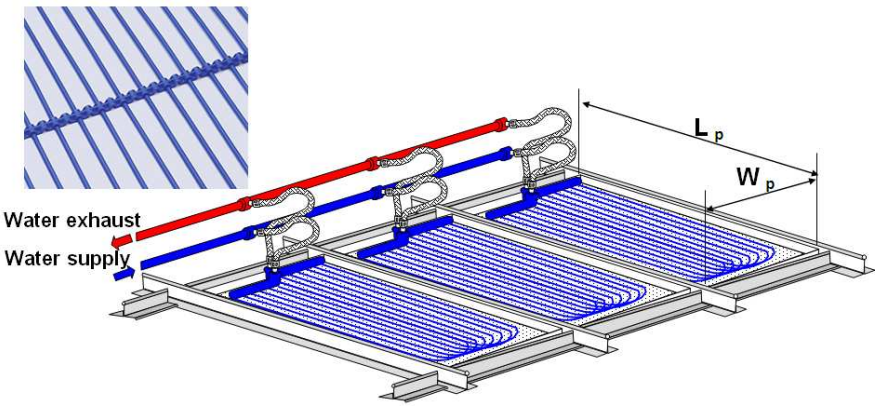

Figure 1.4: View of Synthetic capillary tube mats radiant ceiling

The radiant mats in this system can be incorporated into the ceiling in three configurations: placed on top of the metal ceiling panels with a layer of mineral wool installed above, embedded into a ceiling plaster layer, or stretched between insulation and gypsum plasterboard (Figure 1.5).

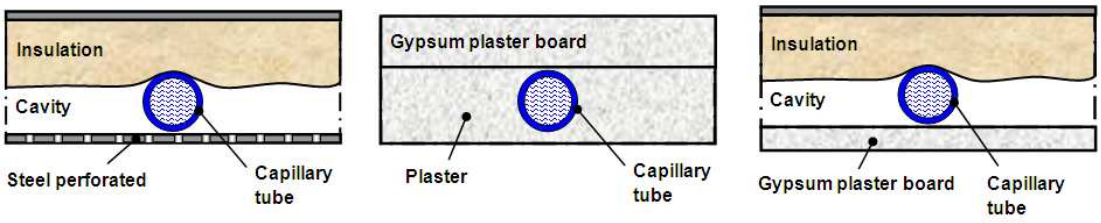

Figure 1.5: Capillary tube mats radiant surfaces

The capillary tube mats present also different configurations depending on the application. The “U” mats shown in Figure 1.4, are suitable for application in metal panel ceilings. The “G” and “S” mats (Figure 1.6) are suitable in particular for application on plaster ceiling and gypsum plasterboards.

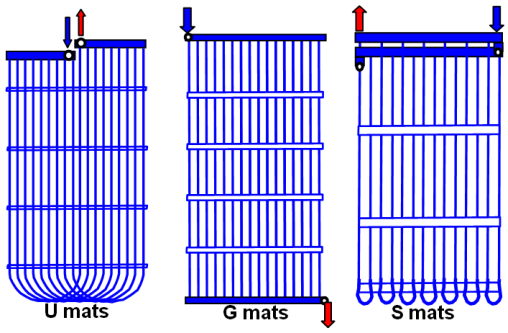

Figure 1.6: Capillary tube mats configurations

The main characteristics of radiant ceilings tested are presented in Table 1.2, for the tube mats tested according to the standard test (**DIN**) and in laboratory test (**TG**).

Table 1.2: Main characteristic of the tested capillary tube mats radiant ceilings

Characteristic	DIN U	DIN S	DIN G	TG
Radiant surface	On top of a steel plate. Thickness 0.8mm	Embedded in plaster Thickness 26 mm	On top of gypsum plaster board Thickness 10 mm	On top of a steel plate. Thickness 0.8 mm
L_p: Panel length	1.37 m.	3.5 m	3.7 m	1.78 m.
W_p: Panel width	0.617 m.	0.87 m	0.23 m	0.53 m.
w_t: Tube separation	10 mm.	15 mm	10 mm.	10 mm.
Panel surface:	0.845 m^2	3.06 m^2	0.85 m^2	0.845 m^2
Perforated area (ρ)	16 %	-------	-------	16 %
N_s: Panels in series	1	1	2	2 or 6 (Heating or Cooling)
N_p: Panels in parallel	12	4	6	3
Upward insulation:	20 mm mineral wool.	-------	30 mm mineral wool.	30 mm mineral wool.
Tube-radiant surface union system	Directly placed on top of the plate	Attached below and then plastered in.	Directly placed on top of the board	Directly placed on top of the plate
D_e	3.4 mm	3.4 mm	3.4 mm	3.4 mm
D_i	2.3 mm	2.3 mm	2.3 mm	1 mm

1.4 WORKING CONDITIONS

The radiant ceiling systems are usually mounted in the false ceiling or embedded into the ceiling and are designed to cover the sensible cooling of heating load or the room. The heating or cooling ceiling systems are connected to a closed circuit containing chilled or heated water and coupled to an air distribution system. The principle scheme of such a system is given in Figure 1.7.

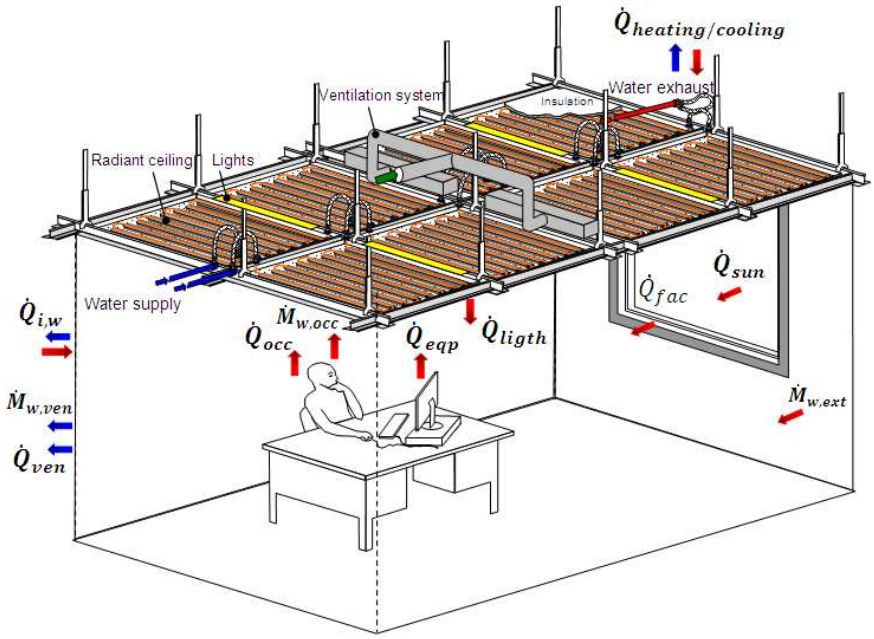

Figure 1.7: Sensible and latent heat loads for a radiant ceiling system

In the following thermal balances, by convention, the algebraic value of each term is positive if the energy flux goes into the control volume and negative if it comes out of the control volume. The energy and water mass balances of the office room control volume defined in Figure 1.7 are given by the following equations, valid in both heating and cooling modes:

$$\dot{Q}_{heating/cooling} + \dot{Q}_{fac} + \dot{Q}_{ven} + \dot{Q}_{void} + \dot{Q}_{i,w} + \dot{Q}_{occ} + \dot{Q}_{sun} + \dot{Q}_{eqp} + \dot{Q}_{lightt} = C\frac{dT}{d\tau}\,[\mathrm{W}] \qquad (1.1)$$

$$\dot{M}_{w,ven} = \dot{M}_{w,occ} + \dot{M}_{w,ext} \qquad [\mathrm{kg\ s^{-1}}] \qquad (1.2)$$

As the radiant elements are part of the room architecture and exposed directly to the occupant (placed above the occupancy zone) they are supposed to operate only in dry regime, as shown in Eq. (1.1).

Therefore, the water supply temperature in the ceiling must exceed the dewpoint corresponding to the setpoint of indoor humidity ratio. Consequently the latent (moisture) load of the room can be controlled by the auxiliary ventilation system, which is also designed to provide air renewal for hygienic requirements (Eq. 1.2). A humidity and temperature control system can be used to avoid the condensation risk. A schematic diagram of this control system is showed in Figure 1.8. As long as the sensor is registering a condensation risk, either the flow to the ceiling is cut off by closing the control valve, or the water supply temperature is raised. When natural ventilation of the room is allowed, the limitation is related to the outdoor dewpoint.

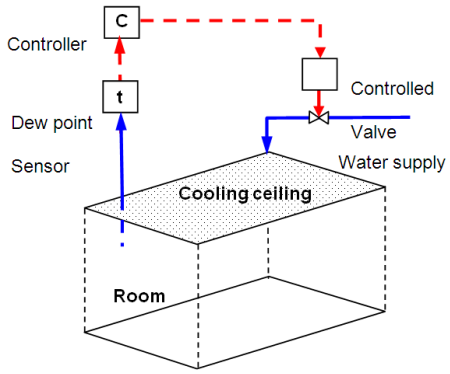

Figure 1.8: Simplified scheme of ceilings control system.

The water flow rate must be sufficient to maintain a turbulent regime, in order to increase the heat exchange. The water circuit should be designed to favor the parallel flow and minimize pressure drops.

The ventilation slot diffusers are usually located between the ceiling panels and above the occupancy zone. The air should be blown horizontally along the ceiling surface to increase the heat transfer coefficient and to avoid, thanks to “Coanda effect” (Behhe, 1999) a jet fall in occupancy zone.

The contact quality (bonds between water pipes and ceiling panels) is crucial for radiant ceiling effectiveness. Identical ceiling modules (as designed) might provide completely different results only due to a bad contact quality.

In most applications, the thermal and sound insulation of the room ceiling void is recommended (in some cases required) and direct contact (cold bridges) between ceiling elements and room surfaces is prohibited. The free air circulation between rooms ceiling voids is allowed only if both rooms are equipped with the same radiant ceiling system and have identical destination (office room for example) (Ternoveanu *et al.,* 1999).

The air velocity pattern at the occupancy zone must fulfill the comfort requirements. This means a maximum accepted average velocity in the range of 0.15-0.2 m/s with peak values limited to 0.25-0.3 m/s and a maximal allowed vertical temperature gradient of 2-3 K on the total height of the room.

Besides ensuring the heating or cooling of a building, the operation of a radiant ceiling system has also to prevent or minimize two side-effects associated with the presence of the radiant surface in the building (prevention of these adverse side-effects limits the heating or cooling power of the system). The first side-effect is the deterioration of comfort conditions due to the asymmetrical character of the radiant exchange in a room with a radiant surface. The second side-effect is the condensation risk in cooling mode.

1.5 RADIANT CEILING HEAT EXCHANGE

The two typical individual elements of radiant ceiling considered in this study are presented in Figure 1.9, where:

$t_{a\ void}$ is the air temperature in the ceiling void, [℃]

$t_{a\ cavity}$ is the air temperature in the radiant ceiling cavity, [℃]

$t_{a\ room}$ is the dry air temperature of the room, [℃]

$t_{res\ room}$ is the resultant temperature of the room, [℃]

t_{t} is the temperature of the tube external surface, [℃]

t_{w} is the average water temperature inside the tubes, [℃]

$t_{RC,0}$ is the radiant ceiling fin base temperature, [℃]

$t_{RC,\ ave}$ is the average temperature of the radiant ceiling surface, [℃]

w_{t} is the tube separation, [m]

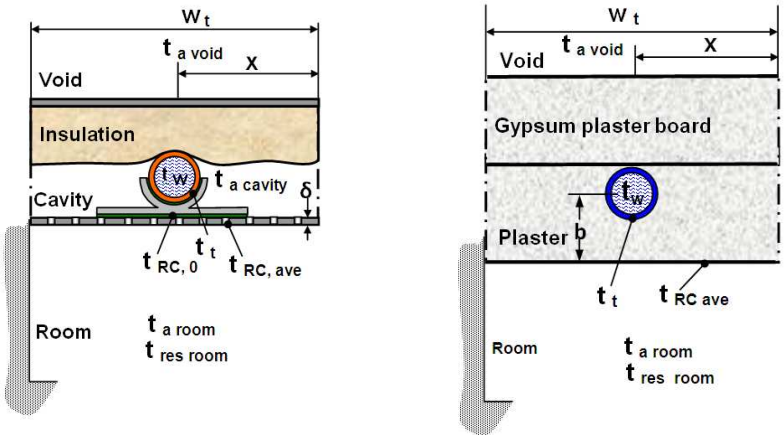

Figure 1.9: Schemes of typical radiant ceiling elements

The radiant ceiling can be represented as a fin. The heat exchange of the system considers the convective resistances on the water side, conduction through the tube shell and union system (tube-ceiling surface) or through a plaster layer and convective-radiative resistances from the tube and radiant ceiling surfaces to the cavity and the room. The fin effectiveness, the mixed convection close to the radiant ceiling surface (generated by the ventilation system) and the panel perforations influence must be considered.

The connection between the panel surface and the tubes is therefore a critical factor. Poor connections (higher thermal contact resistance) provide only limited heat exchange between the tubes

and the panel, resulting in increased temperature differences between the panel surface and the cooling or heating fluid. Each one of these parameters will be considered here after.

1.5.1 Heat transfer coefficient for internal flow in circular tubes

Heat transfer and pressure drop may have to be identified in the three flow regimes: laminar, transition and turbulent. In the case of circular tubes, laminar regime exists at Reynolds numbers lower than 2300. Transition between laminar and turbulent regimes occurs in the range of 2300 ≤ Re ≤ 10000. According to the design criteria, the radiant ceiling should operate in turbulent flow. However this choice may generate too high pressure drops and also too high pumping energy consumption. This is why the system is often operating in the transition regime. In this regime, the Gnielinski equation (Eq. 1.3) (Celata *et al.,* 2007) can be used:

$$Nu_w = \frac{\frac{f_r}{8}(\mathrm{Re}-1000).\mathrm{Pr}_w}{1+12.7\left|\frac{f_r}{8}\right|^{1/2}.(\mathrm{Pr}_w^{2/3}-1)} \quad [-] \quad (1.3)$$

where:

$$f_r = (1.82.\log(\mathrm{Re})-1.64)^{-2} \quad [-] \quad (1.4)$$

And:

$$\mathrm{Re} = 4.\frac{\dot{M}_w / N_p}{\pi.D_i.\mu_w} \quad [-] \quad (1.5)$$

N_p: number of panels in each blocks connected in parallel

1.5.2 Heat transfer from extended surfaces

The temperature distribution along a one-dimensional fin is described by the following equation:

$$\frac{d^2 t_{RC}}{dx^2} = \frac{h_{RC} P}{A_c k_{RC}}\left(t_{RC,average} - t_{a,RC}\right) \quad (1.6)$$

where the air temperature close to the radiant ceiling surface ($t_{a,RC}$) is defined in Chapter 3.

And ***P*** is the fin perimeter and A_c is the cross-sectional area of the fin (Figure 1.10). h_{RC} is the radiant ceiling heat transfer coefficient. It is calculated according to methodology described in Chapter 3.

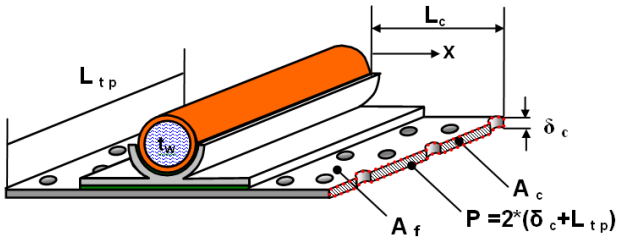

Figure 1.10: Individual ceiling element as a fin

The solution of Eq. 1.6 gives the following expression for the fin temperature in a section "*x*":

$$\frac{t_{RC,x} - t_{a,RC}}{t_{RC,0} - t_{a,RC}} = \frac{\cosh(m * (L_c - x))}{\cosh(m * L_c)} \tag{1.7}$$

with

$$m^2 = h_{RC} * \frac{P}{A_c * k_{RC}} \tag{1.8}$$

and

$$L_c = \frac{w_t - D_e}{2} \quad [\text{m}] \tag{1.9}$$

The effectiveness of this equivalent fin can be defined by:

$$\varepsilon_{fin} = \frac{M_f * \tanh(m * L_c)}{h_{RC} * A_f} \quad [-] \tag{1.10}$$

where A_f is the surface area of the fin (Figure 1.10) and:

$$M_f = \sqrt{h_{RC} * P * k_{RC} * A_c} \tag{1.11}$$

1.5.3 Radiant ceiling heat transfer coefficient definitions

Both convection and radiation have to be considered:

$$h_{RC,room} = h_{RC,room,conv} + h_{RC,room,rad} \quad [W\ m^{-2}\ K^{-1}] \quad (1.12)$$

a. Room-Radiant Ceiling convection ($h_{RC\ room\ conv}$)

The convective heat exchange inside the room equipped with a radiant ceiling becomes a complex process due to the combined effect of ventilation, ceiling perforations, internal thermal load and cooled or heated facade. Existing correlations were developed from experimental measurements in specific conditions of ventilation and internal thermal loads (Alamdari and Hammond, 1983; Spitler and Fisher, 1991; Awbi and Hatton, 2000; Novoselac *et al.,* 2006). Experimental studies were performed considering the individual influence of some parameters on comfort conditions: load distributions (Behne M., 1996), ventilation (Kulpmann, 1993 and Behne M., 1999) and facade (Fredriksson J. *et al.,* 2001).

According to ASHRAE System and Equipment Handbook, (2004) only natural convection (NC) should be considered on the radiant ceiling surface. The law suggested by Incropera, (1996) is:

$$Nu_{RC,room,NC} = C_{h,RC,room}.Ra_{RC,room}^{1/n} \quad [-]$$

The coefficients of this law have the following values:

$C_{h,RC,room}$=0.54 and n=4 (for $10^4 \leq Ra \leq 10^7$) or **$C_{h,RC,\ room}$=0.15** and **n=3** (for $10^7 \leq Ra \leq 10^{11}$). In cooling mode.

And **$C_{h,RC,room}$=0.27 and n=4** (for $10^5 \leq Ra \leq 10^{10}$). In heating mode.

The characteristic length is defined as follows:

$$L_{c,RC,NC} = \frac{A_{s,RC}}{P_{RC}} \quad [m] \quad (1.13)$$

However, among others to make sure that the cooling ceiling system is operating only in dry regime, moisture has usually to be removed from the room through a mechanical ventilation system which generates some air movement. Consequently the above-defined natural convection heat transfer coefficient needs to be corrected by an improvement factor (that is also including the effect of the perforation and fenestration).

According to the criteria defined by Incropera and DeWitt, (1996), forced convection (FC) is negligible if (Gr_L/Re_L^2) » 1. Hence mixed free and forced convection regime is generally one for which (Gr_L/Re_L^2) ≈ 1. In this study, the current order of magnitude found for (Gr_L/Re_L^2) is 0.9 to 0.68. Therefore to combine the effects of natural and forced convection at ceiling surface, the Yuge, (1970) method is used by means of the following function (Figure 1.11):

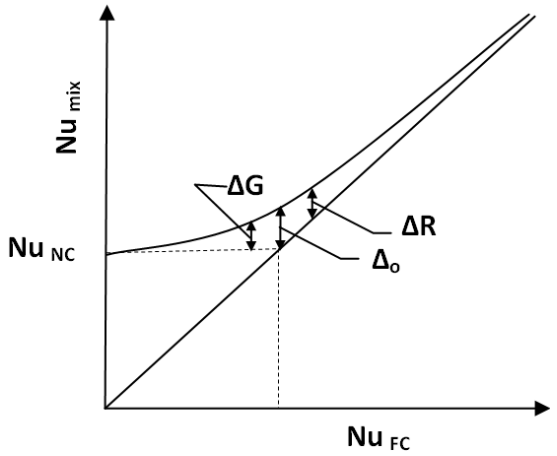

Figure 1.11: Combined convective heat transfer in traverse flow.

$$Nu_{RC,room,mix} = \begin{cases} For: Nu_{RC,room,FC} > Nu_{RC,room,NC} ....; Nu_{RC,room,mix} = Nu_{RC,room,FC} + \Delta R \\ For: Nu_{RC,room,FC} < Nu_{RC,room,NC} ....; Nu_{RC,room,mix} = Nu_{RC,room,NC} + \Delta G \text{ [-]} \\ For: Nu_{RC,room,FC} = Nu_{RC,room,NC} ....; Nu_{RC,room,mix} = Nu_{RC,room,NC} + \Delta_o \end{cases} \quad (1.14)$$

With:

$$\Delta R = \Delta_o \exp\left[-n*(Nu_{RC,room,FC} - Nu_{RC,room,NC}\right]$$

$$\Delta G = \Delta_o \exp\left[-m*(Nu_{RC,room,NC} - Nu_{RC,room,FC}\right]$$

The effect of buoyancy on heat transfer in a forced flow is strongly influenced by the direction of the buoyancy force relative to that of the flow. For a perpendicular direction (transverse flow) caused by ventilation system, buoyancy acts to enhance the rate of heat transfer associated with pure forced

convection. The Yuge method was developed originally for mixed convection on a sphere in transverse flow. For a flat plate in transverse flow, the adaptation of the coefficients *m* and *n* in this study gives the following results:

$$m = \frac{7 + 0.011 Nu_{,room;NC}}{1 + 0.1 Nu_{cc,room,NC}}$$

$$n = \frac{0.993}{2 + 0.2 Nu_{cc,room,NC}}$$

$$\Delta_o = 0.257 * Nu_{cc,room,NC}$$

For a ventilated radiant ceiling, the Reynolds number close to the diffusers is usually of the order of 25000. Therefore the equation (Eq. 1.15) can be used for forced convection (FC) on a horizontal plate in parallel and laminar flow (Incropera and DeWitt, 1996).

$$Nu_{cc,room,FC} = 0.664 \mathrm{Re}_L^{1/2} \mathrm{Pr}^{1/3} \qquad [-] \qquad (1.15)$$

with

$$\mathrm{Re}_L = \frac{u_\infty L_{RC,FC}}{\nu}$$

The air velocity on the radiant ceiling (u_∞) and the characteristic length in forced convection ($L_{RC,FC}$) (distance of the jet detachment) are defined from diffuser manufacturer's catalogue.

Finally, we get that the convective heat transfer coefficient on the radiant ceiling surface in mixed regime is:

$$h_{RC,room,conv} = \frac{k_a}{L_{c,RC}} Nu_{RC,room,comb} \qquad [\mathrm{W\ m^{-2}\ K^{-1}}] \qquad (1.16)$$

The characteristic length ($L_{c,RC}$) has to be experimentally identified due to the fact that, in modern buildings, there are too many different configurations and possible combinations of ventilation systems, thermal load types and distributions, as well as facade effects.

In this study the analysis of ceiling convection is performed by considering that is not possible to get a correlation law which covers all the possible combinations of a real case.

b. Room-Ceiling radiation ($h_{RC\ room\ rad}$)

In order to analyze the internal radiant exchanges, each surface of the enclosure can be characterized by its uniform radiosity and irradiation. The net radiative heat flux of the ceiling surface can be evaluated from Eq. 1.17 and Eq. 1.18 from radiosities (J_i), emissivities (ε_i), areas (A_i), view factors ($F_{i,j}$) and black body emissive powers (E_{bi}):

$$\dot{Q}_{rad,i} = \sum_{j=1}^{N} A_i.F_{i,j}(J_i - J_j) \quad [W] \qquad (1.17)$$

$$\frac{E_{b,i} - J_i}{\frac{1-\varepsilon_i}{\varepsilon_i.A_i}} = \sum_{j=1}^{N} A_i.F_{i,j}(J_i - J_j) \ [W] \qquad (1.18)$$

The view factors can be calculated using the software EES (Alvarado and Klein, 2008) for the surfaces considered in Figure 1.12 according to the experimental test conditions.

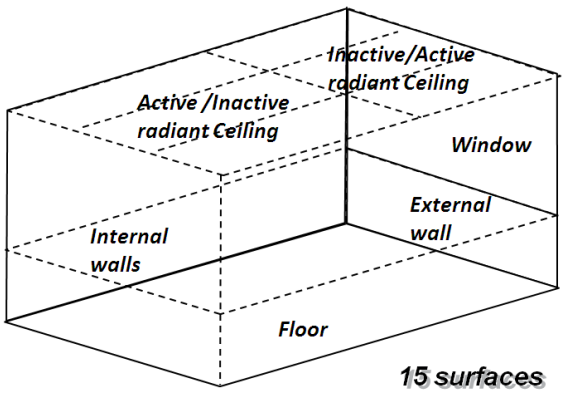

Figure 1.12: Room radiation surfaces

The net radiant heat flux at the ceiling surface can be determined by solving the unknown J_i. This method assumes that the surface temperatures are uniform and known.

According to the method proposed by Davies (2004), the heat transfer coefficient for each surface can be calculated using the transformation “delta to star” to obtain a linearized radiative heat transfer coefficient. For a parallelepiped enclosure (six surfaces) the delta and star networks transformation can be represented in Figure 1.13.

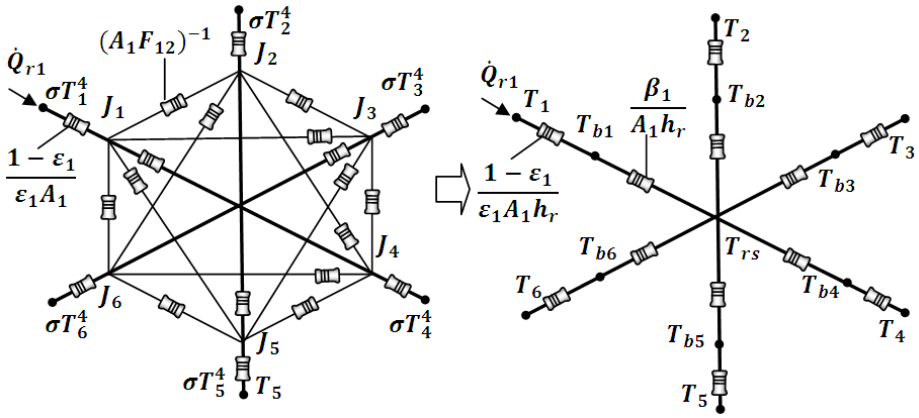

Figure 1.13: Delta and star networks of a parallelepiped enclosure.

Where:

T_{rs}: The radiant star temperature, [K]

T_{bi}: Black-body equivalent radiation temperature of the surface *I,* [K]

βi: Delta-star transform of the surface *i,* [-]

And:

$$T_{rs} = \frac{\sum T_j . S_j}{\sum S_j} \quad [K] \qquad (1.19)$$

$$\frac{1}{S_j} = \frac{1-\varepsilon_j}{\varepsilon_j . A_j . h_{ri}} + \frac{\beta_j}{A_j . h_{ri}}$$

S_i is the total physical conductance between the surface node T_j and the radiant node T_{rs}.

If the room is represented by three surfaces (radiant ceiling, facade and internal walls) the “delta to star” transformation can be presented in Figure 1.14.

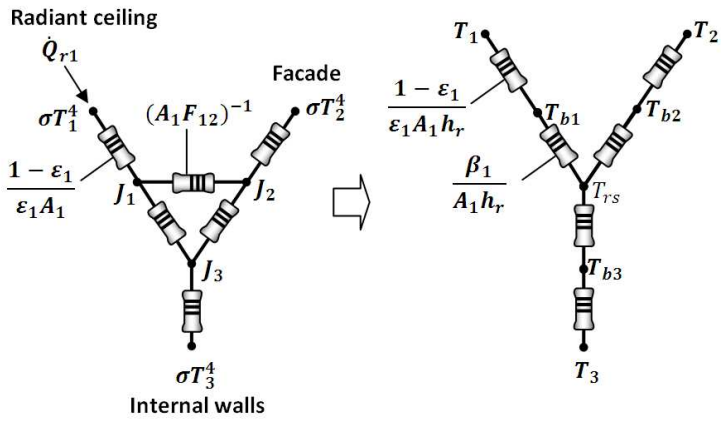

Figure 1.14: Delta and star networks of three rectangular sides of indefinite length.

where

$$\beta_1 = \frac{A_1.A_2.F_{2,3}}{A_1.F_{1,2}.A_2.F_{2,3} + A_2.F_{2,3}.A_3.F_{3,1} + A_3.F_{3,1}.A_1.F_{1,2}}, etc \quad [-] \qquad (1.20)$$

$$T_{rs} = \frac{T_1.S_1 + T_2.S_2 + T_3.S_3}{S_1 + S_2 + S_3} \quad [K] \qquad (1.21)$$

and

$$S_j = \frac{A_j.h_r}{\left(\frac{1-\varepsilon_j}{\varepsilon_j}\right) + \beta_j} \quad [W/K] \qquad (1.22)$$

As the radiosities and temperatures are known and assuming linearization of the heat transfer coefficient, it can be calculated as:

$$h_{ri} = \frac{\dot{Q}_{rad,i}}{A_i * (T_{rs} - T_i)} \quad [W\ m^{-2}\ K^{-1}] \qquad (1.23)$$

This coefficient depends therefore on the surface and radiant star temperature definition, emissivities and view factors between the room surfaces and the radiant ceiling. There is therefore a slight variation if some part of the ceiling is inactive, with respect to the case in which the total ceiling surface is active.

Several methods have been developed to simplify this calculation. For example in the "mean radiant temperature" method (MRT), the thermal radiation interchange inside an indoor space is modeled by assumption that the surfaces radiate to a fictitious, finite surface (representing the room walls including the facade and the floor) that gives about the same heat flux as the real multisurface case (Walton G.N., 1980)**.** The MRT equation for the radiant ceiling surface may be written as:

$$\dot{Q}_{RC,room,rad} = A_{RC,effec} * \sigma * F_{r,room} * ((t_{RC,ave} + 273.15)^4 - (t_{mr,room} + 273.15)^4) \text{ [W]} \quad (1.24)$$

with

$$t_{mr,room} = \frac{\sum_{j=RC,ave}^{n} A_j . \varepsilon_j . t_j}{\sum_{j=RC,ave}^{n} A_j . \varepsilon_j} \quad \text{[K]} \quad (1.25)$$

When the surface emittances of the enclosure are nearly equal and the surfaces directly exposed to the panel are marginally unheated or uncooled, the fictitious temperature $t_{mr,room}$ become the area-weighted average uncooled or unheated temperature (AUST) widely used in the related literature (Kilkis, 1995; Jeong and Mumma, 2004; ASHRAE System and Equipment, 2004). However it has to be considered that there is usually an important temperature difference between the facade and the room surfaces.

As a better approximation, the mean radiant temperature of uncooled or unheated surfaces can be calculated from measurements of the resultant and air temperatures, by correcting the mean radiant temperature of the room (Eq. 1.26) as the radiant ceiling "sees" an environment which excludes its own influence (Ternoveanu *et al.,* 1999).

$$t_{mr,room} = \left[2 * t_{res,room} - t_{a,room} - \frac{A_{RC,s}}{A_{room,f,s}} * t_{RC,ave} \right] * \frac{1}{1 - \frac{A_{RC,s}}{A_{room,f,s}}} \quad [℃] \quad (1.26)$$

Eq. (1.26) is applicable only if: $|t_{mr\ room} - t_{a\ room}| < 4$ K (Külpmann R.W., 1993).

The radiation exchange factor ($F_{r\ room}$) for any two diffuse, gray surfaces that form an enclosure can be calculated from Eq. (1.27) (Incropera and DeWitt, 1996):

$$F_{r,room} = \frac{1}{\frac{1}{F_{RC,f}} + \frac{1}{\varepsilon_{RC}} - 1 + \frac{A_{RC,s}}{A_{room,f,s}} * \left[\frac{1}{\varepsilon_{f,room}} - 1\right]} \text{ [-]} \qquad (1.27)$$

Where $F_{RC,f}$ is the radiation view factor from ceiling to a room fictitious surface giving an equivalent heat transfer, as in the real multi-surface case (1.0 for flat ceiling ASHRAE, 2009).

$A_{RC,s}$, $A_{room,f,s}$ are the area of radiant ceiling and fictitious room surface (other than the ceiling).

ε_{RC} and $\varepsilon_{f,room}$ are emissivities of the ceiling (**model parameter**) and of the fictitious surface (0.98 (ASHRAE 2009)).

The radiation heat transfer coefficient can be expressed as follows:

$$h_{RC,room,rad} = \sigma * F_{r,room} * \frac{(t_{RC,ave} + 273.15)^4 - (t_{mr,room} + 273.15)^4}{t_{RC,ave} - t_{mr,room}} \quad \text{[W m}^{-2}\text{ K}^{-1}\text{]} \qquad (1.28)$$

The radiative heat transfer coefficient can also be linearized according to methodology presented in Figure 1.15.

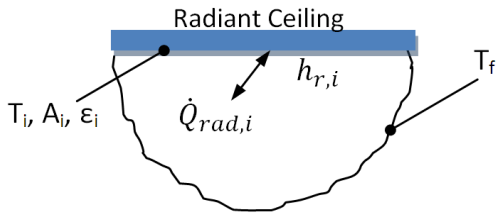

Figure 1.15 Simplified room radiation exchange

where

$$\dot{Q}_{rad,i} = h_{r,i} * A_i * (t_i - t_f) \quad \text{[W]} \qquad (1.29)$$

The heat transfer coefficient in this case can be also linearized as:

$$h_{r,i} = \varepsilon_i * \sigma_i * (T_i - T_f)(T_i^2 - T_f^2) \text{ [W m}^{-2}\text{ K}^{-1}\text{]} \qquad (1.30)$$

If the difference between T_i and T_f is small, the following approximation can be considered:

$$h_{r,i} = 4 * \varepsilon_i * \sigma_i * \overline{T}^3 \quad \text{[W m}^{-2}\text{ K}^{-1}\text{]}$$

where

$$\overline{T} = (T_i + T_f)/2 \qquad [K]$$

The temperature T_f is actually the mean radiant temperature viewed by the surface *i.*

In the previous cases (two and three surfaces), the result of $h_{r,i}$ coefficient linearization is exact. However, for a parallelepiped enclosure of six surfaces, there is an error of about 6 % (Davies 2004). In this study, the radiation heat transfer coefficient of the radiant ceiling is calculated considering the star temperature for three surfaces: facade, internal walls and radiant ceiling as the most representative and useful case for commissioning process.

A comparison is established hereafter between simplified and detailed methods to calculate the radiant heat flow from the ceiling surface:

For example for the radiant ceiling **T1**, if $\dot{Q}_{RC,room,rad}$ is calculated following the detailed method (Eq. 1.17 and 1.18) and the laboratory experimental results (section 3.1) in which all surface temperatures were measured, an average difference of 3.71 % with respect to the simplified method (Eq.1.24) is obtained (see Figure 1.16) (the same result is found for synthetic capillary tube mats: types U, S, G tested with all the radiant ceiling active and reference temperature placed at the room center).

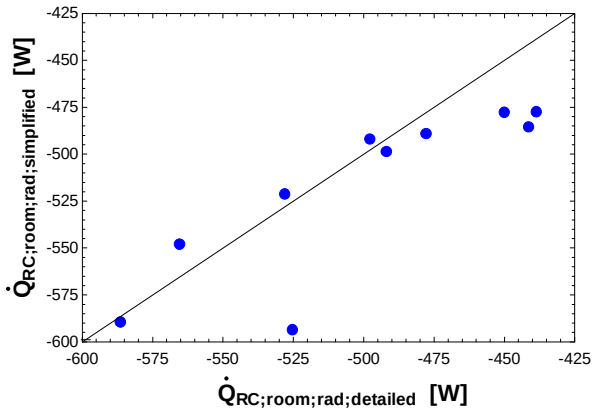

Figure 1.16: Comparison between detailed and simplified methods for room radiant heat exchange

In general the differences between simplified and detailed methods shown in Figure 1.16 are due to the air temperature stratification. For simplified method, the measurements of resultant and air temperatures at 75 [cm] from the floor are used. For the point which is outside the range the stratification was particularly important (1.5 [K]).

If the detailed method is used, it is important to take into account that the surface temperature uncertainties could be significant, specially glazing surface (Fissore and Fonseca, 2007) and the global uncertainty increases with the number of measured variables. This is a typical difficulty in the commissioning process.

1.5.4 Room-resultant temperature

The resultant temperature can be accurately estimated from measured surface temperatures and corresponding view factors between the person and the surfaces. The mean radiant temperature (MRT) viewed by a sphere of 60 [cm] of diameter (representing a seat person) placed in different positions inside the room is calculated according to:

$$MRT = \left[F_{0,j} * T_{s,j}^{4}\right]^{1/4} \quad [K] \qquad (1.31)$$

The view factors ($F_{0,j}$) can be calculated using the software EES (Alvarado and Klein, 2008) for the configuration presented in Figure 1.17 and the surfaces and the sphere position into the room shown in Figure 1.18. The number of surfaces and position of the globe sensor are fixed according to the experimental conditions during laboratory testing and commissioning processes.

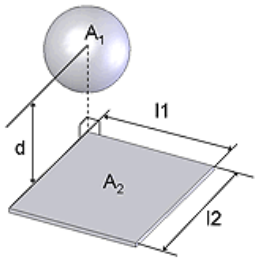

Figure 1.17: MRT view factor calculation

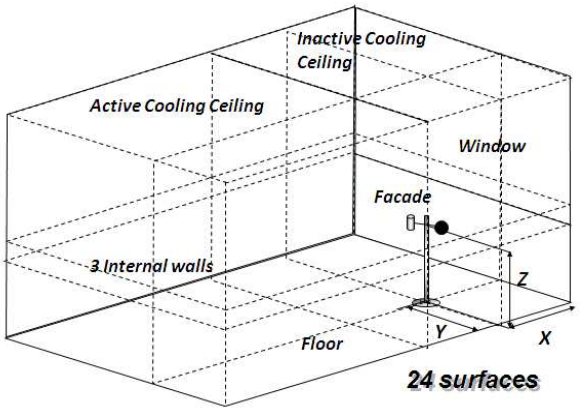

Figure 1.18: Surfaces used for MRT calculation.

The resultant temperature can be calculated as:

$$t_{res,room} = \frac{\left(MRT - 273.15\right) + t_{a,room}}{2} \quad [℃] \qquad (1.32)$$

This estimation can be checked at the point(s) where the globe temperature is measured, in the frame of a commissioning process.

1.5.5 Bi-dimensional Conduction

For one out of the seven radiant ceiling configurations presented in this study, the thermal resistance between the tubes and ceiling surface takes into account the thermal resistance through a plaster layer (Figure 1.19). For this configuration, bi-dimensional conduction effects are important and the tube is considered in the modeling as a horizontal cylinder of characteristic length L_{tp}, midway between parallel planes (Figure 1.19).

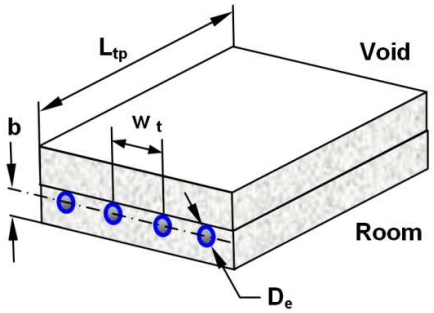

Figure 1.19: Conduction shape factor definition

According to Incropera and DeWiitt (1996), the conduction thermal resistance can be defined as:

$$R'_{s1} = \frac{\ln\left|8.\frac{b}{\pi.D_e}\right|}{2.\pi.k_{s1}} \qquad [\text{K. m W}^{-1}] \qquad (1.33)$$

Where, ***b*** value is the distance between tube shaft and ceiling surface. k_{s1} is the conductivity of the plaster layer. The ***b*** value is obtained using the experimental results (as a model parameter).

1.5.6 Global heat transfer characteristics

In the frame of an experimental analysis, the *A.U* value of the radiant ceiling can be calculated as:

$$A.U = \frac{\left|\dot{Q}_{system}\right|}{\Delta_{T,Ln}} \qquad [\text{W K}^{-1}] \qquad (1.34)$$

where

$$\Delta_{T,Ln} = \left|\frac{t_{w,su} - t_{w,ex}}{Ln(Arg)}\right| \qquad [\text{K}] \qquad (1.35)$$

$$Arg = \frac{t_{w,su} - t_{res,room}}{t_{w,ex} - t_{res,room}} \qquad [-] \qquad (1.36)$$

The resultant temperature measured with a globe sensor at some selected point inside the room is used as reference. This *U* value includes the exchange with the room and also the ceiling void.

The ceiling effectiveness can be defined as follows:

$$\dot{Q}_{system} = \varepsilon.\dot{M}_w.c_{pw}.\left(t_{w,su} - t_{res,room}\right) \qquad [\text{W}] \qquad (1.37)$$

$$\varepsilon = 1 - \exp(-NTU) \qquad [-] \qquad (1.38)$$

$$NTU = \frac{A.U}{\dot{C}_w} \qquad [-] \qquad (1.39)$$

$$\dot{C}_w = \dot{M}_w.c_{pw}. \qquad [\text{W K}^{-1}] \qquad (1.40)$$

1.6 CONCLUSIONS

A brief general description of radiant ceiling systems and a detailed analysis of heat transfer used in this study were developed, covering such topics as materials and working principle, description to finish with a general description of commissioning processes.

In convection and radiation of the radiant ceiling, it was concluded that the most studied and documented heat flow patterns are based on natural convection and simplified radiation exchange between two surfaces. The convective heat exchange on a radiant ceiling surface becomes a complex process, considering specially the combined effect of ceiling perforation, ventilation and fenestration systems. There are too many configurations and possible combinations of these elements in the modern buildings that do not allow to completely describe the phenomenon with a correlative method. In this study the analysis of ceiling convection is performed by considering that it is not possible to get a correlation law which covers all the possible combinations of a real case.

2. Experimental analysis in laboratory

2.1 INTRODUCTION

The aims of this chapter are to give some ideas about the theoretical uncertainty on the different measured variables and a description of different measurement methods and sensors used to test the radiant ceiling systems.

The main objective of this chapter is to present the results of the experimental analysis and its discussion. Another objective is to describe the test benches:

- Two test chambers have been adapted in a way to reproduce as good as possible the characteristics of real offices located in Brussels.

  Fifty-six tests were performed in these two chambers, with the aim to observe the influences of parameters such as the mass flow rate, supply water temperature and thermal load distribution, fenestration and ventilation system effects on the radiant ceiling capacity and comfort conditions.
- A third test bench was used to reproduce the standard test conditions for radiant ceiling systems according to the German standard DIN 4715-1, (1993). Nine tests were performed using this bench.

The aim of this kind of test is to compare the performance of different types of cooling ceiling systems. Therefore a homogeneous load distribution is considered, without influences of ventilation system and/or facade asymmetry (HLK, 1995; C. Kochendörfer, 1996).

2.2 MEASUREMENT SYSTEMS AND UNCERTAINTY ANALYSIS

The basic method to evaluate a measurement uncertainty is universal and applicable to all types of measurements. However this method might be complex, considering that the resulting values are usually function of many independent variables, measured during the experiment.

The uncertainty methodology used in this work is described in detail in Fonseca N., (2009); Fissore and Fonseca, (2007) and ISO GUM, (1995).

All experimental results must be expressed as:

$$Y = \bar{Y} \pm U .....(k_y = ...) \quad (2.1)$$

where

Y is the output magnitude, result whose uncertainty must be estimated.

An estimation of *Y* can be obtained from a functional relation as:

$$Y = f(X_1, X_2, X_3, ...X_N)$$

where the *X* values can be independent measurements or combinations of other variables.

The $\bar{Y}$ value is the statistic average of ***n*** measurements.

U is the expanded uncertainty on *Y* estimate value and can be obtained as:

$$U = u_y * k_y \quad (2.2)$$

where

u_y is the combined uncertainty of *Y*

k_y is the coverage factor. This value depends on the confidence level (it currently varies between 1 and 3).

In order to obtain the combined uncertainty on *Y,* an uncertainty propagation law can be used such as:

$$u_y = \left[\left(\frac{\partial Y}{\partial X_1} * u_{x1} \right)^2 + \left(\frac{\partial Y}{\partial X_2} * u_{x2} \right)^2 + ... \left(\frac{\partial Y}{\partial X_n} * u_{xN} \right)^2 \right]^{0.5} \quad (2.3)$$

When the partial derivatives involved in the estimation of u_y value are defined as functions of other variable x_i, the average values of the ***n*** measurements can be used to perform the calculation.

The u_{xi} values represent the individual uncertainties on estimation of each variable involved in the calculation of u_y (if the uncertainty u_{xi} depends on the measurement of other variables, the equation 2.3 must be used again until the u_{xi} values correspond to a direct measurements).

The combined uncertainty u_{xi} of each variable measured directly can be finally estimated as:

$$u_{xi} = \sqrt{U_{A,xi}^2 + u_{cal,xi}^2 + u_{drift,xi}^2 + u_{tem,xi}^2 + u_{met,xi}^2 + u_{res,xi}^2} \tag{2.4}$$

with

U_A : type A uncertainty, calculated using statistics methods.

u_{cal}: calibration uncertainty.

u_{deriva}: drift uncertainty.

u_{temp}: temperature uncertainty.

u_{met}: method uncertainty.

u_{res}: resolution uncertainty.

All the components of the uncertainty measurements are calculated using the methodology described in ISO GUM, (1995). Required values of accuracy, resolution, calibration, etc., can be taken from manuals and equipment calibration certificates.

The coverage factor is calculated as a function of the effective degree of freedom of the *Y* variable (γ_y). Considering a confidence level of 95.45 %, (which is usual for the available instrumentation), the coverage factor can be calculated as:

$$k_y = 1.95996 + \frac{2.37356}{\gamma_y} + \frac{2.818745}{\gamma_y^2} + \frac{2.546662}{\gamma_y^3} + \frac{1.761829}{\gamma_y^4} + \frac{0.245458}{\gamma_y^5} + \frac{1.000764}{\gamma_y^6}$$

The effective degree of freedom must be calculated from the Welch-Satterthwaite formula as:

$$\gamma_y = \frac{(u_y)^4}{\frac{(u_{x1})^4 * \left(\frac{\partial Y}{\partial x_1}\right)^4}{\gamma_{X1}} + \frac{(u_{x2})^4 * \left(\frac{\partial Y}{\partial x_2}\right)^4}{\gamma_{X2}} + ... \frac{(u_{xN})^4 * \left(\frac{\partial Y}{\partial x_N}\right)^4}{\gamma_{XN}}} \tag{2.5}$$

Temperatures

Temperatures are measured with T thermocouples (copper/copper-nickel) of Class 1 (defined by the Standard IEC 584-3) with a reference temperature of 0 [℃] obtained by a water/ice mixture.

The resultant (globe) and air temperatures as well as room surface temperatures and water temperatures are measured according to ANSI/ASHRAE Standard 41.1-1986 (RA 91). Air temperatures are measured at different position from the facade. Figure 2.1 shows the schematic view of the column used for dry and resultant air temperature measurements.

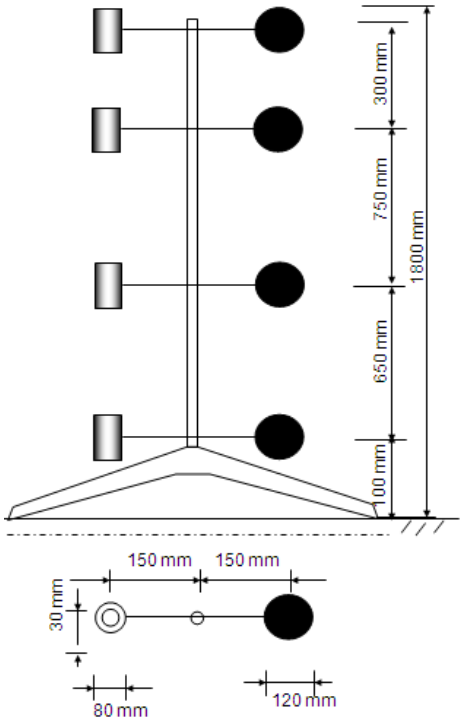

Figure 2.1: Air and globe temperatures measuring columns.

Data acquisition system

The signals given by the sensors are measured with the help of 2 to 6 data acquisition cards, which can measure DC voltage, DC intensities and temperatures. Table 2.1 gives some characteristics of these cards (Cuevas C., 2007). Temperatures are measured directly with the conversion laws suggested by the interface software.

Table 2.1 data acquisition system characteristics

Number of Channels	20
Type of measurements	DC voltage: ±12 V DC current: 0 to 20 mA Thermocouples: B, E, J, K, N, T, R, S
Supply voltage	12 to 50 VDC

For measurements of pressure, differential pressure and electrical power converters, a resistance of 100 Ω was installed in parallel to its outputs to convert its current signals to voltage. Thus, its output signals of 4-20 mA and 0-20 mA are transformed to 0.4-2 V and 0-2V. This resistance has a tolerance of ± 0.1 %. The accuracies of the acquisition system for each transducer are given in Table 2.2.

Table 2.2 Data acquisition accuracies

Measuring	Scale	Accuracy
Temperature	100 to 400 [℃] <	±0,3 K
Pressure	0 – 2,2 V	±[0,01 % rdg + 0,01 % fs]
Electrical power	0 – 2,2 V	±[0,01 % rdg + 0,01 % fs]

Data processing

The time evolutions of temperatures and powers allow for checking the stability of the tests and selecting the “good” period, in which a steady state analysis can be applied.

Figure 2.2 shows an example of air and water temperatures evolution and the “good” period selected to calculate the averages values for further analysis.

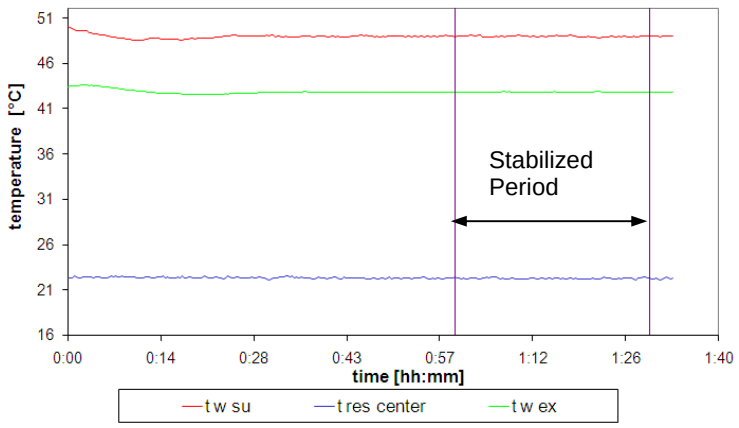

Figure 2.2: Evolution of room and water temperatures.

Measuring uncertainties

All measurements are performed according to ANSI/ASHRAE Standard 41.1-1986 (RA 91), ASHRAE, ANSI/ASHRAE Standard 41.2-1987 (RA92) and ANSI/ASHRAE Standard 41.3-1989. Table 2.3 gives the combined uncertainties (device and data acquisition system) of the main measurements. The air flow rate is measured according to international standard ISO 5167 (1991).

For the temperatures, two sources of uncertainty are considered: one coming from the thermocouple tolerance (±0,5 [K]) and the other one coming from the data acquisition system (±0,3 [K]) (method uncertainty). This gives an overall absolute uncertainty of ±0,6 [K] (the relative uncertainty is smaller). The corresponding cooling effect of the air discharged into the chamber is evaluated with an uncertainty of ±3.5 %. The *A.U* experimental value is evaluated with an uncertainty of ±5.3 %.

Table 2.3: Measuring uncertainties

Variable		Measurement range	Combined uncertainty
Temperature differentials	ΔT_w	2 to 5 [K].	± 0.25 [K].
	ΔT_a	10 [K].	± 0.25 [K].
Flows	$\dot{M}_w$	0.0397 [kg s^{-1}].to 0.103 [kg s^{-1}].	±0.1% of the measured value
	$\dot{V}_a$	96 to 105 [m^3 h^{-1}].	± 3.5 % of the measured value
Electrical powers	$\dot{W}_f$	290 to 500 [W].	± 1 % of the measured value
	$\dot{W}_{in,loads}$	750 to 1060 [W].	± 1 % of the measured value

2.3 TEST BENCHES DESCRIPTION AND EXPERIMENTAL ANALYSIS

2.3.1 Test bench type 1

2.3.1.1 General description

This test bench is used for the experimental analysis of the radiant ceiling type 1 (**T1**) in **cooling mode**. Ten main tests are performed to observe the influences of the mass flow rate, supply water temperature and thermal load distribution on the cooling ceiling capacity and on the comfort conditions. Additionally, during these tests, the facade and ventilation system effects are also considered. Twelve additional tests are performed to evaluate the influences of ventilation system and of different thermal load distributions on the cooling ceiling capacity. The most important disturbances evaluated here are:

- Thermal loads: with or without thermal loads and distributed uniformly or located close to the facade.
- Facade: with or without facade effect.
- Ventilation: with or without cooling or heating air.
- Fan-coil effect: comparative method. In the same loads conditions, the cooling ceiling is replaced by a fan-coil which is controlled in such a way to maintain the same comfort level at the center of the room.

The climatic chamber used is 3.1 [m] in height, 3.6 [m] in width and 6 [m] in length. The cooling ceiling is placed at 2.7 [m] above the floor level. The chamber has a space to simulate facade and an adjacent chamber in order to avoid the ambient influence (Figure 2.3). In order to simulate the external thermal load, the facade air space is heated until reaching the required load in the chamber.

Figure 2.4 shows the water circuit schema. The cooling ceiling (**T1**) consists of 2 modules (left and right) each one composed of 4 radiant panels. Sensors are installed on both sides of the circuit (supply and exhaust), in order to measure temperature and pressure (ISO, 1991). Water flow rate is accurately measured by timing integration (Figure 2.4). The water temperature differential (t_{wex} – $t_{wsu)}$) is also directly measured (Fonseca N *et al*., 2003).

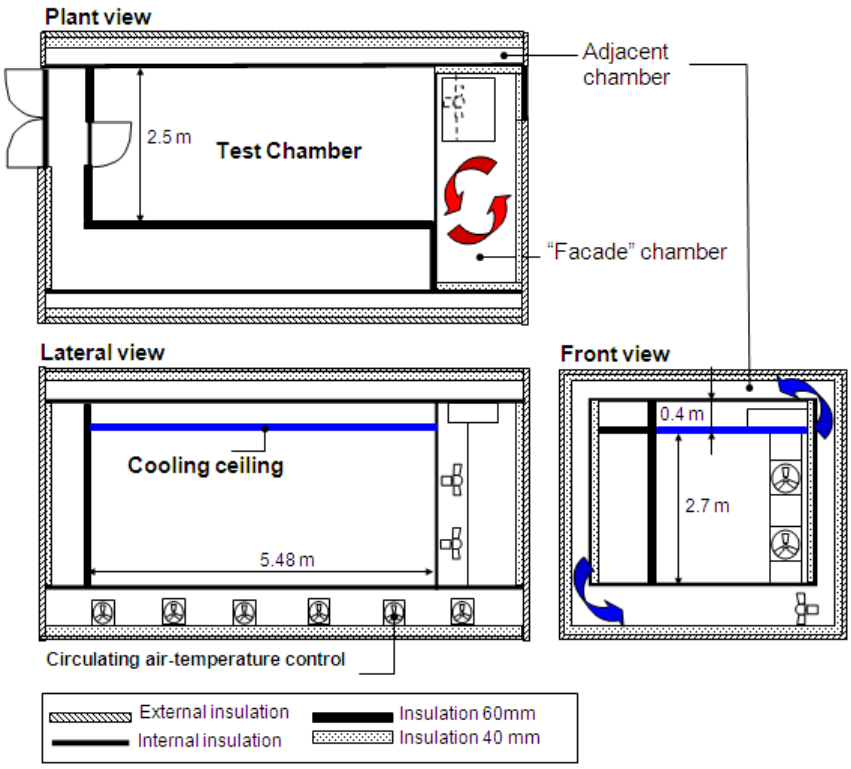

Figure 2.3: Test chamber views.

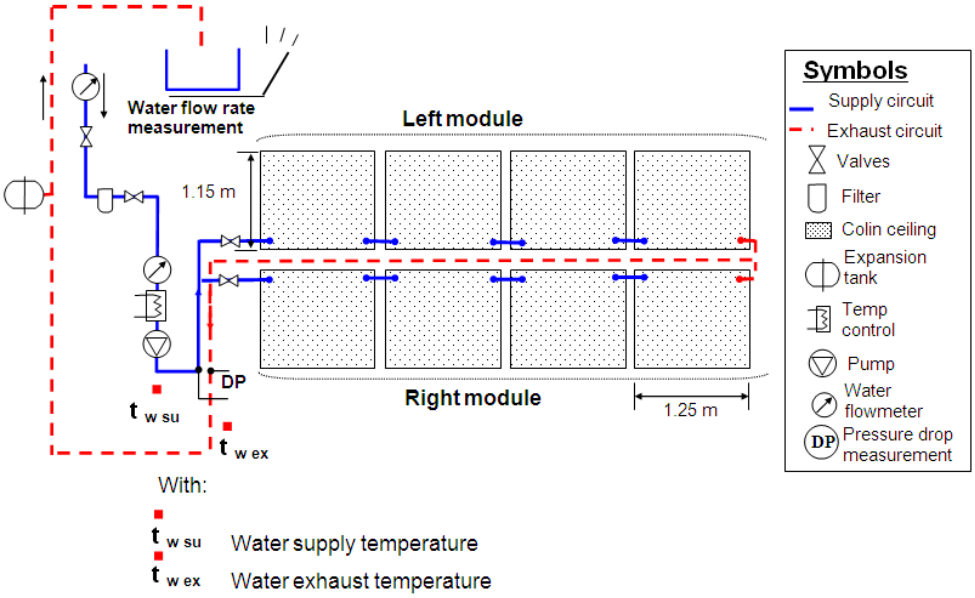

Figure 2.4: Schematic view of the water circuit.

Figure 2.5 shows the air circuit scheme. The ventilation system is provided by the radiant ceiling manufacturer, in order to adapt it to the panels and modules specifications. It is important to note the alternative direction facade-hall for the air discharge. The air flow rate measurement supplied by the discharge boxes is carried out by means of a diaphragm, according to international standard ISO 5167, (1991).

Discharge air temperature is measured downflow of the air flow rate measurement, in the entrance of the chamber ceiling. Air is discharged at 15[℃] in to the chamber, which is at 25 [℃].

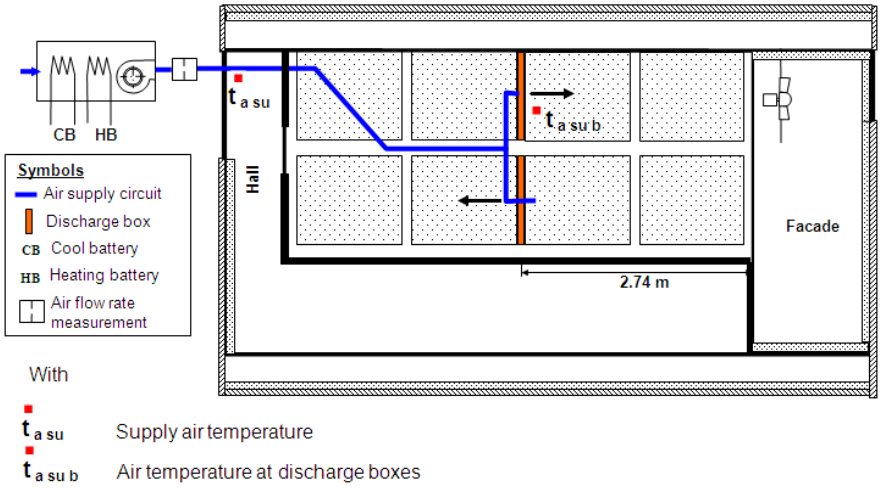

Figure 2.5: Schematic view of the ventilation system.

During the test, the chamber is over-pressurized; this eliminates any parasitic air infiltration and gives an opportunity to study the influences of mechanic ventilation on cooling ceiling performances.

For the thermal balance, it is assumed that the air leaves the chamber at the reference temperature measured at the center of the chamber, considering that there is no specific extraction device.

Internal thermal loads are simulated as shown in Figure 2.6:

- Four fluorescent tubes of 38 W each one (60 % radiative 40 % convective) are placed inside the cooling ceiling, in accordance with the accessories supplied by the manufacturer.
- Seven electrical convection heaters with a total thermal load of 514 W (99 % convective) are installed in the room.

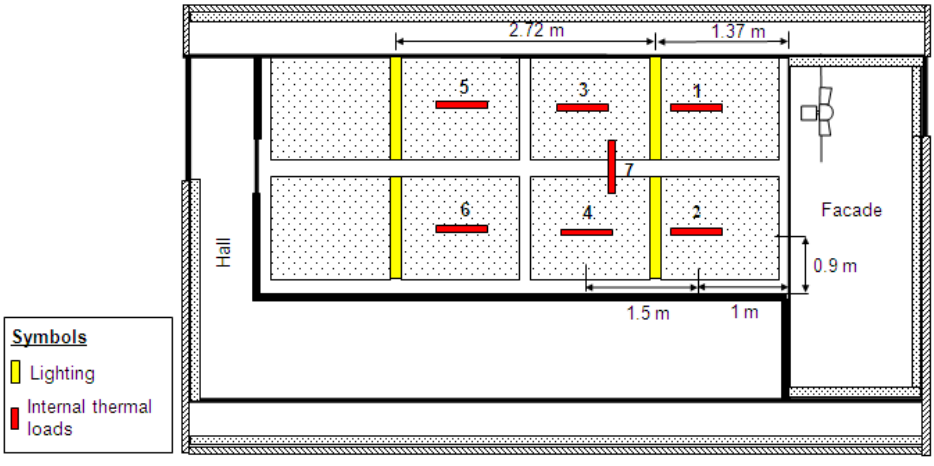

Figure 2.6: Occupation thermal loads distribution.

- The facade air space is heated until reaching the required load in the chamber. Heat transmission through the facade is measured by 20 flux meters (Figure 2.7). For the thermal balance only 12 fluxmeters are used (they are included in the zone limited by dotted line in Figure 2.7). It is considered that the left side zone could be affected by operating conditions of the facade fan and the right side zone is out of the simulated zone.

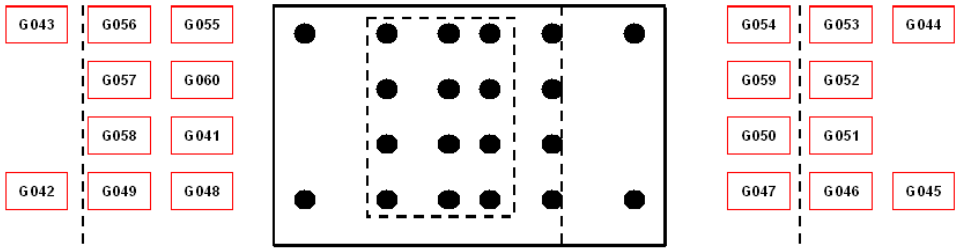

Figure 2.7: Schematic view of heat fluxmeters and temperature distribution on the facade.

At the center of each heat fluxmeter, the internal surface temperature is also measured. For the same reason as presented before, only 12 measurements are considered.

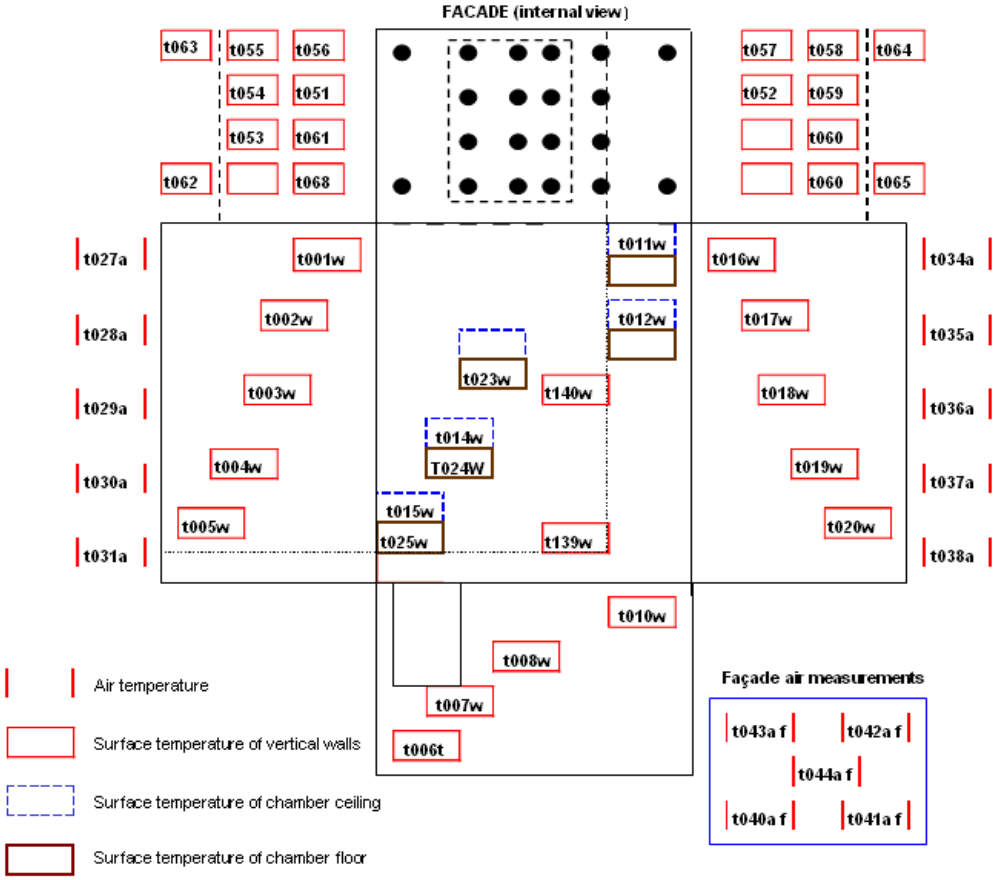

Figure 2.8: Internal surface and air temperature measurements

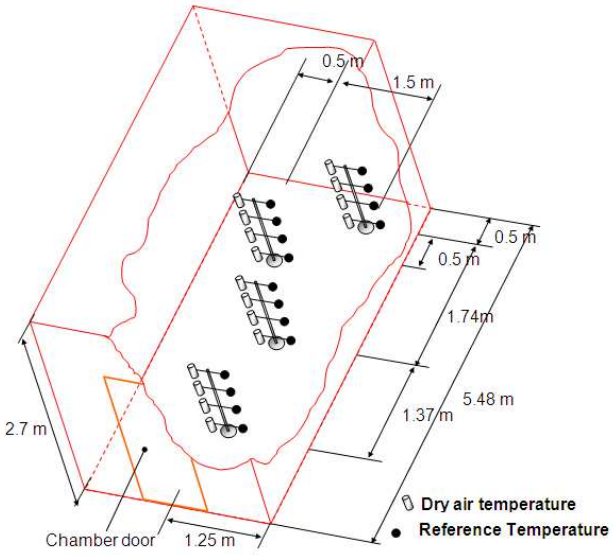

Figure 2.9: Air and globe temperatures measurements.

Internal surface temperatures and air temperatures of lateral and facade chambers are measured at points indicated in Figure 2.8. The combination of heat flow measurement, surface temperature and reference temperature at the center of the chamber, allows for the estimation of a heat exchange coefficient between the facade and the chamber. The reference temperature is always taken at the chamber center, at 75 [cm] above the floor, with one of the globe temperature sensors (Figure 2.9). Figure 2.10 shows the position of air velocity measured during the comfort test. It is carried out at 6 positions inside the chamber, placed vertically at 10 [cm], 75 [cm], 150 [cm] and 200 [cm] height above the floor.

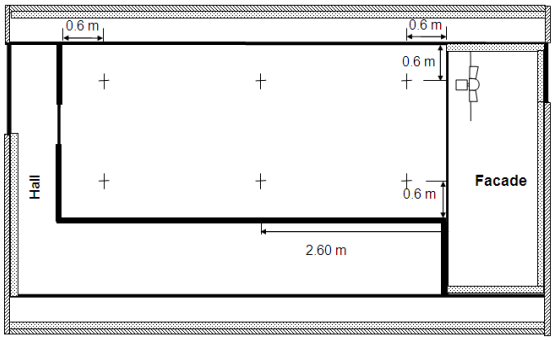

Figure 2.10: Position of air velocity measurements.

Air velocity measurements are performed using a thermal anemometer at intervals of 5 minutes during one hour time. Thermography analyses on modules and walls are carried out for one particular performance test. The aim of the analysis is to detect any cooling ceiling failure, leakage or incorrect thermal contact between piping and radiant panels.

2.3.1.2 Experimental results

Room energy balance

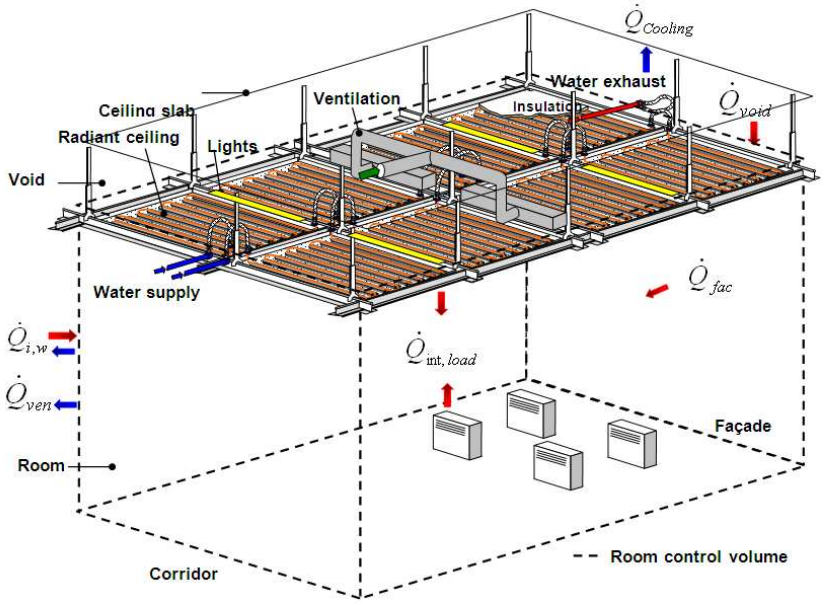

Figure 2.11: Control volume for the room thermal balance

The thermal balance of the test chamber control volume as seen in Figure 2.11 is given by the following equation in cooling mode:

$$\dot{Q}_{\text{int},loads} + \dot{Q}_{void} + \dot{Q}_{i,w} + \dot{Q}_{fac} - \dot{Q}_{ven} - \dot{Q}_{cooling} + \dot{U} = \dot{R}_{global} \quad [\text{W}] \qquad (2.6)$$

Where the heat flow rate extracted by the cooling ceiling system can be defined as:

$$\dot{Q}_{cooling} = \dot{M}_{w,su}.c_{p,w}.\left(t_{w,su} - t_{w,ex}\right) \quad [\text{W}] \qquad (2.7)$$

The internal thermal load (lighting and convectors) $\dot{Q}_{\text{int},loads}$ is measured directly by watt-meters.

The heat gain through internal walls is estimated as a function of the measured surface temperature of each wall and floor surfaces of the enclosure. The internal heat transfer coefficient is estimated at 8 [W m^{-2} K^{-1}]:

$$\dot{Q}_{i,w} = h_{\text{int}} * A_s * (t_{s\_w} - t_{res,room,center})[\text{W}] \qquad (2.8)$$

The void heat gain is estimated as a function of the measured ceiling back surface temperature (in contact with the air in the ceiling void) and the average water temperature. The *U* value is estimated at 1.13 [W m^{-2} K^{-1}] (considering the thermal resistance of 30 [mm] insulation and a not ventilated void of 40 [cm]):

$$\dot{Q}_{void} = A_{ceiling} * U * \left[t_{s,ceiling} - \frac{(t_{w,su} + t_{w,ex})}{2} \right] \text{[W]} \qquad (2.9)$$

The external heat gain through the facade $\dot{Q}_{fac}$ is measured directly by watt-meters.

The heat flow rate extracted by the ventilation system can be defined as:

$$\dot{Q}_{ven} = \dot{M}_a * c_{pa} * (t_{res,room,centre} - t_{a,su}) \qquad \text{[W]} \qquad (2.10)$$

In Eq. 2.6, $\dot{U}$ is the internal energy variation of the control volume. It can be calculated as:

$$\dot{U} = C * \frac{dT_a}{d\tau} \qquad \text{[W]} \qquad (2.11)$$

With:

C : global thermal mass of all components included in the control volume, [J K^{-1}]:

$$C = (m_1 * c_1 + m_2 * c_2 ..... m_n * c_n) \qquad \text{[J K}^{-1}\text{]} \qquad (2.12)$$

As the internal energy variation of the control volume is only around 0.3 % of the total thermal load, the uncertainty of this estimation can be neglected.

$\frac{dT_a}{d\tau}$: air temperature variation (supposed to represent the state variable, hypothesis used as better estimation), [K s^{-1}].

The differential $dT_a / d\tau$ is calculated using the method shown in Figure 2.12. Initial and final temperatures are determined by averaging 5 points at the beginning and 5 other points at the end of each sampling stabilized period, in such a way to define a period of 60 minutes (Cuevas and Lebrun, 2002).

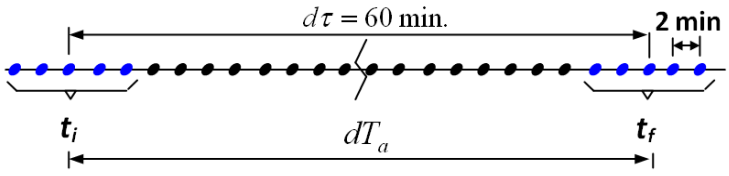

Figure 2.12: Method used to determinate $dT_a / d\tau$.

$\dot{R}_{global}$ is the residual of the thermal balance, [W].

The residuals of the thermal balance give an idea about the precision of the measurements.

Thermal balance results

The estimated values of all terms of the thermal balance are shown in Table 2.4. It is observed that an average of 76.7 % of the room thermal load is compensated by the cooling ceiling system and 23.3 % by the ventilation system. The heat gains from the ceiling void and facade represent an average of 10.2 % and 38.5 % of the total thermal load respectively.

Table 2.4: Thermal balance results

Test	T1C1	T1C2	T1C3	T1C4	T1C5	T1C6	T1C7	T1C8	T1C9	T1C10
$\dot{Q}_{cooling}$ [W]	828.14	808.87	806.19	1065.94	837.53	856.18	849.43	927.21	967.01	1046.48
$\dot{Q}_{ven}$ [W]	314.73	281.94	291.84	350.48	266.55	260.54	247.45	263.50	271.76	179.25
$\dot{Q}_{\mathrm{int},loads}$ [W]	768.51	800	760	1057	637.14	662.09	652.98	655.6	768.53	751.3
$\dot{Q}_{fac}$ [W]	500.64	491.43	471.56	421.16	458.96	505.49	489.49	478.34	308.72	290.79
$\dot{U}$ [W]	-9.77	1.39	1.38	-0.68	6.30	-0.68	1.47	-1.10	-6.82	-4.47
$\dot{Q}_{void}$ [W]	104.70	97.89	97.74	126.14	120.20	111.28	110.10	125.75	148.84	156.90
$\dot{Q}_{i,w}$ [W]	-229.08	-228.78	-213.31	-307.89	11.86	-136.23	-178.20	-91.10	41.27	70.00
$\dot{R}_{global}$ [W]	-7.86	7.13	19.34	-12.69	13.37	25.22	-21.03	-23.20	21.77	38.78

The results are shown in Figure 2.13. In average, they are in the order of ±2 % of the tested cooling ceiling capacity.

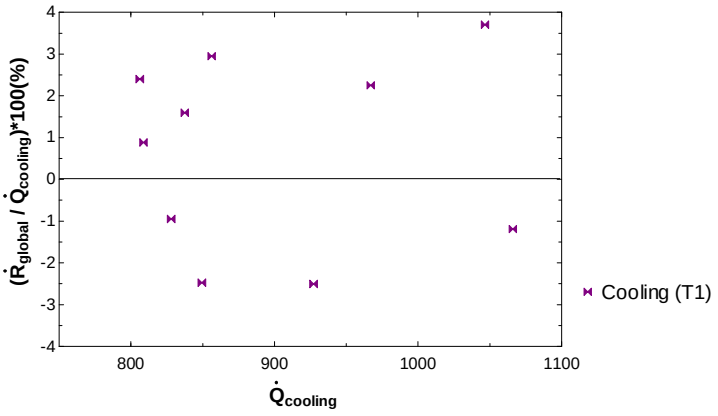

Figure 2.13: Thermal balance residual

Cooling capacity results

Main tests are carried out as a verification of the *A.U* values as a function of $\dot{M}_w$ and $\Delta_{T,Ln}$. The resultant temperature at the center of the chamber and 75 [cm] above the floor is used as reference.

- The water flow rate $\dot{M}_w$ varies from 0.0397 [kg s^{-1}] to 0.103 [kg s^{-1}].
- The log mean temperature difference at the center of the chamber ($\Delta_{T,Ln,center}$) calculated from Eq. (1.35) varies from 7.63 [K] to 9.95 [K].

The experimental cooling ceiling capacity can be calculated from Eq. 2.7.

The experimental *A.U* values at the center of the chamber can be calculated from Eq. 1.34.

The test results are presented in Table 2.5.

Table 2.5: Measurements and *A.U* calculated values

Test	$t_{w\,su}$ [℃]	$t_{w\,ex}$ [℃]	$t_{ref\,center}$ [℃]	$\Delta_{T,Ln}$ [K]	$\dot{M}_W$ [kg s^{-1}]	*A.U* center [W K^{-1}]	*U* center [W $m^{-2}K^{-1}$]	$\dot{Q}_{cooling}$ [W]
T1C1	12.05	15.87	23.9	9.78	0.0656	107.0	9.3	1046.5
T1C2	14.04	17.66	25.1	9.17	0.0638	105.4	9.2	967
T1C3	14.88	17.03	24.5	8.47	0.103	109.5	9.5	927.2
T1C4	14.89	17.26	24.1	7.93	0.0856	107.2	9.3	849.4
T1C5	14.82	18.7	25	8.02	0.0519	106.8	9.3	856.2
T1C6	15.68	19.44	25.6	7.91	0.0532	105.9	9.2	837.5
T1C7	14.03	18.87	26.6	9.95	0.0526	107.1	9.3	1065.1
T1C8	14.66	19.51	25	7.63	0.0397	105.7	9.2	806.2
T1C8	14.64	19.41	25.1	7.79	0.0405	103.8	9.0	808.9
T1C10	14.38	19.4	25	7.84	0.0394	105.6	9.2	828.1

In the experimental test domain considered, it is observed that the influence of the selected parameters ($\dot{M}_w$, $\Delta_{T,Ln}$) on *A.U* is negligible. An $A.U_{center}$ average value of 106.4 [W K^{-1}] is observed (Table 2.5). However, this value is significantly affected by the choice of the indoor reference temperature as, shown in Table 2.6. The *A.U* value is reduced when choosing a reference temperature nearer to the frontage. This decrease reaches 10 % when using as reference the globe temperature at 0.5 m from the frontage.

Table 2.6: *A.U* calculated values using reference temperatures at 1 m and 0.5 m from the facade

Test	$t_{ref\ center}$ [℃]	$t_{ref\ 1m}$ [℃]	$t_{ref\ 0.5\ m}$ [℃]	$\dot{M}_w$ [kg s^{-1}]	$A.U_{center}$ [W K^{-1}]	$A.U_{1m}$ [W K^{-1}]	$A.U_{0.5\ m}$ [W K^{-1}]
T1C1	23.9	24.65	24.77	0.0656	107.0	99.28	98.15
T1C2	25.1	25.97	26.1	0.0638	105.4	96.59	95.34
T1C3	24.5	25.32	24.77	0.103	109.5	99.45	105.7
T1C4	24.1	24.93	25.25	0.0856	107.2	96.5	93.1
T1C5	25	26.04	26.35	0.0519	106.8	94	90.86
T1C6	25.6	26.62	26.85	0.0532	105.9	93.81	91.42
T1C7	26.6	27.28	27.28	0.0526	107.1	94.69	100.1
T1C8	25	25.91	26.21	0.0397	105.7	93.76	90.52
T1C8	25.1	25.88	26.46	0.0405	103.8	93.66	87.63
T1C10	25	25.85	26.49	0.0394	105.6	94.96	88.31

The test results for the additional tests are presented in Table 2.7, in order to evaluate the influences of the ventilation system and different thermal load distributions. The resultant and air temperatures are measured in this case at the center of the chamber.

Table 2.7: Additional tests results

Test	$A.U_{Center}$ [W/K]	$\Delta_{T,Ln}$ [℃]	$\Delta T_{a\ vent}$ [K]	$\dot{M}_w$ [kg s^{-1}]	Thermal loads distribution	Cooling ceiling ON	Without Facade	Fan-Coil ON.
2705a	104.46	9.32	7.3	0.0612	Left	X		
0506a	104.59	7.48	8.84	0.0526	Without	X		
0606a	106.78	4.35	5.40	0.0507	Without	X	X	
0606b	110.84	8.45	2.28	0.0521	Facade	X		
1206a	106.84	7.47	10.72	0.0398	Without	X		X
1206b2	119.46	7.32	9.98	0.0403	Facade	X		X
1206b3	115.99	7.49	Without	0.0398	Facade	X		X
1206b4	-	-	Without	0	Facade	-		X
1205b5	-	-	Without	0	Facade	-		X
1206c1	101.5	7.66	Without	0.0375	Facade	X		
1206c2	105.57	7.84	4.89	0.0394	Facade	X		
1306b	103.25	7.55	11.73	0.0396	Uniform	X	X	

For the test 1206b3 and 1206b2, an increase of 13.6 % and 10.4 % of *A.U* value with respect to the main test is observed at the same test conditions. This is due to the air movement inside the chamber, induced by the fan-coil. For the test 1206a, the fan-coil is also active, but in this case the thermal loads are off. This explains the reduction of *A.U* value.

For the test 0606b, the air is injected into the chamber with a temperature close to the room air temperature, which produces an average increase of the cooling capacity of 4.4 %. Finally, if the ventilation system is off (test 1206c1) for the same test conditions of the main tests, an average reduction of the cooling ceiling capacity of 5.6 % is observed. For the other variations the differences are not significant.

The heat transfer coefficient in the facade $h_{int,fac}$ obtained for ten main tests (with the cooling ceiling active, Table 2.8) is compared to the one obtained in the tests carried out with the fan-coil (Table 2.7 test 1206b4 and 1206b5). In case of the main tests, the average heat transfer coefficient is of the order of 7.1 [W m^{-2} K^{-1}]. When using a fan coil $h_{int,fac}$ is reduced to an average value of 6.6 [W m^{-2} K^{-1}], reducing the heat transfer by 7 %.

Table 2.8: Facade internal heat transfer coefficient

Test	$\dot{q}_{fac}$ [W m^{-2}]	$t_{ave,s,fac}$ [℃]	$t_{a,ave,fac}$ [℃]	$t_{ref,center}$ [℃]	$h_{in,fac}$ [W m^{-2} K^{-1}]
T1C1	-32.2	28.3	30	23.9	7.32
T1C2	-33.9	29.7	31.5	25.14	7.43
T1C3	-53.7	32.3	34.3	24.47	6.86
T1C4	-54.6	31.9	34.2	24.06	6.96
T1C5	-56.9	32.8	35.4	24.97	7.27
T1C6	-51.2	32.7	35.1	25.62	7.23
T1C7	-47.4	33.1	35.3	26.6	7.29
T1C8	-52.7	32.3	34.7	24.97	7.19
T1C8	-55	32.7	35.2	25.06	7.20
T1C10	-55.8	32.8	35.3	25	7.15

Pressure drop results

Results of pressure drop measurements are shown in Figure 2.14. Pressure drops can be calculated as a function of the water flow rate from Eq. 2.13 for Reynolds number varying from 2178 to 5763 and friction factor varying from 0.036 to 0.048 (commercial copper or plastic pipe with effective roughness 1.5 µm (ASHRAE, 2009)):

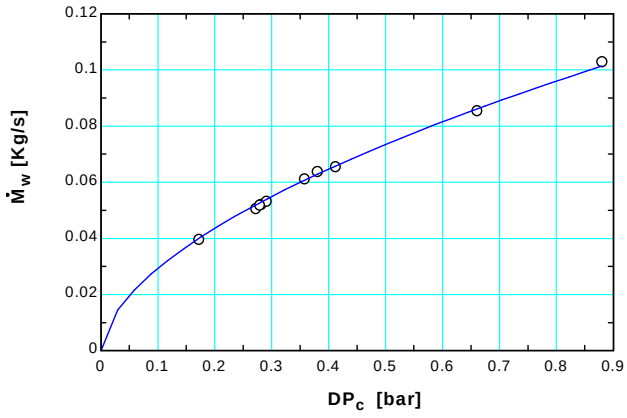

Figure 2.14: Measurement results of Pressure drop.

$$\dot{M}_W = 0{,}10905 * DP_C^{\,0{,}57} \quad [\text{kg s}^{-1}] \qquad (2.13)$$

For a nominal water flow rate of 0.0648 [kg s^{-1}], the pressure drop calculated using experimental equation 2.13 is 0,40 [bar].

It appears that with this type of cooling ceiling, the water flow rate influence on the cooling capacity is small. Even if the mass flow rate is reduced by 50 %, the *A.U* values in Table 2.5 remain almost the same. However, the pumping energy consumption is not negligible. It also appears that the system COP could be significantly improved by choosing correctly the water mass flow rate.

Comfort conditions results

Measurements of air velocity at the occupation zone are shown in Figures 2.15 and 2.16 in [cm s^{-1}].

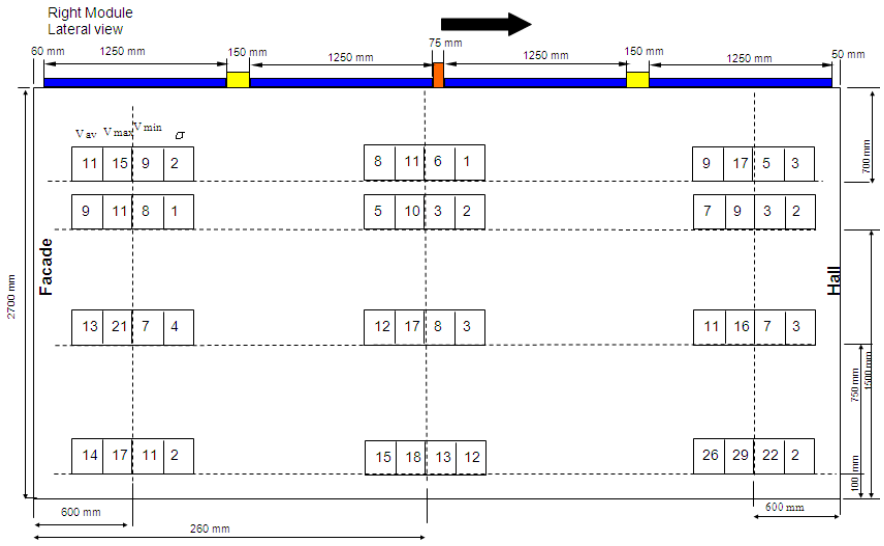

Figure 2.15: Right module-Lateral view of the air velocity distribution and measuring results

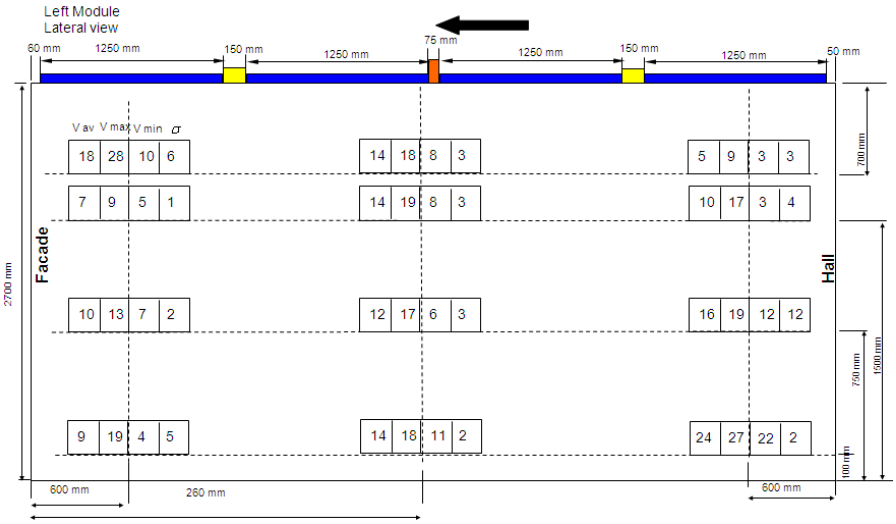

Figure 2.16: Left module-Lateral view of the air velocity distribution and measuring results.

It is observed that, except from the back side of the chamber, close to the floor, where an air velocity of around 25 [cm s^{-1}] was measured (Coanda effect), the air velocity inside the occupancy zone is always lower than 20 [cm s^{-1}]. This value fulfills the recommended levels of thermal comfort (ASHRAE, 2009; Behne, 1996; Kulpmann, 1993) in order to reduce the draft risk in spaces (undesired local cooling of the human body caused by the air movement).

Thermography results

The results of thermographic measurements are shown in Figures 2.17 and 2.18. A rather homogeneous temperature distribution of the cooling ceiling panels is observed.

An average temperature of 31.7 [℃] and 24 [℃] can be observed for facade and back wall respectively (Figures 2.17).

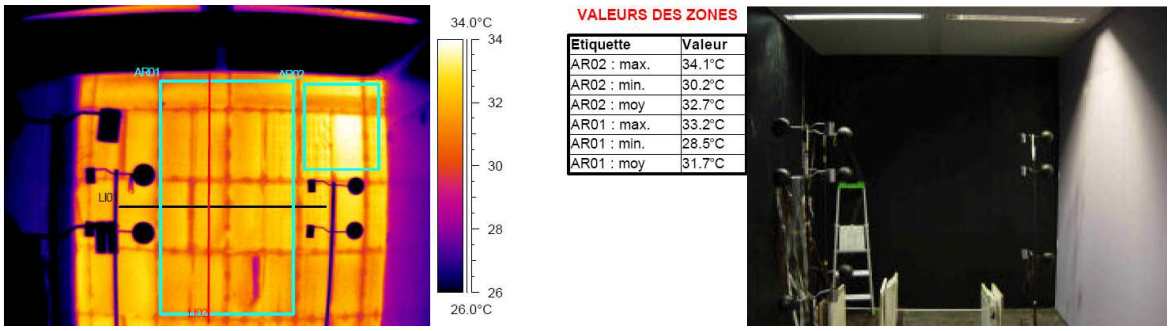

a)

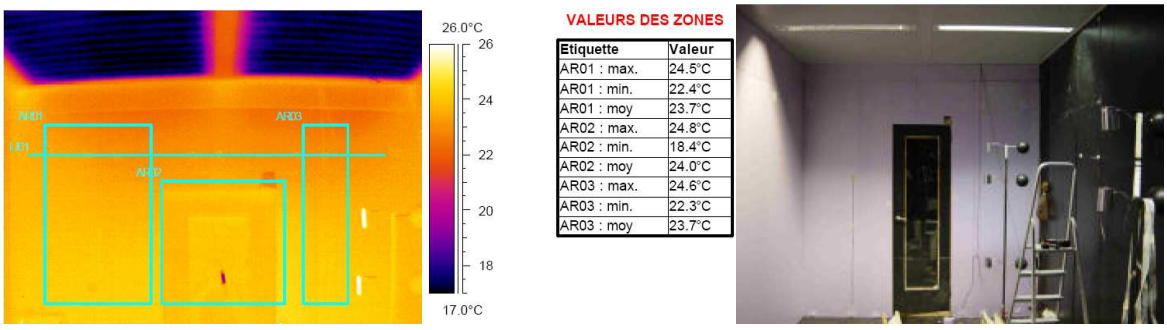

b)

Figure 2.17: Thermography of the facade a) and back wall b)

The surface temperature of the panels close to the facade is around 19.5 [℃], while the panels close to the back wall have a surface temperature around 16.8 [℃]. The average temperature of the cooling ceiling is 17.8 [℃] (only the active area of the c ooling ceiling is considered) (Figure 2:18).

Thermography results show that the heat sources distribution has a strong influence on the surface temperature of the cooling ceiling. However the radiant temperature asymmetry defined according to ASHRAE, (2009) remains within the allowed values for thermal comfort requirements.

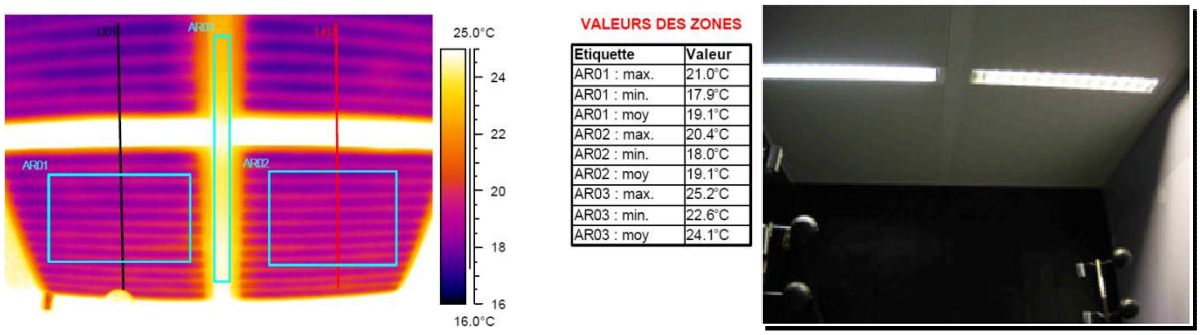

a)

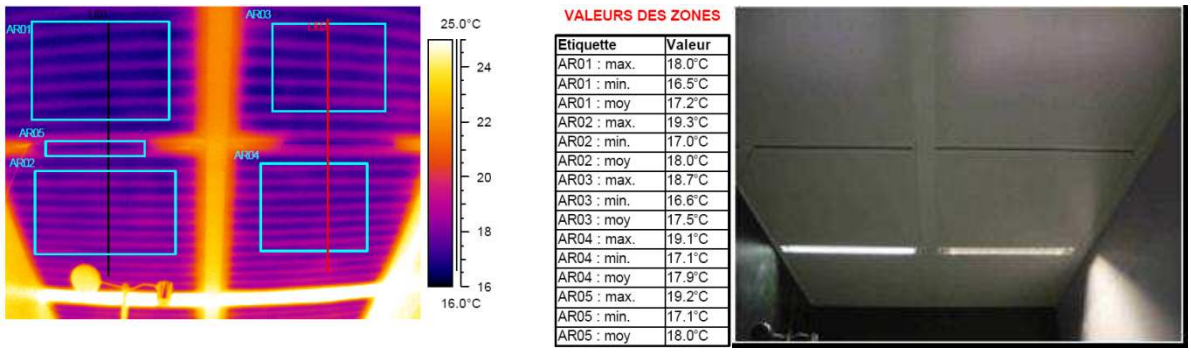

b)

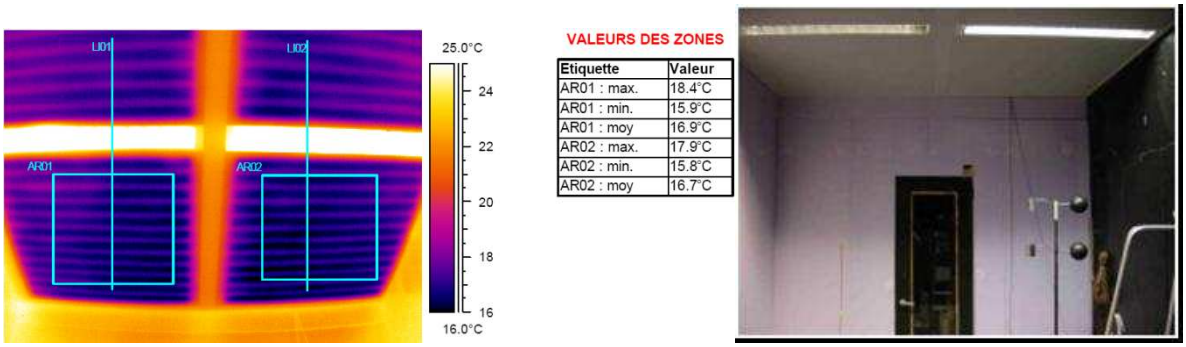

c)

Figure 2.18: Thermography of the ceiling panels close to facade (a), center (b) and back wall (c).

2.3.2 Test bench type 2

2.3.2.1 General description

This test bench is used for the experimental analysis of the radiant ceiling types **T2, T3** and **TG**, (see Table 1.1), in **cooling or heating** mode. Forty six tests were performed to observe the influences of ventilation system, thermal load type (convective, convective+radiative, with or without thermal load) and active ceiling position on the comfort conditions and on the radiant ceiling capacity.

The climatic chamber used during the tests was built in such a way to reproduce as accurately as possible the structure and characteristics of a large commercial building located in Brussels according to the experiment work developed by Bourdouxhe *et al.,* 1998.

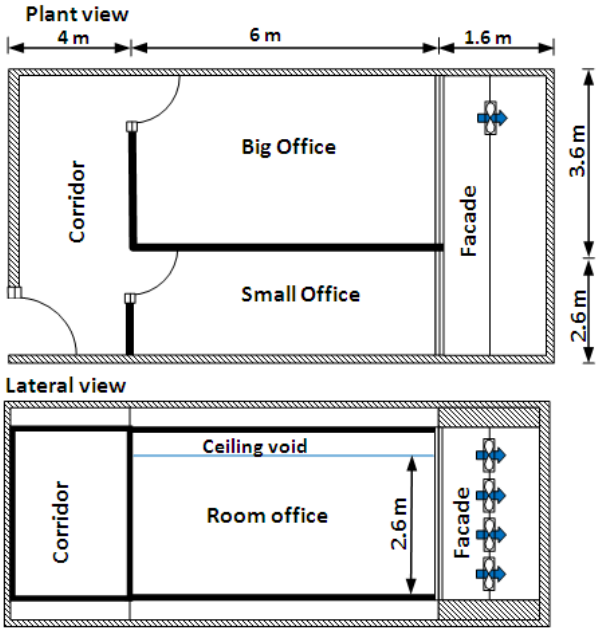

Figure 2.19: Climatic chamber: plan and lateral views

Figure 2.20: Climatic chamber: external and internal views

The climatic chamber (See Figure 2.19 and 2.20) is a wood structure, strongly insulated, 11.6 [m] long, 6 [m] wide and 3.5 [m] high. It is divided into two principal zones by a facade: the first “external” zone simulates the exterior climate and the second “internal” zone contains the equipment to be tested and the hydraulic and ventilation systems used during the test.

As shown in Figure 2.19, the “external zone” is divided into two parts by a mobile partition wall. Four axial fans, placed on the height of this partition wall are used to create an air circulation all along the facade. Correct placement of the mobile partition helps to obtain the required air speed along the facade and the partition wall (4 [m s^{-1}] heating mode and 1 [m s^{-1}] for cooling mode).

In order to carry out the test with as much realism as possible, the “internal” zone containing the testing equipment is itself subdivided into two zones with the dimensions of two type offices of the real building (big and small offices). The usable height in the offices is 2.6 [m].

The facade structure is the same as in the real building. It is composed of a double glazing window and an insulated wall. The windows frame is made of aluminum with warm-edge spacer. The heat transfer coefficient of the window without the frame is 2.6 [W m^{-2} K^{-1}] and it has a surface of 8.5 [m^2] for the big office and 5.7 [m^2] for the small office.

According to the test to be performed, the facade space is set at a temperature that can vary between -10 [℃] and 30 [℃].

The high recirculation flow rate allows for the reduction of the temperature variation along the air space to less than 1 [K] in both cooling and heating modes.

The maximum heat exchange at the facade occurs in heating mode.

The facade *A.U* coefficients for the small and big offices are 11.8 [W K^{-1}] and 17.5 [W K^{-1}] respectively (facade: window and external wall) (Bourdouxhe *et al.,* 1998).

As can be seen in Figure 2.19, the main access to the offices is from the corridor. The latter is also thermally controlled (humidity and temperature). The two offices and the corridor are covered by a metal false floor and a fitted carpet. The false floor is in the shape of metal paving 4 [cm] thick placed on metal supports to allow for an air space of 6 [cm] between the metal paving and the chamber external wood floor. The vertical walls of the offices are metallic, 6 [cm] thick and filled with mineral wool. These partitions are attached between the false floor and the false ceiling.

The false ceiling of the offices is composed of “active” radiant panels installed by modules. Each module is composed of three rows of two panels. The big office is equipped with three modules and

the small office with two modules. The dimensions of these panels and modules depend on each radiant ceiling type. Modules are separated by a 'C' profile suspension grid (inactive structure) where the ventilation boxes (two by module) and fluorescent lightings (two by module) are installed.

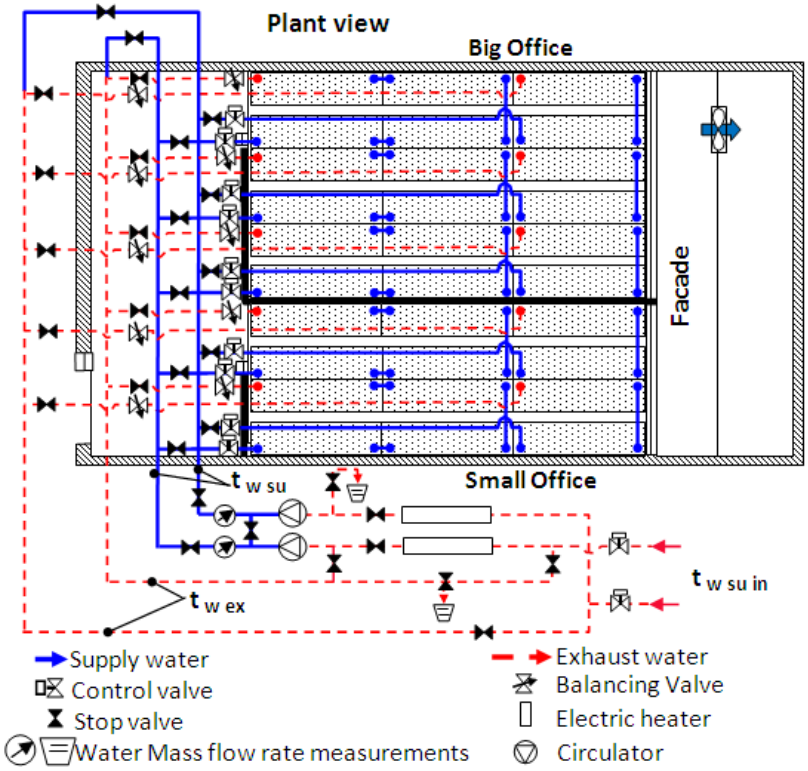

Figure 2.21: Hydraulic circuits

Figure 2.21 shows the hydraulic diagram of the active panels. Each panel module is supplied by two parallel water circuits. The first circuit in each module supplies hot or cold water to the two active panels connected in series and situated at the facade level. The second circuit supplies only cold water the other two panel rows of each module. These panels are inactive in heating mode.

As it can be seen in Figure 2.21, each pipe leaving toward a module is equipped with a stop valve and a control valve. Each return of a module is equipped with a balancing valve and a stop valve. The circuit also includes a by-pass valve, circulators, electric resistances and water mass flow rate meters. The entire circuit is thermally insulated.

Due to the thermal insulation of the water supply circuit (located in the corridor), the power released by the circulators and by the electric resistances is almost entirely injected in the water (the thermal loss of the supply water circuit is around 0.5 % of the total power of the system). The electric power supply is measured by electronic watt-meters. The total mass flow rate in the circuit is measured by time integration and also by water counters.

In heating mode, the supply and exhaust valves of the cold circuits are closed. Once the three hot circuits close to the facade are balanced, the mass flow rate is adjusted by a main balancing valve. The electrical power supplied by the resistances is adjusted in order to maintain the air set point temperature in the office.

In cooling mode, the six circuits of the modules are open and balanced. The electric resistances are not used and the cold supply and exhaust water valves are adjusted in order to reach the desired supply water temperature toward the panels of the active cooling ceiling (to avoid condensation risk).

The ventilation system is shown in Figure 2.22. The supplied air is injected into the office through a circular diffusers (Figure 2.23) placed close to the facade (105 [$m^3 h^{-1}$] for the big office and 70 [$m^3 h^{-1}$] for the small office). The return air is extracted from the office bottom and then treated by an Air-Handing Unit (AHU) to be re-injected into the conditioned space.

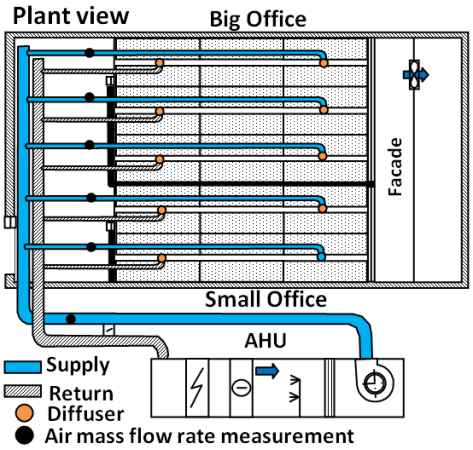

Figure 2.22: Ventilation system

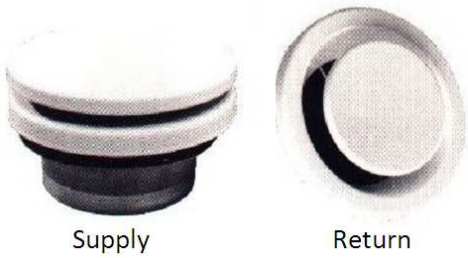

Figure 2.23: Supply and return Diffusers

The supply air mass flow rates in the ducts are measured with the help of a thermo-anemometer probe. This probe is installed at the supply duct of each module (80 mm diameter) in the ceiling void of the corridor (range 0 to 5 [m s^{-1}]). For a volumetric flow rate of 35 [$m^3 h^{-1}$], the air velocity is 1.9 [m s^{-1}],

the Reynolds number is then 10000 and the measurement precision is ±0.05 [m s^{-1}]. The internal thermal loads are injected into the offices by electric convectors or heating carpets adjusted in order to maintain a set point temperature of 25 [℃] in cool ing mode or 22 [℃] in heating mode.

Measurements

Internal surface temperatures (facade, mobile wall into the facade, room internal walls, floor, room side active ceiling and active ceiling surface toward the ceiling void) are measured at 5 points distributed symmetrically on each surface. Air temperatures of the corridor, facade, chambers and ceiling void are also measured in 5 points in each space. Air temperature and globe temperatures are measured using two columns placed inside the chamber at the positions shown in Figure 2.24 and measurements are vertically placed at 10 [cm], 75 [cm], 150 [cm] and 200 [cm] above the floor.

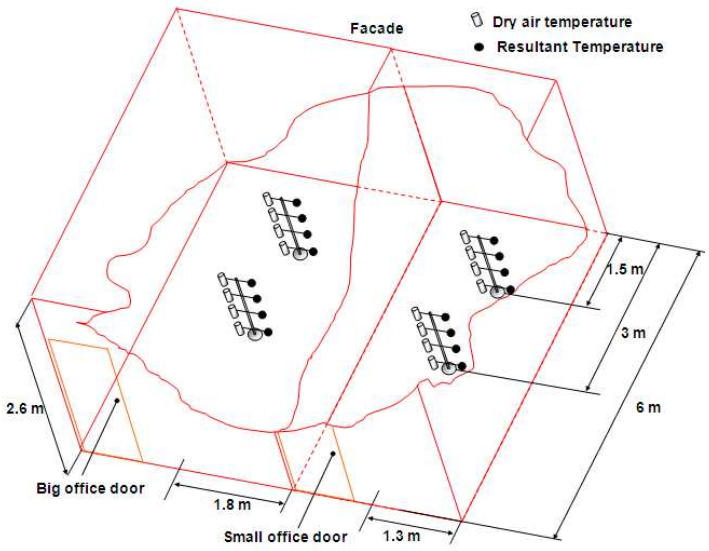

Figure 2.24: Air and globe temperatures measurements.

The reference temperature is taken at the chamber center, at 75 [cm] above the floor, with globe temperature sensor. A maximal vertical variation of air temperature of 1.5 [K] is observed in heating mode. In cooling mode the variation is around 0.5 [K].

Six watt-meters equip the climatic chamber and enable measuring the electric power consumed by all the electric circuits in the chamber.

The stability of the temperature in the chamber is relatively good for all the tests. The maximal variation of the resultant temperatures during the tests period (after stabilization: 1.5 [h]) is lower than 0.1 [K h^{-1}]. The average relative humidity during the test is 53 %.

2.3.2.2 Experimental results

Thermal balances

a. Radiant ceiling balance

Because of the weak water temperature difference across the supply conduits, due to the extend heat exchange surface, a balance based on water mass flow rate and temperatures is too imprecise. Therefore, the supply and exhaust conduits "losses" or "gains" to the ceiling void must be estimated. The total thermal power of the radiant ceiling includes the exchange with the ceiling void.

The thermal balance of the radiant ceiling is given therefore by the following equation in both heating and cooling modes:

$$\dot{Q}_{heating/cooling} = \dot{Q}_{su} + \dot{Q}_{con} \quad [W] \qquad (2.14)$$

Where:

$\dot{Q}_{heating/cooling}$ is the total thermal power of the radiant ceiling, [W]

$\dot{Q}_{su}$ is the total thermal power supplied to the radiant ceiling, [W]

$\dot{Q}_{con}$ is the conduits thermal loss (supply and return circuits) in the ceiling void, [W]

And for heating mode:

$$\dot{Q}_{su} = \dot{Q}_{ER} + \dot{Q}_{cir} - \dot{Q}_{cor} \quad [W] \qquad (2.15)$$

Where:

$\dot{Q}_{ER}$ is the power dissipated by the electric resistance immersed into the water supply circuit, [W].

$\dot{Q}_{cir}$ is the electric power consumed by the circulators, [W].

$\dot{Q}_{cor}$ is the thermal loss of the conduits in the corridor, [W].

The thermal test stability is such that the transients are negligible (drift lower than 0.1[K h^{-1}]).

The total thermal power supplied to the system calculated from Eq. 2.14 is accurate to be used as reference.

Still in heating mode, a check can be made by calculating, with less accuracy, $\dot{Q}_{su}$ by means of a water energy balance:

$$\dot{Q}_{su} = \dot{M}_w . c_w . \left(t_{w,su} - t_{w,ex}\right) \quad [W] \qquad (2.16)$$

The water mass flow rate $\dot{M}_w$ is determined by counters placed inside the circuits (see Figure 2.21).

In cooling mode, the electric resistance is not used. The cooling power is obtained by injection of cold water into the circuit.

In cooling mode the power supplied by the system can be calculated as:

$$\dot{Q}_{su} = \dot{M}_{w,in} . c_w . \left(t_{w,ex} - t_{w,su,in}\right) - \dot{Q}_{cir} + \dot{Q}_{cor} \quad [W] \qquad (2.17)$$

Where:

$\dot{M}_{w,in}$ is the water mass flow rate injected into the circuit and measured by weight time integration, [kg s^{-1}] (see Figure 2.21).

$t_{w,su,in}$ is the temperature of the cold water injected into the circuit, [℃].

In this case, Eq. 2.16 can be also used to verify the estimation of the power supplied by the system.

For the systems tested in climatic chamber 2, supply conduits, thermal losses or gains into the ceiling void vary between 10 % and 20 % of the radiant ceiling power. The heat flow of the radiant ceiling upward to the ceiling void varies between 5 % and 10 % of the radiant ceiling power. This is not negligible, however in a real building this energy is not considered as lost. Contrary it is also used for heating or cooling of the adjacent rooms but its effect is perceived after some time delay, related to the thermal inertia of the ceiling slab (see Figure 2.25).

b. Room thermal balance

Figure 2.25 shows the control volume and the different terms used to establish the room global balance.

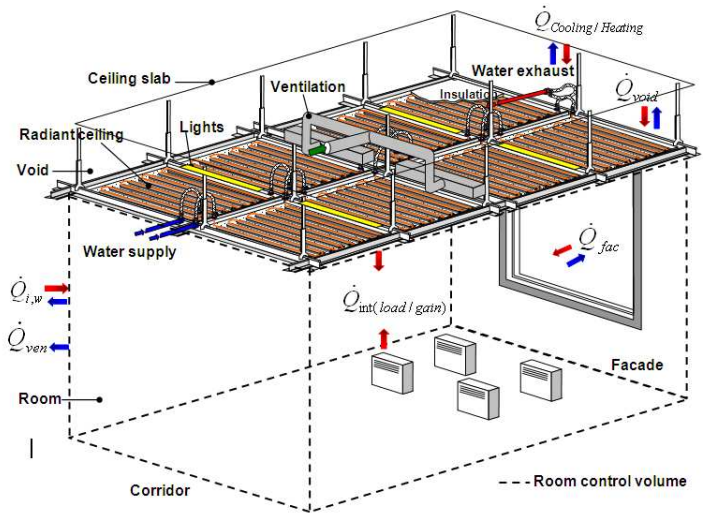

Figure 2.25: Control volume for the room global balance

The thermal balance of the air contained in this control volume (limited by internal walls, facade and radiant ceiling) is given by the following equation (in both heating and cooling modes):

$$\dot{Q}_{heating/cooling} + \dot{Q}_{void} + \dot{Q}_{\text{int},gains} + \dot{Q}_{i,w} + \dot{Q}_{fac} + \dot{Q}_{ven} + \dot{U} = \dot{R}_{global} \quad [W] \qquad (2.18)$$

The thermal gains (from lighting and electric convectors) are measured by watt-meters.

The heat flow rates are evaluated by using the method already discussed in the section 2.3.1.

Test results

a. Copper radiant ceiling type 2 (T2)

The tests are performed in the small office of the climatic chamber 2. These results allow to determine the radiant ceiling emissions in heating (H) and cooling modes (C) respectively (Figure 2.26), with and without ventilation, with and without internal thermal loads and with different types of thermal loads (Table 2.9).

Table 2.9: T2: Tests description

Test	T2H1	T2H2	T2C1	T2C2	T2C3
ventilation	ON	OFF	ON	OFF	ON
Heating	X	X	-	-	-
Cooling	-	-	X	X	X
Effective area m^2	6.5	6.5	19.4	19.4	19.4
Without thermal load	X	X	-	-	-
Convective thermal loads	-	-	X	X	-
Convective and radiative thermal loads	-	-	-	-	X

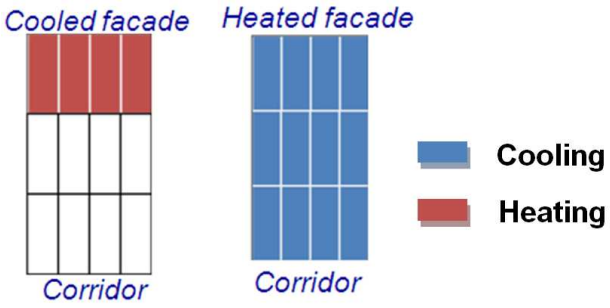

Figure 2.26: T2: Active radiant ceiling panels in heating and cooling mode

The estimated values of all terms of the thermal balance are shown in Table 2.10.

From experimental results, it is observed that, in heating mode, an average of 84 % of the total room heat losses are compensated by the radiant ceiling system.

In cooling mode an average of 74 % of room heat gains are compensated by the cooling ceiling and 14 % by the ventilation system.

Table 2.10: T2: Thermal balance results

Test		T2H1	T2H2	T2C1	T2C1	T2C1
$\dot{Q}_{cooling}$	[W]	-	-	1484	1502	1368
$\dot{Q}_{heating}$	[W]	806	670	-	-	-
$\dot{Q}_{ven}$	[W]	156	-	289	-	269
$\dot{Q}_{\mathrm{int},loads\,/\,gains}$	[W]	46	42.4	1748	1570	1716
$\dot{Q}_{fac}$	[W]	750	797	290	237	216
$\dot{U}$	[W]	-9.8	-5.2	-7.2	6.3	4.5
$\dot{Q}_{void}$	[W]	32.5	26	54.3	30.5	50.2
$\dot{Q}_{i,w}$	[W]	90.4	108.6	-317	-315	-312.6
$\dot{R}_{global}$	[W]	-5.9	-7.2	-4.9	26.8	37.1

The residuals of the thermal balance are shown in Figure 2.27. On average, they are in the order of ±3 % of the tested radiant ceiling capacity.

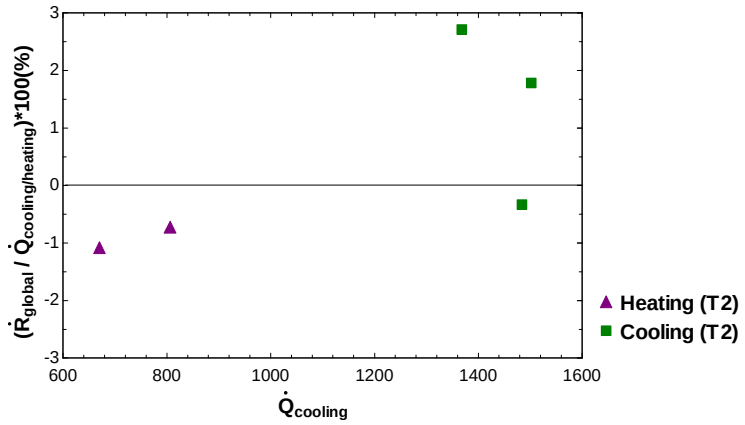

Figure 2.27: T2: Thermal balance residuals

The global heat transfer coefficient of the radiant ceiling is based on the total cooling or heating power of the active ceiling and therefore includes the power dissipated toward the ceiling void. As well in cooling as in heating mode its value is affected by four parameters: water mass flow rate and temperatures, thermal load distribution into the room and ventilation system.

The test results are presented in Table 2.11.

Table 2.11: T2: Measurements and *A.U* calculated values

Test	ventilation	Thermal loads	$t_{w\,su}$ [°C]	$t_{w\,ex}$ [°C]	$t_{ref\,center}$ [°C]	$\Delta_{T,Ln}$ [K]	$\dot{M}_w$ [kg s^{-1}]	*A.U* center [W K^{-1}]	*U* center [W m^{-2} K^{-1}]	$\dot{Q}_{cooling}$ [W]	$\dot{Q}_{heating}$ [W]
T2H1	ON	Without	35.91	32.6	21.88	11.78	0.06798	68.4	10.5	-	806
T2H2	OFF	Without	36.92	34.27	21.65	14.27	0.06798	46.92	7.2	-	670
T2C1	ON	Convective	16.34	18.31	25.65	8.18	0.1998	181.4	9.3	1484	-
T2C2	OFF	Convective	16.32	18.28	26.21	8.86	0.1998	169.4	8.7	1502	-
T2C3	ON	Conv+Rad	15.47	17.29	24.21	7.71	0.1998	177.3	9.1	1368	-

In the experimental domain considered, it is observed that in heating mode, the influence of the ventilation system on *A.U* values is considerable. The ventilation plays a beneficial role in the thermal performance of the radiant ceiling system.

The increase of the ceiling emission is due to the Coanda effect: the air supplied in the office “sticks” to the ceiling and produces an increase of thermal exchange of about 30 % in heating mode.

In cooling mode the apparent enhancement is of the order of 6 %. However this result must be taken with a certain caution because it falls within the measurement uncertainty.

b. Copper radiant ceiling type 3 (T3)

The experimental tests are performed in the small office of the climatic chamber 2. These results allow to determine the radiant ceiling emissions in heating and cooling modes. In heating mode, ten tests also allow to evaluate the influences of the water log mean temperature difference, outside air temperature difference (room-facade zone), internal temperature difference (room-upper zone) and ventilation system, according to the tests listed in Table 2.12.

In cooling mode, eight tests are performed to analyze the influences of effective ceiling area and its position inside the room (close to the facade (FC) or to the corridor (CR)) (Figure 2.28), the type or internal thermal loads (convective (Conv) or radiative (Rad)) and ventilation effect, according to the test listed in Table 2.13.

Table 2.12: **T3**: Test description in heating mode

Test	T3H1	T3H2	T3H3	T3H4	T3H5	T3H6	T3H7	T3H8	T3H9	T3H10
ventilation	ON	ON	ON	ON	OFF	OFF	ON	ON	ON	ON
$\Delta_{T,Ln}$ **[K]**	22.8	24.2	22.6	23.7	25	24.6	23.5	24.1	16.1	15.1
$\Delta_{t,out}$ **[K]**	19.9	31.1	30.6	22.8	27.8	12.4	9.9	31.4	30.5	31.6
$\Delta_{t,\mathrm{int}}$ **[K]**	0	0.5	-1.2	0.1	0.6	4.2	4.5	7.3	8.9	4.4
Ceiling position	FC	FC	FC	FC	FC	FC	FC	FC	FC	FC
Effective area [m^2]	3.7	3.7	3.7	3.7	3.7	3.7	3.7	3.7	3.7	3.7

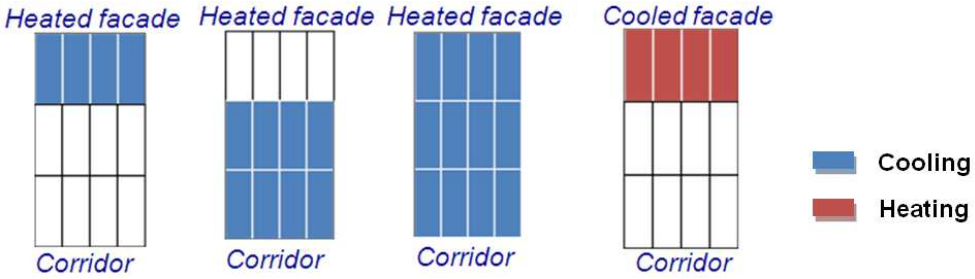

Figure 2.28: T3: Active radiant ceiling panels in heating and cooling mode

Table 2.13: **T3**: Test description in cooling mode.

Test	T3C1	T3C2	T3C3	T3C4	T3C5	T3C6	T3C7	T3C8
ventilation	ON	ON	ON	OFF	ON	ON	ON	ON
Effective area [m^2]	11.2	11.2	11.2	11.2	11.2	7.4	3.7	3.7
Ceiling position	-	-	-	-	-	CR	FC	FC
Thermal load: Conv	-	-	-	X	-	-	-	-
Thermal loads: Conv +Rand	X	X	X	-	X	X	X	X

The estimated values of all terms of the thermal balance are shown in Tables 2.14 and 2.15. It is observed that, in heating mode, an average of 95 % of the room heat losses are compensated by the radiant ceiling system.

In cooling mode, an average of 78 % of room heat gains are compensated by the cooling ceiling system and 22 % by the ventilation system.

Table 2.14: **T3**: Thermal balance results for heating mode.

Test	T3H1	T3H2	T3H3	T3H4	T3H5	T3H6	T3H7	T3H8	T3H9	T3H10
$\dot{Q}_{heating}$ [W]	911	991	946	957	702	702	1018	1004	624	585
$\dot{Q}_{ven}$ [W]	173.9	145.7	145.7	152.72	-	-	171.5	162.1	124.5	145.7
$\dot{Q}_{\mathrm{int},gains}$ [W]	15	15	15	15	15	15	15	15	15	15
$\dot{Q}_{fac}$ [W]	234	365.7	359.8	338.7	326.9	143.5	139.9	369.3	358.7	371.6
$\dot{U}$ [W]	-8.3	5.2	-7.8	-6.5	6.4	-10.2	12.1	9.2	-4.1	-3.2
$\dot{Q}_{void}$ [W]	74	76.96	79.9	79.9	74	68	71	62.2	23.7	32.6
$\dot{Q}_{i,w}$ [W]	-458.2	-461.2	-337.3	-418.8	-303.5	-511.6	-622.4	-475.6	-117.6	-53.9
$\dot{R}_{global}$ [W]	-22.4	-38.4	30.4	-24.6	19	-16.4	40.2	-41	10.4	-7

Table 2.15: **T3**: Thermal balance results for cooling mode.

Test	T3C1	T3C2	T3C3	T3C4	T3C5	T3C6	T3C7	T3C8
$\dot{Q}_{cooling}$ [W]	704	739	765	872	955	540	309	312
$\dot{Q}_{ven}$ [W]	91.6	101	117.48	-	-30.5	148	150.4	148
$\dot{Q}_{\mathrm{int},loads}$ [W]	200	200	200	200	200	200	200	200
$\dot{Q}_{fac}$ [W]	41.2	78.8	74	85.8	87	89.4	88.2	84.7
$\dot{U}$ [W]	5.2	6.7	-6.1	-4.9	-5.4	2.5	3.4	2.8
$\dot{Q}_{void}$ [W]	74	77	79.9	79.9	74	68.1	74	62.2
$\dot{Q}_{i,w}$ [W]	461.7	489.4	555	488.9	551.8	339.3	108.5	124.8
$\dot{R}_{global}$ [W]	-13.6	11.8	20.4	-22.2	-17	11.2	11.8	14.4

According to Figure 2.29, the residuals correspond to an average of ±4.5 % of the tested radiant ceiling capacity**.**

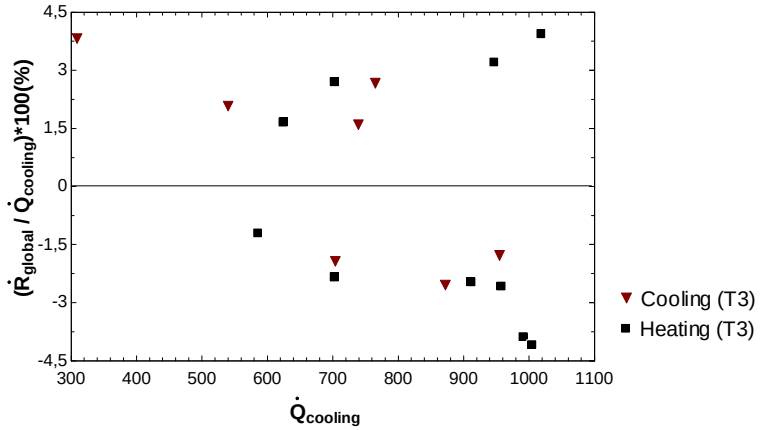

Figure 2.29: **T3**: Thermal balance residuals

The test results are presented in Table 2.16 and 2.17.

Table 2.16: **T3**: Measurements and *A.U* calculated values: heating mode

Test	ventilation	Thermal loads	$t_{w\,su}$ [℃]	$t_{w\,ex}$ [℃]	$t_{ref\,center}$ [℃]	$\Delta_{T,Ln}$ [K]	$\dot{M}_w$ [kg s^{-1}]	*A.U* center [W K^{-1}]	*U* center [W m^{-2}K^{-1}]	$\dot{Q}_{heating}$ [W]
T3H1	ON	Without	49	42.8	23	22.9	0,035	39.8	10.7	911
T3H2	ON	Without	49	42.7	21.5	24.2	0,0375	40.9	11.1	991
T3H3	ON	Without	49.1	43	23.3	22.5	0,0369	42	11.3	946
T3H4	ON	Without	49	42.8	22.1	23.6	0,0369	40.5	10.9	957
T3H5	OFF	Without	49.1	44.4	21.7	25	0,03555	28.1	7.6	702
T3H6	OFF	Without	49.1	44.5	22.1	24.6	0,03639	28.5	7.7	702
T3H7	ON	Without	49	43	22.4	23.6	0,0405	43.1	11.6	1018
T3H8	ON	Without	49	42.8	21.7	24.1	0,03861	41.6	11.2	1004
T3H9	ON	Without	39.3	35.2	21	16.1	0,03638	38.7	10.4	624
T3H10	ON	Without	39.3	35.4	22.2	15.1	0,03583	38.7	10.7	585

Table 2.17: Measurements and *A.U* calculated values: cooling mode

Test	ventilation	Thermal loads	Effective area m^2	$t_{w\,su}$ [℃]	$t_{w\,ex}$ [℃]	$t_{ref\,center}$ [℃]	$\Delta_{T,Ln}$ [K]	$\dot{M}_w$ [kg s^{-1}]	*A.U* center W K^{-1}]	U center [W m^{-2} K^{-1}].	$\dot{Q}_{cooling}$ [W]
T3C1	ON	Conv+Rad	11.2	15.1	17.7	23.1	6.6	0.06567	106.7	9.5	704
T3C2	ON	Conv+Rad	11.2	15.2	17.8	23.5	6.9	0.06639	106.9	9.5	739
T3C3	ON	Conv+Rad	11.2	15.1	17.9	23.5	6.9	0.06664	110.8	9.9	765
T3C4	OFF	Conv	11.2	15.0	18.3	25.2	8.4	0.06369	103.6	9.2	872
T3C5	ON	Conv+Rad	11.2	15.0	18.5	25.6	8.7	0.0644	110	9.8	955
T3C6	ON	Conv+Rad	7.4	15.2	18.4	25	8.0	0.04053	67	9.0	540
T3C7	ON	Conv+Rad	3.7	15.4	18.7	24.4	7.2	0.02233	42.8	11.6	309
T3C8	ON	Conv+Rad	3.7	15.4	18.7	24.3	7.1	0.02236	43.9	11.9	312

As with the radiant ceiling types **T1** and **T2**, the ventilation plays a beneficial role in the thermal performance of the radiant ceiling: the heat transfer increases are of about 32 and 5 % in heating and cooling modes, respectively.

In general, the global heat transfer coefficient of the radiant ceiling system in heating mode is 10 % higher than in cooling mode, when the ventilation system is active. This is due to a higher temperature difference between the room air and the ceiling surface in heating mode.

In cooling mode there is a reduction of 8 % of the heat transfer coefficient when the active panels are placed close to the corridor (Test T3C6 in Table 2.17), due to the “contact interruption” between the radiant ceiling and the facade (Figure 2.28). For the same reason, if the active ceiling is placed close to the facade there is an increase of the heat transfer coefficient of 20 % due to the higher air velocity and the temperature gradient in this zone (Tests T3C7 and T3C8 in Table 2.17).

c. Capillary tube mats: type “G” (TG)

The tests performed in the big office of the climatic chamber 2, allow to determine the radiant ceiling emissions in heating and cooling modes, with and without ventilation and without thermal loads except for the lightings, (Table 2.18).

Table 2.18: **TG**: Test description

Test	TGH1	TGH2	TGH3	TGH4	TGH5	TGH6	TGH7	TGH8	TGC1	TGC2	TGC3
Ventilation	ON	ON	ON	ON	OFF	OFF	OFF	OFF	ON	ON	ON
Heating	X	X	X	X	X	X	X	X	-	-	-
Cooling	-	-	-	-	-	-	-	-	X	X	X
Without thermal load	X	X	X	X	X	X	X	X	-	-	-
Thermal loads Con +Rand	-	-	-	-	-	-	-	-	X	X	X
Effective area [m^2]	6.5	6.5	6.5	6.5	6.5	6.5	6.5	6.5	19.4	19.4	19.4

The estimated values of all terms of the thermal balance are shown in Table 2.19.

In heating mode, an average of 95 % of the room heat losses are compensated by the radiant panels.

In cooling mode, an average of 6 7 % of the room heat gains are compensated by the cooling ceiling system and 19 % by the ventilation system.

Table 2.19: **TG**: Thermal balance results

Test		TGH1	TGH2	TGH3	TGH4	TGH5	TGH6	TGH7	TGH8	TGC1	TGC2	TGC3
$\dot{Q}_{cooling}$	[W]	-	-	-	-	-	-	-	-	1102	1404	758
$\dot{Q}_{heating}$	[W]	874	1106	881	618	1058	846	861	567	-	-	-
$\dot{Q}_{ven}$	[W]	173	162	162	132	-	-	-	-	304	281	278
$\dot{Q}_{\text{int},gains/loads}$	[W]	15	15	15	15	15	15	15	15	1592	1941	1045
$\dot{Q}_{fac}$	[W]	498.7	745.6	751.6	317.3	770.2	559	573.5	419.7	63.4	3.1	174.1
$\dot{U}$	[W]	-7.2	-4.4	-9.8	-6.3	5.5	-3.2	4.2	7.1	-6.2	4.9	-9.2
$\dot{Q}_{void}$	[W]	81.2	96.5	80.3	55.9	124.3	112.7	104	76.4	9.3	7.7	8.9
$\dot{Q}_{i,w}$	[W]	-150.3	-135.7	-129.9	-101.6	-149.7	-218.6	-182.7	-76.8	-239.2	-288	-200.2
$\dot{R}_{global}$	[W]	-21.4	-23.2	-22.2	-19.9	34.3	-32.5	20	16.2	-13.3	-16.3	-17.4

According to Figure 2.30, the residuals correspond to an average of ±4 % of the tested radiant ceiling capacity.

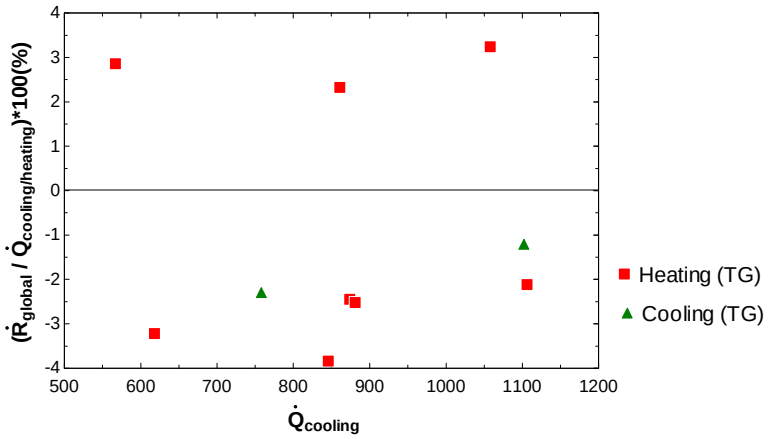

Figure 2.30: **TG**: Thermal balance residuals

The test results are presented in Table 2.20.

Table 2.20: **TG**: Measurements and *A.U* calculated values

Test	ventilation	Thermal loads	$t_{w\,su}$ [°C]	$t_{w\,ex}$ [°C]	$t_{ref\,center}$ [°C]	$\Delta_{T,Ln}$ [K]	$\dot{M}_w$ [kg s^{-1}]	$A.U_{center}$ [W K^{-1}]	U_{center} [W m^{-2}K^{-1}]	$\dot{Q}_{cooling}$ [W]	$\dot{Q}_{heating}$ [W]
TGH1	ON	Without	42.8	39.9	21.8	19,8	0.09	44.8	6.9	-	874
TGH2	ON	Without	47.1	43.3	21.3	24,2	0.086	46.5	7.1	-	1106
TGH3	ON	Without	43.1	40	21.8	19,9	0.085	44.7	6.9	-	881
TGH4	ON	Without	35.5	33.4	20.3	13,9	0.085	43.8	6.7	-	618
TGH5	OFF	Without	48.3	45	21.4	25,6	0.0925	41.81	6.4	-	1058
TGH6	OFF	Without	44.1	41.4	21.5	21,45	0.0925	39.9	6.1	-	846
TGH7	OFF	Without	44.4	41.4	20.8	22,29	0.0836	38.95	6.0	-	861
TGH8	OFF	Without	37.0	35.1	21.4	14,88	0.0903	38.57	5.9	-	567
TGC1	ON	Conv+Rad	15.2	17.7	25.9	9,472	0.117	118.5	6.1	1102	-
TGC2	ON	Conv+Rad	13.2	16.5	26.2	11,42	0.116	125.4	6.5	1404	-
TGC3	ON	Conv+Rad	17.3	19	24.5	6,394	0.117	120	6.2	758	-

For capillary tube mats as for copper tubes ceiling, ventilation plays a beneficial role.

In heating mode, the air supply permits an increase of about 11 % of the thermal exchange.

If the ventilation system is active, the global heat transfer coefficient is 9 % higher in heating than in cooling mode.

In similar test conditions, one observes a reduction of global heat transfer coefficient when passing from the capillary mats to the copper ceiling systems (**T1, T2** and **T3**).

The reductions are of the order of 23 % and 15 % with and without ventilation, respectively.

This is due to the increase of the thermal contact resistance for capillary tubes mats considering the additional air layer between the tubes and the ceiling metal panel.

2.3.3 Test bench type standard DIN 4715-1

2.3.3.1 General description

This test bench is used for the experimental analysis according to the standard test conditions of the German norm DIN 4715-1, (1993) for the radiant ceiling types (DIN U, DIN S and DIN G see Table 1.2) from test reports of HLK laboratory of Stuttgart University, (1995, 2002 and 2003), in cooling mode. Nine tests are performed to compare the performance of the different types of cooling ceiling configurations.

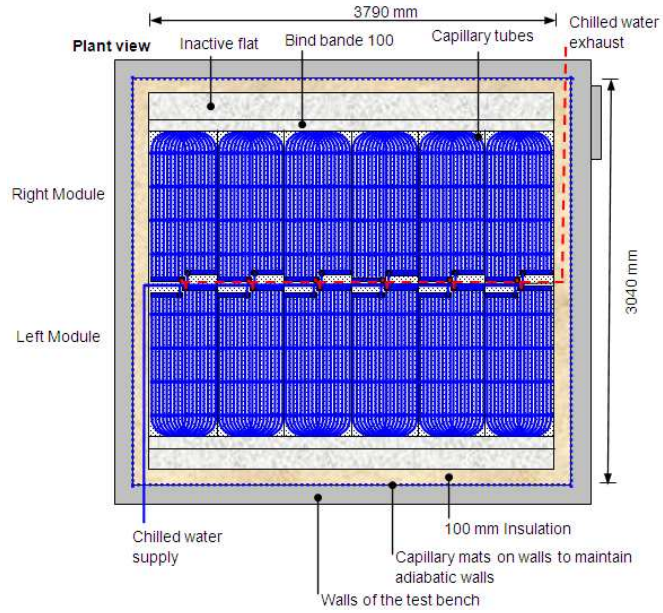

Figure 2.31: Plant view of test chamber according to DIN 4715-1

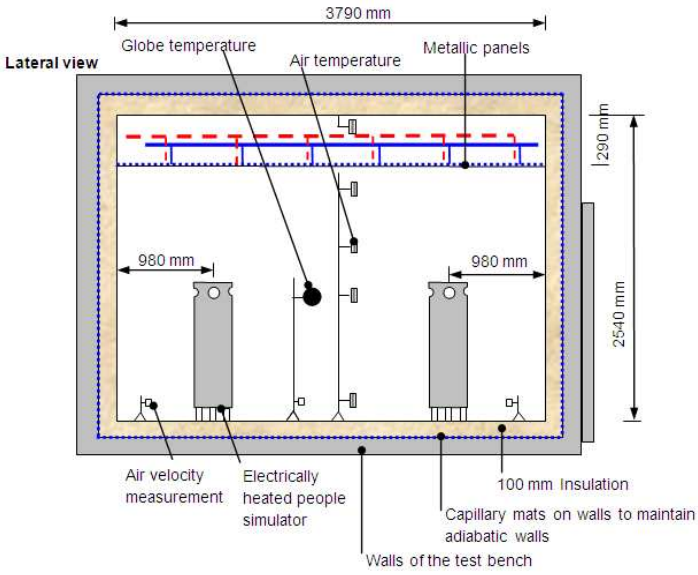

Figure 2.32: Lateral view of test chamber according to DIN 4715-1

The climatic chamber used in this case is strongly insulated, 2.54 m high, 3.79 m wide and 3.79 m long. The cooling ceiling is placed at 2.25 m above the floor level, the ceiling surface is 14.36 m^2 (Figure 2.31 and 2.32). The active cooling ceiling surface is 10.14 m^2 (70.6 % of ceiling surface). Hydronic system is performed by panels connection following Tichelmann loop principle (Figure 2.31).

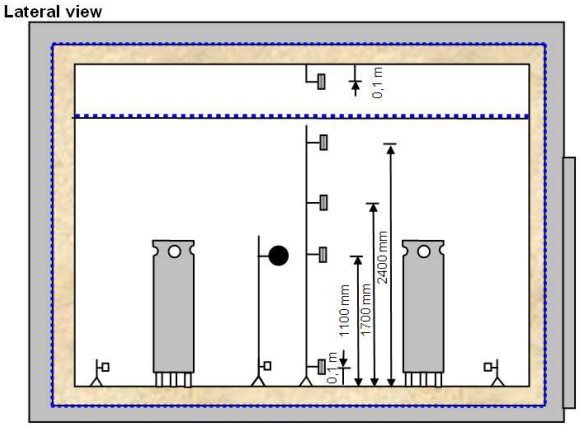

Figure 2.33: Air velocity and globe temperatures measurements positions.

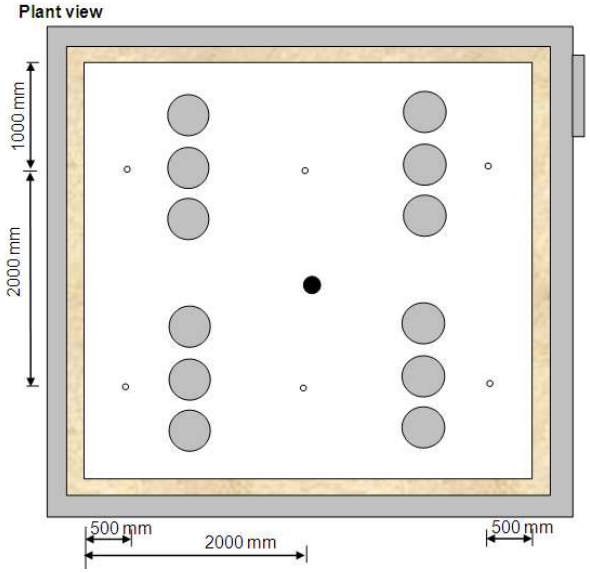

Figure 2.34: Positions of air velocity and temperature measurements and thermal loads distribution

Figure 2.31 shows the water circuit scheme. The cooling ceiling consists of 2 modules (left and right), each one formed by 6 radiant ceiling panels, all of them connected in parallel. The thermal occupancy load is generated by electrically heated people simulators. In this case, the tests are performed without ventilation and without facade effect. The resultant (globe) temperature is always taken at the center of the chamber at 1.1 m above the floor. Air and globe temperatures are measured inside the room at the position shown in Figure 2.33 and Figure 2.34. Figure 2.34 shows the six positions of air velocity measurements for comfort test.

2.3.3.2 Experimental results

The main test results for cooling ceiling mats configurations tested are presented in Table 2.21. The cooling power is measured with ±3 % accuracy. Water temperature difference and globe temperature were measured with PT100 sensors with a deviation lower than ±0.02 K and ±0.04 K respectively. The mass flow rate is measured with a magnetic inductive volumetric flow meter with uncertainty of ± 0.5 % of the measured value.

Table 2.21: Main results of cooling ceiling mats tested.

Variable		**"U" mats** On top of a steel plate.			**"S" mats** Embedded in plaster			**"G" mats** On top of gypsum plaster board		
Test N°		**1**	**2**	**3**	**1**	**2**	**3**	**1**	**2**	**3**
$\dot{M}_w$	[kg h^{-1}]	379.3	379.1	380.6	393.1	392.11	391.51	289.54	290.73	284.53
$t_{a\ res}$ **(Globe 1.1m)**	[℃]	26.34	26.03	26.75	25.79	25.79	25.79	26.06	26.07	26.54
$t_{w\ su}$	[℃]	19.47	16.01	13.74	17.02	14.68	12.07	18.67	16.06	13.22
$t_{w\ ex}$	[℃]	20.67	17.82	16.14	18.68	16.80	14.78	19.96	17.85	15.72
$\dot{q}_{exp}$	[W m^{-2}]	52.2	78.8	105.0	62.2	79.6	101.9	42.7	59.3	81.4
$A.U_{center}$	[W K^{-1}].	84.4	87.7	90.2	95.8	96.8	108.8	64.8	66.7	68.5
U_{center}	[W m^{-2} K^{-1}]	8.3	8.6	8.9	7.8	7.9	8.2	6.3	6.5	6.7
$t_{w\ void\ average}$	[℃]	26.5	26.4	26.4	**19.91**	**18.45**	**16.61**	25.8	26.2	26.8
$t_{f\ room\ average}$	[℃]	26.7	26.6	26.6	25.7	25.6	25.6	26.1	26.5	27.1
$t_{av\ w\ room\ West}$	[℃]	26.6	26.5	26.6	25.7	25.8	25.7	26.1	26.5	27.1
$t_{av\ w\ room\ North}$	[℃]	26.8	26.8	26.8	25.7	25.8	25.7	25.9	26.3	26.9
$t_{av\ w\ room\ South}$	[℃]	26.7	26.6	26.6	25.9	25.8	25.8	25.9	26.3	26.9
$t_{av\ w\ room\ Est}$	[℃]	26.5	26.4	26.4	25.8	25.7	25.8	25.8	26.2	26.8

According to DIN 4715-1 the tests were also performed with the half of the water mass flow rate.

It is observed that for the considered conditions, the influence of the water mass flow rate on $\dot{q}$ value is negligible. For "S" mats configuration embedded in plaster (without upward insulation) the results show that the system is submitted to some heat gain from the ceiling cavity ($t_{w\ void\ average}$ in Table 2.21). Therefore, a thermal (and acoustical) insulation is recommended to reduce cooling of the floor above.

If the two capillary mats configurations on top of a ceiling surface are compared, the results show that the cooling capacity of the system is reduced by 24 % when the gypsum plaster board is used as a radiant surface.

Comfort conditions

Air velocity measurement results for the cooling mats configurations tested are shown in [m s^{-1}] in Figures 2.35. The measured air velocity inside the chamber is always lower than 0.18 [m s^{-1}]. Lower values were measured for **"G"** mats on top of the gypsum plasterboards with a maximal value of 0.06 [m s^{-1}], which corresponds to the lower cooling ceiling capacities.

Figure 2.35: Air velocity measurement results for **"U" "S"** and **"G"** mats.

These values fulfill the recommended levels of thermal comfort according to ASHRAE, (2009). Since, the tests were performed without ventilation, they are only an indicative of the buoyancy natural convective air movement inside the chamber.

Thermography

Thermographic results for **"U"** mats configuration are shown in Figure 2.36. A maximal water temperature difference of 1K between supply and exhaust condition is observed in each panel.

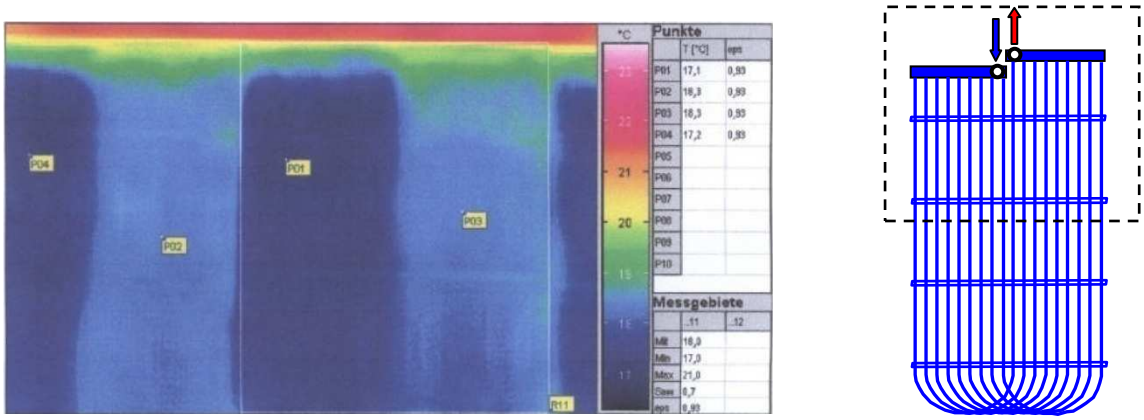

a) Half of the ceiling panels on the connection side (supply and exhaust capillary tube mats)

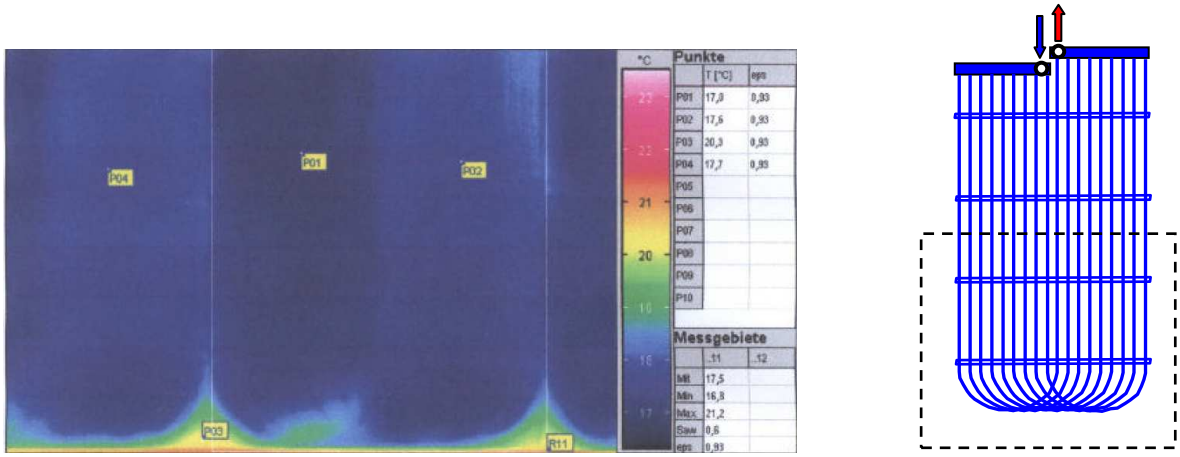

b) Half of the ceiling panels on the return side

Figure 2.36: Thermography of the ceiling panels for capillary **"U"** mats configuration

2.4 CONCLUSIONS OF THE EXPERIMENTAL ANALYSIS

For the radiant ceiling system tested, the water mass flow rate has a small influence on the radiant ceiling capacity, but the corresponding pressure drop deserves to be carefully identified.

The test results also show that the influences of heat sources distribution and surfaces temperatures inside the room are considerable.

The resultant temperature varies significantly close to the facade, therefore the cooling or heating ceiling capacity evaluated at the center of the room could be insufficient to assure the comfort of the occupants.

The applicability of a certain heat sources concentration, which is closely related to the actual conditions, must be taken into account and the radiant ceiling must therefore be evaluated together with its designed environment and not as a separate HVAC equipment.

In the experimental domain considered, it is observed that, in heating mode, the influence of ventilation system on *A.U* values is significant. An increase of the thermal exchange with the active panels, of about 30 % in heating mode is observed. In cooling mode the enhancement is apparently in the order of 6 %, however this result must be taken with a certain caution, because it can be due to the measurement uncertainty.

For the test conditions presented in this study and when the ventilation system is activated, the global heat transfer coefficient of the radiant ceiling system in heating mode is always 10 % higher than in cooling mode.

It is also observed that, a “contact interruption” between the radiant ceiling and the facade (an inactive ceiling zone for example) can produce a reduction of 8 % of the cooling capacity.

Due to the increase of the thermal contact resistance for capillary tubes mats (considering the air layer between the tubes and the ceiling metal panel) for similar test conditions, the global heat transfer coefficient on the ceiling surface is lower than the radiant ceiling systems with copper tubes (**T1, T2** and **T3**). Therefore, for the test performed (in heating or cooling mode) and average reduction of 23 % and 15 % is observed, with and without ventilation respectively.

From the standard tests (used to compare different systems) it is observed that the cooling capacity of the system with capillary tubes mats on top of the gypsum plaster board is reduced by 24 % with respect to the traditional metal plate as radiant surface.

3. Static modeling of the radiant ceiling systems

3.1 INTRODUCTION

A few currently available computer models of radiant ceiling systems were developed specially as design tools for radiant cooling systems and usually as stand-alone programs to evaluate their performance. In general, these models cannot be used to determine the global behavior of radiant ceiling systems (cooling and heating) in any conditions other than specific design conditions and without considering, for example, the effect of fenestration and ventilation systems or ceiling perforation.

The model developed by Kilkis *et al*., (1995) proposes a design procedure for radiant cooling systems that assumes steady-state conditions where the radiant and convective heat exchange is simplified as in most of the cases considered in the related literature (ASHRAE System and Equipment, 2004; Jeong and Mumma, 2004; Udagawa, 1998).

This chapter presents the results of a theoretic-experimental study performed to develop a computational model of radiant ceiling systems. The model considers the radiant ceiling as a fin. Only the dry regime is considered. From ceiling and room dimensions, cooling ceiling material description and room surface temperature measurements, supply water and air mass flow rates and temperatures, the model calculates the cooling ceiling capacity, average ceiling surface temperature, water exhaust temperature and room resultant temperature as a comfort parameter.

Fin efficiency, mixed convection close to the cooling ceiling (generated by the ventilation system) and panel perforations influence are studied. The theoretical approach gives to the user an appropriate tool for preliminary calculation, design and diagnosis in commissioning processes where the main objective is to support a Functional Performance Test of the system in order to verify the main radiant ceiling performance of the system in cooling or heating mode. A series of experimental results obtained on seven types of cooling ceilings are used in order to validate the model.

3.2 COPPER TUBE RADIANT CEILING MODELING

The main geometric characteristics of this configuration are summarized in Table 1.1. An individual element for the modeling can be chosen, as shown in Figure 3.1 for the copper tube ceiling **T1** in cooling mode.

Considering the symmetry between tubes, the applicable boundary conditions are:

- No heat flow in the fin representing the ceiling at midway between the tubes
- Ceiling fin base temperature ($t_{RC,0}$) corresponding to the fin temperature immediately below the tube.

On the axial orientation, a nominal tube length inside the panel of L_{tp} has to be chosen (Figures 3.1).

The following basic assumptions are used in the simulation model:

- Uniform air temperature and humidity inside the room
- Steady-state, one-dimension heat transfer
- Mechanical ventilation in the space above the ceiling
- Transition or turbulent flow inside the tubes (design condition).

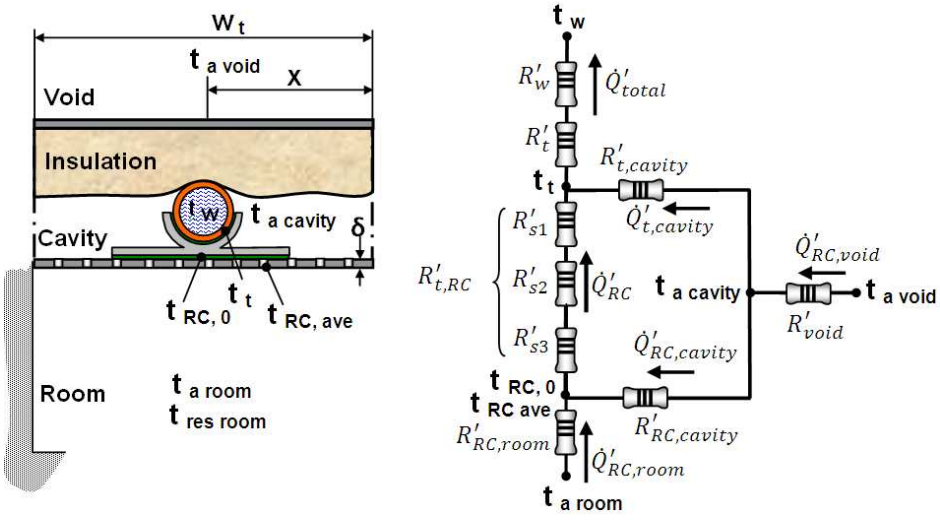

Figure 3.1: Individual copper tube cooling ceiling element and its equivalent thermal circuit

3.2.1 Model description

The cooling ceiling can be characterized by its inputs, outputs and parameters: Figure 3.2 and Table 3.1.

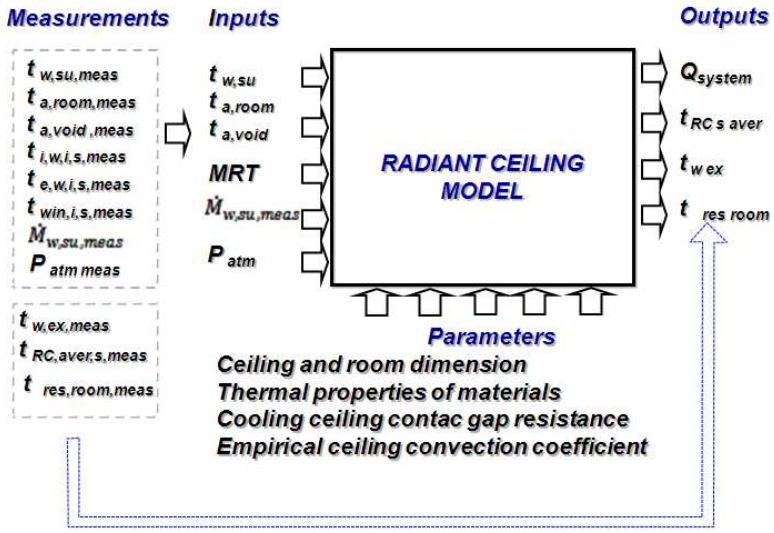

Figure 3.2: Definition of the model inputs outputs and parameters

The performance test for commissioning process (see Annex 1) consist of measuring the variables defined as model inputs (including the verification measurements, see Figure 3.2) and calculates and compares the radiant ceiling capacity, ceiling surface average temperature, water exhaust temperature and resultant temperature. The experimental data provided by the manufacturer can also be used in order to identify the model parameters (first parameter identification).

a. Heat flow definitions

According to Figure 3.1, in cooling mode, the total water enthalpy flow rate per unit of length corresponds to the addition of the total thermal energy extracted by the radiant ceiling panel ($\dot{Q}'_{RC}$) with the heat gain through the tube external surface from the ceiling cavity ($\dot{Q}'_{t,cavity}$):

$$\dot{Q}'_{total} = \dot{Q}'_{RC} + \dot{Q}'_{t,cavity} \qquad [W\ m^{-1}] \qquad (3.1)$$

with

$$\dot{Q}'_{total} = \frac{t_{w,ave} - t_t}{R'_w + R'_t} \quad [\text{W m}^{-1}] \quad (3.2)$$

Table 3.1: Model inputs, outputs and parameters description

Outputs		$t_{RC\ ave}$: Average radiant ceiling temperature, [℃].
		$\dot{Q}_{system}$: Total heat power of the radiant ceiling system, [W].
		$t_{w\ ex}$: Exhaust water temperature, [℃].
		$t_{res,room}$: Resultant temperature, [℃].
Inputs		$t_{w,\ su}$: Supply water temperature, [℃].
		$\dot{M}_w$: Water mass flow rate, [kg s^{-1}].
		$t_{i,w,i,s}$: Surface temperature of room walls and window, [℃].
		$t_{a,\ room}$: Room air temperature, [℃].
		$t_{a,\ void}$: Void air temperature, [℃].
		P_{atm} : Atmospheric pressure, [Pa].
Parameters	**Radiant ceiling and Room geometry**	$L_{p,}\ L_{room}$: Panel and room length, [m].
		W_p, W_{room} : Panel and room width, [m].
		H_{room} : Room height, [m].
		N_p : Number of panel's blocks connected in parallel [-].
		N_s : Number of panels connected in series [-].
		D_i : Tube internal diameter, [m].
		D_e : Tube external diameter, [m].
		w_t : Tube separation, [m].
		ρ : Panel porosity factor [%].
		δ_{RC} : Ceiling plate thickness, [m].
		δ_{ins} : Insulation thickness, [m].
	Contac gap resistance	δ_{s1} : Thickness gap of tube- interconnection profile, [m].
	Thermal properties of materials	k_{RC} : Ceiling panel thermal conductivity, [W m^{-1} K^{-1}]
		k_t : Tube thermal conductivity, [W m^{-1} K^{-1}]
		k_{ins} : Insulation thermal conductivity, [W m^{-1} K^{-1}]
		k_{s1} : Gap thermal conductivity, [W m^{-1} K^{-1}]
		k_{s2} : Interconnection profile thermal conductivity, [W m^{-1} K^{-1}]
	Convection coefficients	$h_{RC,room}$, $h_{RC,cavity}$: Empirical ceiling convection coefficients from diffuser air velocity and characteristic length (u_∞, $L_{RC,FC}$).

Definition of the radiant ceiling parameters such as geometry and ventilation indicated in Table 3.1 allows for the use of manufacturer technical information on radiant ceiling systems and diffusers. On the other hand the choice of the resultant temperature as a comfort indicator enables a relatively easy verification of this parameter in the room.

Considering constant tube surface temperature, the water average temperature is estimated from the log mean temperature difference for each block of panels connected in series by:

$$\frac{t_t - t_{w;ave}}{t_t - t_{w;su}} = \exp\left[\frac{\frac{-\pi}{D_i} \cdot h_w \cdot \frac{L_t}{2}}{\frac{\dot{M}_w}{N_p} \cdot c_{p;w}}\right] \quad [℃] \qquad (3.3)$$

The total heat flow extracted by the radiant ceiling panel ($\dot{Q}'_{RC}$) corresponds to the sum of the heat flows (convection + radiation) coming from the ceiling cavity ($\dot{Q}'_{RC,cavity}$) and from the room ($\dot{Q}'_{RC,room}$) according to:

$$\dot{Q}'_{RC} = \dot{Q}'_{RC,room} + \dot{Q}'_{RC,cavity} \quad [W\ m^{-1}] \qquad (3.4)$$

The radiant ceiling average temperature is one of the outputs of the model. It can be calculated with reference to the fin effectiveness according to Eq. 3.5 (Figure 3.3).

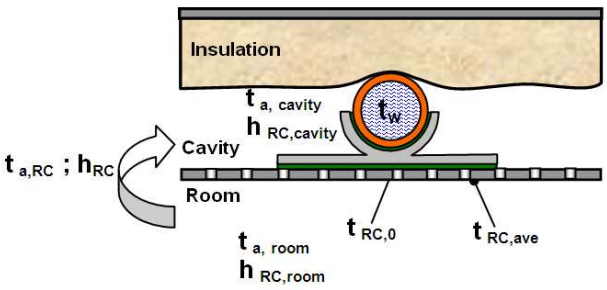

Figure 3.3: Heat transfer definition on an individual ceiling element considered as a fin

$$t_{RC,ave} = t_{a,RC} - \varepsilon_{fin} \cdot (t_{a,RC} - t_{RC,0}) \quad [℃] \qquad (3.5)$$

The radiant ceiling heat transfer coefficient h_{RC} as a fin can be defined as follows:

$$h_{RC} = h_{RC,room} + h_{RC,cavity} \quad [\text{W m}^{-2}\text{ K}^{-1}] \quad (3.6)$$

The air temperature close to the radiant ceiling surface ($t_{a,RC}$) is defined as a weighted average of $t_{a,cavity}$ and $t_{a,room}$. The weighting factors are the heat transfer coefficients:

$$t_{a,RC} = \frac{h_{RC,room}.t_{a,room} + h_{RC,cavity}.t_{a,cavity}}{h_{RC,room} + h_{RC,cavity}} \quad [\text{°C}] \quad (3.7)$$

Total heat transfer capacity of a radiant surface to the room and cavity are determined by two heat transfer mechanisms: convection and radiation:

$$h_{RC,room} = h_{RC,room,conv} + h_{RC,room,rad} \quad [\text{W m}^{-2}\text{ K}^{-1}] \quad (3.8)$$

$$h_{RC,cavity} = h_{RC,cavity,conv} + h_{RC,cavity,rad} \quad [\text{W m}^{-2}\text{ K}^{-1}] \quad (3.9)$$

The radiant ceiling heat transfer coefficient of the ceiling to the room and cavity are defined using the methodology described in section 1.5.3. The simplified method for radiant heat exchange can be used to calculate the heat transfer coefficient between the radiant ceiling and the cavity. Only natural convection is considered between the cavity surfaces and the air into the cavity.

The air velocity on the cooling ceiling surface (u_{∞}) and characteristic length in forced convection ($L_{RC,FC}$) (distance of the jet detachment) are considered here as model parameters and defined from diffuser manufacturer's catalogue. The characteristic length of mixed convection ($L_{c,RC}$) is a parameter to be identified on the basis of experiments, considering that there are too many possible configurations of ventilation systems, thermal load types and distributions and possible facade effects to find a correlative method for the entire possible combinations of a real case in a building.

The effectiveness of this equivalent fin can be defined by the methodology discussed in section 1.5.2. In the current technical literature, the perforations effect of the metal panels commonly used as radiant ceiling surface is not considered (ASHRAE, 2004; Kilkis, 1995; Udagawa 1998; Miriel *et al*., 2002; Jeon and Mumma, 2004). In this modeling, a simplified approach is used. It is based on the definition of a fin porosity factor ρ (% percentage of perforated area). The following effects are considered: environmental heat transfer area, heat conduction inside fin and surface temperature.

The fin geometry (see Figure 1.10) can be therefore redefined as:

$$P = 2.\left[\frac{\delta_{RC}}{L_{tp}} + 1\right].(1+\rho) \qquad [-] \qquad \text{(Per unit of length)} \qquad (3.10)$$

$$A_c = \delta_{RC}.(1-\rho) \qquad [m] \qquad \text{(Per unit of length)} \qquad (3.11)$$

$$A_f = P.L_c.(1-\rho) \qquad [m] \qquad \text{(Per unit of length)} \qquad (3.12)$$

where ***P*** is the fin perimeter, $\boldsymbol{A_c}$ is the cross-sectional area of the fin and $\boldsymbol{A_f}$ is the surface area of the fin.

Finally, the heat gain from ceiling void through the insulation (Figure 3.1) can be expressed as a function of the air void temperature (taken as an input in this model) and the void thermal resistance (combination of conduction and convection through the insulation).

b. Thermal resistance definitions

Water to internal tube surface thermal resistance ($R_w^{'}$):

$$R_w^{'} = \frac{1}{A_w.h_w} \qquad [\text{K. m W}^{-1}] \qquad (3.13)$$

The Reynolds number Re calculated from the conditions of the model experimental validation varies between 2168 ~5743 for the copper tubes and 4108~12214 for the capillary tubes which will be considered later. The Gnielinski equation (Eq. 1.3) can be used for forced convection inside tubes in transition or turbulent flow (Celata *et al.*, 2007).

Tube shell thermal resistance ($R_t^{'}$):

$$R_t^{'} = \frac{\ln\left|\frac{D_e}{D_i}\right|}{2.\pi.k_t} \qquad [\text{K. m W}^{-1}] \qquad (3.14)$$

Radiant ceiling thermal contact resistance ($R'_{t,RC}$):

Thermal resistance between tube and ceiling plate for the radiant ceiling **T1** is divided into 3 parts (Figure 3.1): contact resistance between tube external surface and interconnection profile (R'_{s1} bond contact gap 1), conductive resistance through the interconnection profile (R'_{s2}) and contact resistance between interconnection profile and ceiling plate (R'_{s3} bond contact gap 2).

The total resistance is:

$$R'_{t,RC} = R'_{s1} + R'_{s2} + R'_{s3} \qquad [\text{K. m W}^{-1}] \qquad (3.15)$$

with

$$R'_{s1} = \frac{\ln\left|\frac{D_e + 2.\delta_{s1}}{D_e}\right|}{\pi.k_{s1}} \qquad [\text{K. m W}^{-1}] \qquad (3.16)$$

where δ_{s1} is the bond thickness gap; this parameter is experimentally identified.

As the cross section shape and geometry of the interconnection profiles are difficult to evaluate, a fictitious rectangular cross section is defined for the modeling, with base A_{s2} (contact surface) and thickness δ_{s2} (see Figure 3.4):

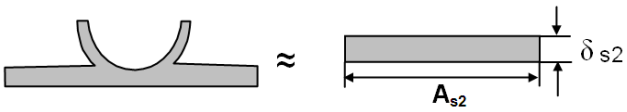

Figure 3.4: Interconnection profile modeling assumption: relation between A_{s2} and the “true” area.

Therefore:

$$R'_{s2} = \frac{\delta_{s2}}{A_{s2}.k_{s2}} \qquad [\text{K. m W}^{-1}] \qquad (3.17)$$

The net effect of these simplifications on R'_{s2} calculation is relatively small, considering the high thermal conductivity of the interconnection profile (usually made of aluminum).

For R'_{s3}, the same methodology is used, but it is assumed that:

$$R'_{s3} = \frac{\delta_{s3}}{A_{s3}.k_{s3}} \quad [\text{K. m W}^{-1}] \quad (3.18)$$

where $\delta_{s3} = \delta_{s1}$ and $A_{s3} = A_{s2}$.

For type **T2** radiant ceiling, R'_{s1} (bond contact gap 1) is replaced by the contact resistance of an air layer considering that the tubes are secured to the interconnection profile by pressure during its manufacturing process. Type **T3** is considered in a similar way to **T2**; but takes into account the thermal resistance of an additional layer of paper between the plate and the profile used as sound insulation (Figure 1.3).

Ceiling plate thermal resistances (R'_{RC}):

$$R'_{RC,cavity} = \frac{1}{h_{RC,cavity}.A_{RC,cavity}} \quad [\text{K. m W}^{-1}] \quad (3.19)$$

$$R'_{RC,room} = \frac{1}{h_{RC,room}.A_{RC,room}} \quad [\text{K. m W}^{-1}] \quad (3.20)$$

$A_{RC,\ cavity}$ and $A_{RC,\ room}$ are the ceiling element surfaces in contact with the air ceiling cavity and room respectively. A similar approach is used to define the thermal resistance of the tube surface inside the ceiling cavity.

For radiant ceiling **T1**, the convective heat transfer coefficient of the copper tube radiant ceiling tested is currently found in the range of 5.9 ~ 6.5 [W m^{-2} K^{-1}] with Ra ≈ $3*10^8$ (see section 1.5.3). If only natural convection is considered and the effect of the perforations is neglected, this coefficient would be underestimated by about 47 %.

In order to analyze the internal radiant exchanges between the room internal surfaces and the radiant ceiling, the detailed method discussed in section 1.5.3 is used. The current order of magnitude found for $h_{RC,room,rad}$ using this methodology is 5.25 [W m^{-2} K^{-1}] for the radiant ceiling **T1**.

The simplified method described in section 1.5.3 is used to calculate the radiative heat transfer coefficient between the ceiling and the cavity and tube surface. A difference of 4 % is found between the results obtained with detailed and simplified methods.

c. Room-resultant temperature

The room-resultant temperature can be calculated according to the methodology described in section 1.5.4. The mean radiant temperature can be calculated in a simplified way from Eq. 1.26 using the resultant and air temperatures measurements. However in this model, it is accurately estimated on the basis of the calculated mean radiant temperature (*MRT* calculated at the same position of the globe sensor position) from Eq. 1.31 and the measurements of air and surfaces room temperatures.

From the experimental results on the radiant ceiling **T1**, it is observed that if the mean radiant temperature is calculated using the simplified method ($t_{mr,room}$ Eq. 1.26), there is no significant difference with respect to the detailed method (Eq.1.31). This result is valid only in the case of measurements of air and resultant temperatures at the center of the chamber (average difference of 0.1 [K]) (see Table 3.2). On the other hand, if the measurements are performed close to the facade (0.5 m) the difference can reach 1.8 [K] (see Table 3.3). The difference is due to the temperature gradient between the facade, ceiling and other surfaces, underestimated by the globe thermometer.

Table 3.2: Simplified ($t_{mr,room}$) and detailed (*MRT*) mean radiant temperature calculation at the center of the room.

$t_{res;room;meas;i}$ [°C]	$t_{a;room;meas;i}$ [°C]	MRT_i [°C]	$t_{mr;room;i}$ [°C]
23,9	23,8	26,33	26,38
25,1	25,1	27,67	27,28
24,5	24,4	26,8	26,69
24,1	24	26,15	26,16
25	24,9	27,09	27,08
25,6	25,5	27,98	27,64
26,6	26,7	28,01	28,84
25	24,9	26,68	27
25,1	25	26,69	27,13
25	25	26,69	26,9

Table 3.3: Simplified ($t_{mr,room}$) and detailed (*MRT*) mean radiant temperature calculation at 0.5m from the facade.

$t_{res;room;meas;i}$ [°C]	$t_{a;room;meas;i}$ [°C]	$MRT_{05m;i}$ [°C]	$t_{mr;room;05m;i}$ [°C]
24,77	24,26	26,35	27,98
26,1	25,49	27,69	29,32
24,77	25,21	26,81	26,26
25,25	24,86	26,18	27,95
26,35	25,81	27,12	29,29
26,85	26,32	28,01	29,72
27,28	27,33	28,03	29,71
26,21	25,86	26,71	28,76
26,46	25,78	26,72	29,53
26,49	25,79	26,72	29,61

d. Global heat transfer characteristics

The global heat transfer characteristics can be calculated according to the methodology described in section 1.5.6. From the panel geometry and the total water enthalpy flow rate per unit of length, the total heat flow transferred to the water is calculated as follows:

$$\dot{Q}_{system} = \dot{Q}'_{total} . L_{tp} . \frac{W_p . N_p . N_s}{w_t} \quad [W] \qquad (3.21)$$

3.2.2 Validation of the copper tube radiant ceiling model

The model has four main parameters: two of them (room and ceiling dimensions and thermal properties of materials) are set with the help of manufacturer datasheets, whereas the two others (contact gap resistance and empirical ceiling coefficients) require some experimentation. It is considered that there are too many possible configurations and combinations of these elements in modern buildings what enables the complete description of the phenomenon with a correlative method.

As an example of the validation process, the model parameters are identified by using separately the tests carried out with the radiant ceiling type **T1**. The *A.U* experimental values (from the resultant temperature $t_{res,room}$ measured at the center of the room) are presented in Table 3.4.

Table 3.4: Experimental and calculated values for copper tube radiant ceiling

AU_i [W/K]	$AU_{exp,i}$ [W/K]	$Error_{AU,i}$ [W/K]	$t_{w,ex,i}$ [°C]	$t_{w,ex,exp,i}$ [°C]	$Error_{t,w,ex,i}$ [°C]	$t_{cc,average,i}$	$t_{a,void}$ [°C]	$t_{res,room}$ [°C]	$t_{a,room}$ [°C]	$t_{w,su}$ [°C]	M_w [kg/s]
107.6	107	-0.5943	15.89	15.87	-0.02071	16.5	22.9	23.9	23.8	12.05	0.0656
106.9	105.4	-1.548	17.69	17.66	-0.02893	18.22	24.17	25.1	25.1	14.04	0.0638
106.3	109.5	3.151	16.98	17.03	0.04758	18.03	23.97	24.5	24.4	14.88	0.103
105.3	107.2	1.892	17.23	17.26	0.02522	18.02	23.38	24.1	24	14.89	0.0856
105.9	106.8	0.9086	18.75	18.7	-0.04656	18.86	24.24	25	24.9	14.82	0.0519
106	105.9	-0.07153	19.44	19.44	0.004503	19.58	25.01	25.6	25.5	15.68	0.0532
107.9	107.1	-0.7934	18.9	18.87	-0.0285	19.14	24.88	26.6	26.7	14.03	0.0526
105.4	105.7	0.3008	19.52	19.51	-0.005421	19.13	23.97	25	24.9	14.66	0.0397
105.4	103.8	-1.641	19.48	19.41	-0.07322	19.13	23.9	25.1	25	14.64	0.0405
105.7	105.6	-0.07846	19.4	19.4	-0.003516	19.02	24.18	25	25	14.38	0.0394

The model parameters are identified with the help of the EES software (Klein and Alvarado 2001), by minimization of the error function θ, which depends on the relative errors of the following variables: heat transfer coefficients and water exhaust temperatures. This function is defined as follows:

$$\theta = \sqrt{\frac{1}{n}\sum_{j=1}^{m}\sum_{i=1}^{n}\left(\frac{V_{j,i,sim} - V_{j,i,meas}}{V_{j,i,meas}}\right)^2} \quad [-] \qquad (3.22)$$

where V_j is the variable "j", m is the number of variables considered for the minimization and n is the number of tests.

After minimization of the function θ, the following parameters are identified for **T1** radiant ceiling:

δ_{s1} = 0.41 [mm] (bond thickness gap)

$L_{c,RC}$ = 0.41 [m] (Radiant ceiling characteristic length)

ε_{RC}=0.90 [-] (Radiant ceiling thermal emissivity)

k_{RC}= 52 [W m^{-1} K^{-1}] (Radiant ceiling panel thermal conductivity)

The model results for these conditions are also shown in Figures 3.5 and Table 3.4.

Figure 3.5 shows the comparison between measured and simulated water exhaust temperatures**.**

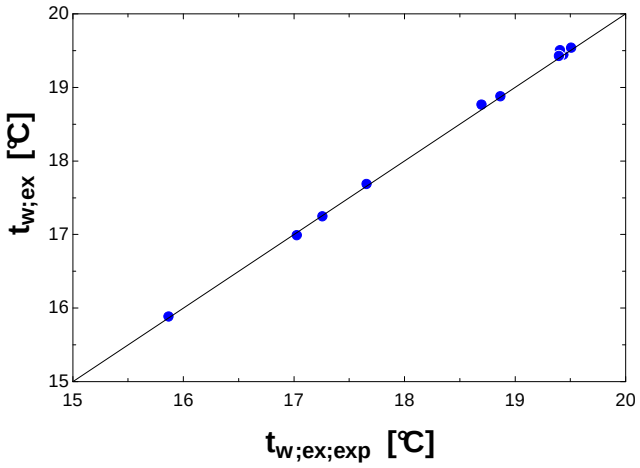

Figure 3.5: Simulated versus measured water exhaust temperature

The model error is defined here with a method similar to that recommended by the ASHRAE Guideline 2, (2005) for experimental data analysis. An average error and standard deviation are defined as follows:

$$\bar{\varepsilon} = \frac{1}{n}\sum_{i=1}^{n}\left(V_{i,meas} - V_{i,sim}\right) = \frac{1}{n}\sum_{i=1}^{n}\left(\varepsilon_i\right) \qquad \sigma = \left[\frac{1}{n}\sum_{i=1}^{n}\left(\varepsilon_i - \bar{\varepsilon}_i\right)^2\right]^{0,5} \tag{3.23}$$

where $V_{i,meas}$ is the measured variable and $V_{i,sim}$ is the simulated one. The model errors are presented in Table 3.5. The confidence limits are defined by the following equation:

$$\bar{\varepsilon} \pm \frac{Z\sigma}{\sqrt{n}} \tag{3.24}$$

with a coefficient Z = 1.96 for a probability of 95 %

Table 3.5: Cooper tubes radiant ceiling model errors

Variable	Average error	Standard deviation	Minimal deviation	Maximal deviation	Confidence limits
A.U **[W K^{-1}]**	0.15	1.5	-1.64	3.15	1.08 -0.77
$t_{w,ex}$ **[K]**	- 0.013	0.034	-0.07	0.05	0.008 -0.03

A good agreement is observed between simulated and measured values.

It is also important to note that, for this type of radiant ceiling, the obtained values for the heat transfer coefficient on the water side (forced convection in tubes with diameters 10 mm, h_w =1513 [W m^{-2} K^{-1}]) are much bigger than on the air side ($h_{RC,room}$ = 11.5 [W m^{-2} K^{-1}]). This explains that the *A.U* values presented in Table 3.4 do not vary very much as a function of the mass flow rate.

3.2.3 Sensitivity analysis

The objective of this analysis is to observe the influence of a possible error due to for example information uncertainty of selected parameters on the model response (after minimization procedure for the radiant ceiling **T1**). This is explained by the fact that some of them are taken from manufacturer information or laboratory test estimation. The influence of the main parameter variation on the model is evaluated by means of the error function θ. Three global parameters are considered:

- Thermal contact resistance: by the influence of the bond thickness gap (δ_{s1})

- Convective coefficient: by the influence of the characteristic length ($L_{c,RC}$), diffuser air velocity (u_{∞}) and panel porosity factor (ρ).
- Thermal properties of materials: by the influences of panel conductivity (k_{RC}), emissivity (ε_{RC}) and tubes conductivity (k_t).

The sensitivity analysis is performed varying the identified parameters within ± 5 %. The response of the model is evaluated through the ratio between the error function θ and the minimum error θ_{min} (with the selected parameter values after minimization of the function θ) (see Figure 3.6).

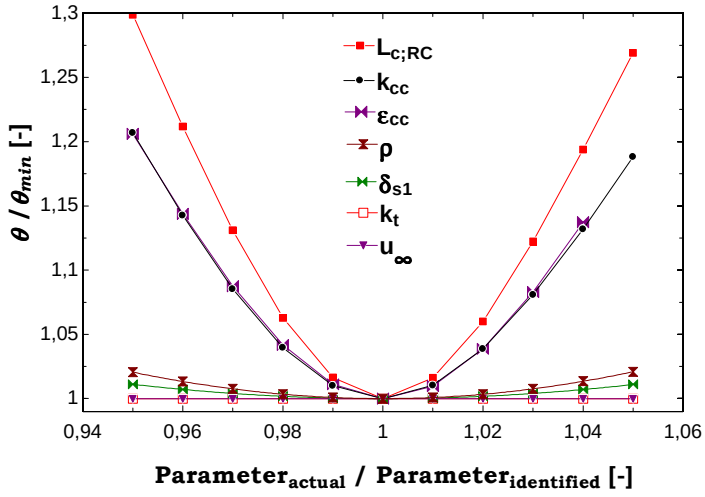

Figure 3.6: Sensitivity analysis results

It is observed that the model is highly sensitive to the error on the characteristic length ($L_{c,RC}$) and to the thermal properties of the radiant ceiling surface (k_{cc}, ε_{cc}). In a smaller degree, it is also sensitive to the panel porosity factor (ρ) and the bond thickness gap (δ_{s1}). An error of the other parameters slightly disturbs the response of the model.

3.3 SYNTHETIC CAPILLARY TUBE MATS RADIANT CEILING MODELING

The main geometric characteristics of this configuration are summarized in Table 1.1. An individual element and its equivalent thermal circuit for each tested configuration are shown in Figures 3.7, 3.8 and 3.9.

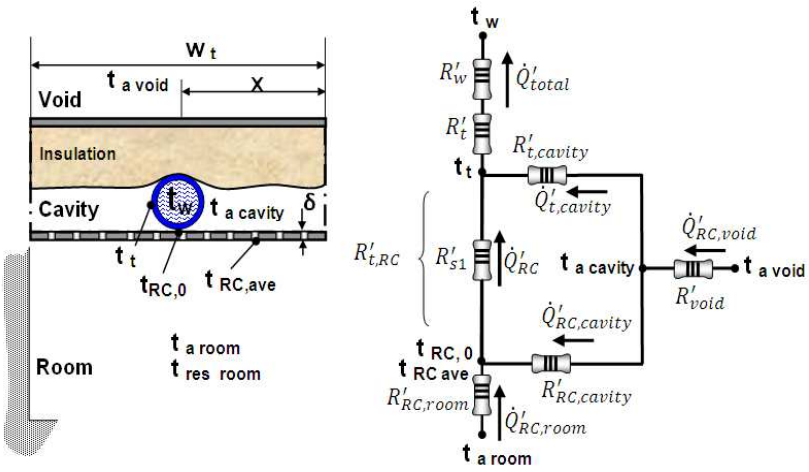

Figure 3.7: Tube mats on top of the metal ceiling panels

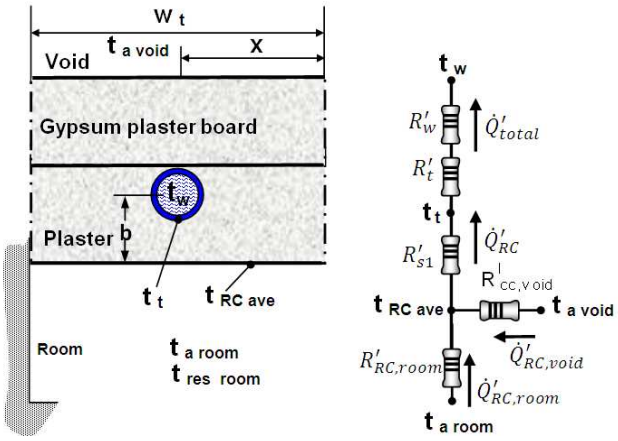

Figure 3.8: Tube mats embedded into the ceiling plaster.

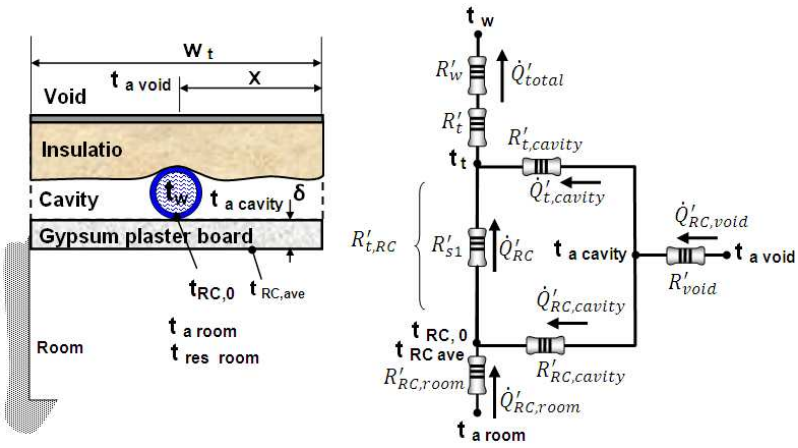

Figure 3.9: Tube mats on top of the gypsum plasterboards

3.3.1 Model description

Almost the same model as the copper radiant ceiling is used, with the following changes:

- For tube mats on the top of the metal panels (Figure 3.7), the thermal resistance between the tubes and ceiling plate ($R'_{t,RC}$) is reduced to a fictitious thermal resistance (R'_{s1}) through a reduced air layer of thickness δ_{s1}, which is a parameter to be identified on the basis of experimental results. In addition, considering the reduced space between the capillary tubes and the corresponding reduced fin length L_c (Figure 1.10), the model assumption made for holes influence considers that the fin surface (A_f) increases as a function of perimeter increase, therefore A_f must be defined as follows:

$$A_f = P.L_c \qquad \text{[m] (Per unit of length)} \qquad (3.25)$$

- For tube mats embedded into the ceiling plaster (Figure 3.8), two-dimensional steady-state conduction heat transfer is considered. According to the experimental measurements and theoretical studies on the basis of numerical and analytical solutions for transient heat conduction, for capillary tubes embedded into the ceiling plaster, the time reaction of the ceiling is less than 15 minutes (the ceiling construction is thinner than 15 mm), then the thermal inertia can be neglected. (C. Rao *et al.,* 2006; Tadeu and Simoes, 2005; J Miriel *et al*., 2002; Antonopoulos A., *et al.,* 1997). The thermal resistance between the tubes and ceiling surface (R'_{s1}) is defined therefore by reference to a horizontal circular cylinder of characteristic length L_{tp}, midway between parallel planes according to Eq. 1.33 and methodology described in section 1.5.5. The distance between the tube axis and the ceiling surface (***b*** value in Figure 3.8) is a model parameter which must be experimentally identified.
- For tube mats on the top of the gypsum plasterboards (Figure 3.9), there is no air circulation between room and ceiling cavity.

3.3.2 Validation process

The *A.U* experimental values can be calculated using the methodology described in section 1.5.6 according to:

$$AU_{exp} = A_{RC,effect}.U_{exp} \qquad [W\ m^{-2}\ K^{-1}] \qquad (3.26)$$

$$U_{exp} = \dot{q}_{exp} / \Delta_{T,Ln,exp} \qquad [W\ m^{-2}\ K^{-1}] \qquad (3.27)$$

For the tested mats configurations, the radiant ceiling thermal power $\dot{q}_{exp}$ in [W m^{-2}] is obtained from experimental results according to DIN 4715-1 in cooling mode, with constant water mass flow rate and 3 levels of water supply temperature (laboratory reports: FTZ, 2000,2003 and HLK Stuttgart University, 1995). The experimental log mean temperature difference at the center of the chamber is also calculated from Eq.1.35. The results are shown in Table 3.6.

Without ventilation and without facade effect, the heat transfer coefficient $h_{RCroom,conv}$ varies between 3.3 and 3.8 [W m^{-2} K^{-1}] for Ra ≈5.6*10^{7} [-] and $h_{RCroom,rad}$ ≈ 5.2 [W m^{-2} K^{-1}].

After error minimization, the model parameters are:

For "**U**" mats configuration is δ_{s1}= 0.28 [mm].

For "S" mats *b*=11.9 [mm].

For "G" mats δ_{s1}= 0.36 [mm].

The model results for these conditions are shown in Table 3.6.

Figure 3.10 shows the comparison between measured and simulated results of the exhaust water temperature**.**

Table 3.6: Experimental and calculated values for synthetic capillary tube mats.

Mats	AU [W/K]	AU_{exp} [W/K]	$Error_{AU}$ [W/K]	$\Delta_{T,Ln,exp}$ [K]	$\Delta_{T,Ln}$ [K]	$t_{w,ex,exp}$ [°C]	$t_{w,ex}$ [°C]	M_w [kg/s]	q_{exp} [W/m2]	$t_{w,su}$ [°C]	$t_{a,room}$ [°C]	$t_{a,void}$ [°C]	$t_{res,room}$ [°C]	$t_{cc,average}$ [°C]
U	84.63	84.43	-0.1985	6.251	6.251	20.67	20.67	0.1054	52.2	19.47	27.01	22.3	26.34	21.42
	87.61	87.7	0.08324	9.085	9.087	17.82	17.82	0.1053	78.8	16.01	26.85	20.57	26.03	18.95
	90.14	90.2	0.06068	11.77	11.77	16.14	16.14	0.1057	105	13.74	27.7	20.04	26.75	17.64
S	100.4	100.8	0.3874	12.32	12.31	14.78	14.78	0.1088	101.9	12.07	26.2	16.7	25.79	15.43
	96.93	96.83	-0.1009	10.01	10.01	16.8	16.81	0.1089	79.6	14.68	26.1	18.1	25.79	17.31
	96.47	95.76	-0.7013	7.911	7.906	18.68	18.69	0.1091	62.2	17.02	26.1	19.9	25.79	19.09
G	65.34	64.85	-0.4942	6.724	6.717	19.96	19.97	0.08043	42.7	18.67	26.32	22.68	26.06	21.13
	66.55	66.65	0.09806	9.086	9.086	17.85	17.85	0.08076	59.3	16.06	26.34	21.6	26.07	19.44
	68.1	68.55	0.4422	12.13	12.13	15.72	15.72	0.07904	81.4	13.22	27.09	21.08	26.64	17.86

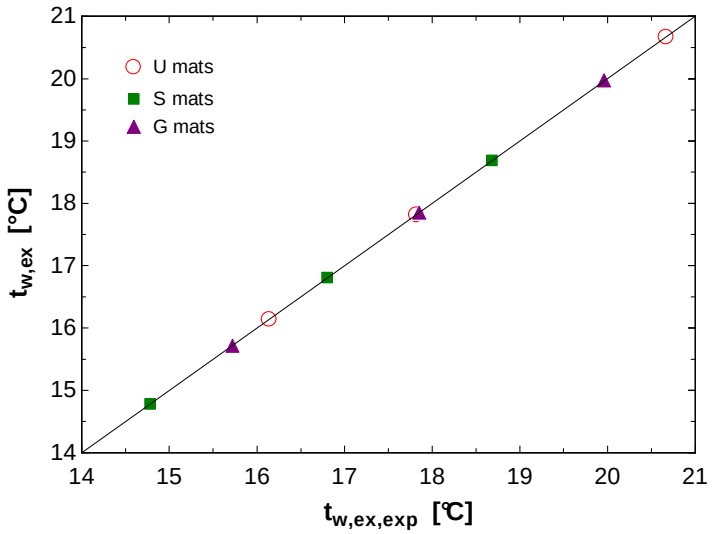

Figure 3.10: Simulated versus measured exhaust water temperature for capillary tube mats

The model errors are presented in Table 3.7. A very good agreement is observed between simulated and measured values. It appears that, with the capillary tube mats radiant ceiling, the heat transfer coefficients (forced convection in tubes with diameters of 2.3 mm, h_w = 9341 [W m^{-2} K^{-1}]) are much bigger on water side than on air side ($h_{cc,room}$ = 8.8 [W m^{-2} K^{-1}]). This also makes that, (and even more than the previous case), the water flow rate influence on *A.U* value is negligible. But the pressure drop is important as well. This makes that pumping energy consumption is no longer negligible and can significantly affect the global COP of the cooling system.

Table 3.7: Cooper tubes radiant ceiling model errors

Mats	Variable	Average error	Standard deviation	Minimal deviation	Maximal deviation	Confidence limits
U	***A.U*** **[W K^{-1}]**	-0.018	0.15	-0.2	0.08	0.15 -0.19
	$t_{w,ex}$ **[K]**	0.003	0.001	0.001	0.004	0.005 0.001
S	***A.U*** **[W K^{-1}]**	-0.14	0.54	-0.7	0.38	0.47 -0.75
	$t_{w,ex}$ **[K]**	- 0.007	0.002	-0.009	-0.005	-0.005 -0.009
G	***A.U*** **[W K^{-1}]**	-0.015	0.47	-0.5	0.44	0.51 -0.54
	$t_{w,ex}$ **[K]**	- 0.003	0.009	-0.001	0.003	0.007 -0.013

3.4 CONCLUSIONS

The modeling and experimental validation of four different radiant ceiling systems are presented here as a part of the study of the system in cooling mode. A good agreement is found between simulated and measured values. The results show that the average difference between simulated and measured *A.U* values and exhaust water temperatures are lower than ±0.15 [W K^{-1}] and ±0.01 [K] respectively.

The definition of the radiant ceiling geometry and ventilation parameters allows for the use of the manufacturer technical information of radiant ceiling systems and diffusers in order to simplify the commissioning process. On the other hand the choice of the resultant temperature as comfort indicator enables a relatively easy verification of this parameter in the room.

The steady state model permits to support a Functional Performance Test of the system to verify the main radiant ceiling performance and to compare them with data given in AS-BUILT files. The experimental data provided by the manufacturer can be used in order to identify the model parameters (first parameter identification).

It is also observed that if only natural convection is considered (as a current modeling practice) the heat transfer coefficient can be underestimated by around 47 % (due to the ventilation, panel perforation and facade effects).

4. Dynamic thermal modeling of radiant ceiling systems and its environment

4.1 INTRODUCTION

The analysis of the radiant ceiling system becomes even more complex considering that its behavior must be studied by coupling it with the corresponding structure of the building (facade, walls, internal loads and ventilation system), climate and functioning conditions (Fonseca *et al*., 2009 b). This is due to the fact that the resultant temperature in a space is not only depending on the air temperature, but also on the transient variation of the surface temperatures in the conditioned space.

The model developed by Kilkis, (1995) proposes a design procedure for radiant cooling systems that assumes steady-state conditions where the radiant heat exchange with the facade and walls is simplified as in most of the model developed in the related literature (ASHRAE system and equipment, 2004; Jeong and Mumma, 2004); Koschenz and Dorer, (1996) propose that the design of radiant cooling systems should be done based on dynamic calculations. However, their design procedure does not use a truly dynamic method. Niu and van der Kooi, (1994) suggest a similar approach. The usual practice (Koschenz and Dorer, 1996) connects a model of cooled or heated ceiling with TRNSYS, (2009) modules for the other room surfaces.

The specific TRNSYS module developed for radiant ceiling, considers it as an “active layer” added to the wall, floor or ceiling definition. Two types of radiant ceilings are considered: concrete core cooling or heating and capillary tube mats system. This model is based on the German norm DIN 4715-1, (1993) for the chilled ceiling panels. Therefore, additional parameters to define the performance in this type of test conditions are needed. These parameters, such as the specific nominal power, mass flow rate, area and number of loops can be obtained from the producer of chilled ceiling panels. However, as the aim of this kind of test (DIN 4715-1, 1993) is only to compare the performance of different types of cooling ceiling systems, a homogeneous load distribution was considered without the influence of the ventilation system and/or the facade asymmetry effect (HLK, 1995; Kochendörfer C., 1996).

The ENERGYPLUS, (2008) program that is based on the most popular features and capabilities of BLAST and DOE-2 (and Zweifel, 1993 and Bruce *et al*., 1994), considers only the case of tubes embedded in a wall, ceiling, or floor or runs current through electric resistance wires embedded in a surface or a panel. This model considers that the building element that contains the hydronic loop is stationary and that its temperature along the length of the tubing is constant. In other words, it is assumed that the water tubing itself has no significant effect on the heat transfer process being modeled. The radiant ceiling is then simplified using these assumptions and the effectiveness-NTU method, as a heat exchanger with laminar or turbulent flow into the tubes (despite that operating regime of the radiant ceiling is often transition flow). Consequently, none of the large building energy programs publicly available (TRNSYS, ENERGYPLUS) has the capability to simulate buildings cooling or heating by radiant ceiling systems with the required detailed level. In this study, a separate dynamic model simulates the specifics of radiant cooling systems performance, but integrated with its environment. The resultant temperature is therefore calculated as a comfort parameter for design purposes and especially for commissioning processes.

4.2 DYNAMIC MODELING

The dynamic model developed in this study basically focuses on the heat exchange between a room and the adjacent zones. The dynamic thermal balances in dry regime of the active radiant ceiling, room and ceiling void, the external and internal walls thermal balance (including a possible inactive ceiling zone) as well as ceiling and floor slabs are considered. The window behavior is modeled assuming steady-state condition, considering the low thermal inertia of the fenestration system. Therefore, the main model inputs are the air temperature of the adjacent zones (lateral rooms, corridor ceiling and floor adjacent zones and facade outside conditions), the water temperature and mass flow rate, the internal thermal loads or gains and the supply air temperature and mass flow rate at the diffuser discharge. The cooling ceiling model can be characterized by the inputs, outputs and parameters shown in Figure 4.1.

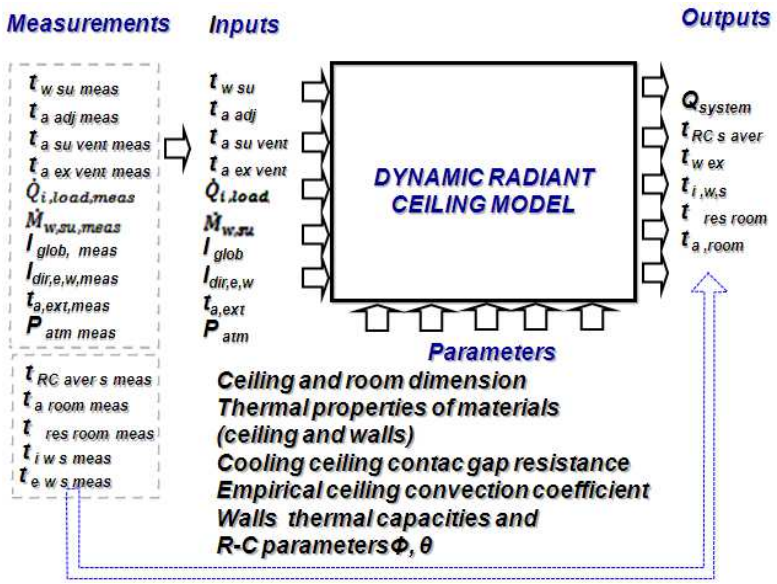

Figure 4.1: Definition of the cooling ceiling model inputs, outputs and parameters

The model allows for the estimation of the water exhaust temperature, radiant ceiling average surface temperature, resultant and dry air room temperatures, radiant ceiling power and also internal surface temperatures of the room in order to compare with measurements taken during the commissioning process.

4.2.1 Radiant ceiling system model

For the dynamic radiant ceiling modeling, the treatment of convection, radiation and conduction heat transfer is almost the same as the static modeling described in details in Chapter 3 and Fonseca *et al.*, (2009). Basically, to consider the transient behavior, the internal energy variation of the ceiling and of the water is included in the energy balance. For the copper tube radiant ceiling (for example) (see Figure 3.1), the total thermal power extracted by water ($\dot{Q}_{total}$) in cooling mode can be calculated from the dynamic water and ceiling thermal balances as:

$$\dot{U}_w = \dot{Q}_{total} - \dot{Q}_{RC} - \dot{Q}_{t,cavity} \quad [W] \quad (4.1)$$

$$\dot{U}_{RC} = \dot{Q}_{RC} - \dot{Q}_{RC,cavity} - \dot{Q}_{RC,room} - \dot{Q}_{i,load,RC} \quad [W] \quad (4.2)$$

and

$$\Delta U_w = \int_{\tau_1}^{\tau_2} \dot{U}_w . d_\tau \quad [J] \quad (4.3)$$

$$\Delta U_{RC} = \int_{\tau_1}^{\tau_2} \dot{U}_{RC} . d_\tau \quad [J] \quad (4.4)$$

$$\Delta U_w = C_w . \left(t_{w,ave} - t_{w,ave,1} \right) \quad [J] \quad (4.5)$$

$$\Delta U_{RC} = C_{RC} . \left(t_{RC,ave} - t_{RC,ave,1} \right) \quad [J] \quad (4.6)$$

where

$t_{w,ave,1}$ is the initial water average temperature, [℃]

$t_{RC,ave,1}$ is the initial radiant ceiling average temperature, [℃]

$\dot{Q}_{RC}$ is the total thermal energy extracted by the radiant ceiling panel, [W].

$\dot{Q}_{t,cavity}$ is the heat flow rate through the tube external surface from the ceiling cavity, [W].

$\dot{Q}_{RC,cavity}$ is the heat flow (convection + radiation) coming from the ceiling cavity, [W].

$\dot{Q}_{RC,room}$ is the heat flow (convection + radiation) coming from the room, [W].

$\dot{Q}_{i,load,r,RC}$ is the radiative fraction of the room internal thermal load on the radiant ceiling, [W].

C_w is the thermal mass of the water into the active radiant ceiling, [J K^{-1}]

C_{RC} is the global radiant ceiling thermal mass (tubes, union system and metalic plates) , [J K^{-1}]

The water average temperature is estimated from the log mean temperature difference for each block of panels connected in series from Eq. 3.3.

4.2.2 Thermal zone model

Two zones are considered in this global model: the room and the ceiling void. Each zone is represented by means of a sensible convective thermal balance. The dynamic behavior of each zone is modeled by an air thermal capacity corrected by taking into account the thermal capacity of the furniture or ducts included in the zones.

The main sensible air room thermal balance can be expressed by:

$$\dot{U}_a = \dot{Q}_{RC,conv,i,s} + \dot{Q}_{inac,RC,conv,i,s} + \dot{Q}_{i,w,left,conv,i,s} + \dot{Q}_{i,w,right,conv,i,s} + \dot{Q}_{i,w,bottom,conv,i,s} + \dot{Q}_{i,w,floor,conv,i,s} + \dot{Q}_{e,w,conv,i,s} + \dot{Q}_{win,conv,i,s} + \dot{Q}_{i,load,conv} + \dot{Q}_{ven} \quad [W] \quad (4.7)$$

$$\Delta U_a = \int_{\tau_1}^{\tau_2} \dot{U}_a . d_\tau \quad [J] \quad (4.8)$$

$$\Delta U_a = C_a . \left(t_{a,room} - t_{a,room,1} \right) \quad [J] \quad (4.9)$$

$$C_a = F_{f,i,c} . c_{p,a} . \rho_a . V_{room} \quad [J\ K^{-1}] \quad (4.10)$$

The thermal balance considers the convective heat flow rate on each surface in contact with the air room, including the possibility of an inactive ceiling surface. The air capacity is corrected by a hypothetical factor ($F_{f,i,c}$), supposed to consider the capacity of all internal surfaces and equipment (walls and furnitures) inside the room. Lebrun *et al*., (2006) proposes a factor of 5.

The $\dot{Q}_{i,load,conv}$ value is the convective portion of the internal thermal load and $\dot{Q}_{ven}$ is the sensible contribution of mechanical ventilation system.

The convective heat transfer coefficients on the internal side of the room walls (external, left, right and back (close to the corridor)) are calculated using the Churchill and Chu correlations (Incropera and DeWitt, 1996), over the entire range of Rayleigh number (*Ra*):

$$Nu = \left[0.825 + 0.387. \frac{Ra^{1/6}}{\left(1 + \left[\frac{0.492}{\Pr} \right]^{9/16} \right)^{8/27}} \right]^2 \quad [-] \quad (4.11)$$

And for the external surface of the external wall for Reynolds number (*Re*) from $5*10^5$ to 10^8 and Prandtl number (*Pr*) from 0.6 to 60 by:

$$Nu = \left(0.037.\mathrm{Re}^{4/5} - 871\right).\Pr^{1/3} \quad [-] \quad (4.12)$$

For the floor surface the Mc Adams correlations are used (Incropera and DeWitt, 1996):

- For an upper cooled surface: Ra from 10^5 to 10^{10}

$$Nu = 0.27.Ra_{RC,room}^{1/4} \quad [-] \quad (4.13)$$

- Or for an upper heated surface: Ra from 10^4 to 10^5

$$Nu = 0.54.Ra_{RC,room}^{1/4} \quad [-] \quad (4.14)$$

The convective heat exchange on the radiant ceiling surface (active or inactive) are calculated according to the methodology described in Chapters 1 and 3.

The thermal balance of air inside the ceiling void can be expressed in a similar way as:

$$\dot{U}_{a,void} = \dot{Q}_{RC,void,conv} + \dot{Q}_{inac,RC,void,conv} + \dot{Q}_{ceiling,slab,void,conv} + \dot{Q}_{ducts,void,conv} + \dot{Q}_{light,back,void,conv} \text{ [W] (4.15)}$$

The void thermal balance considers the convective heat flow rate on each surface in contact with the air void, including the convective heat gain or load from lighting back and water and air conduits (determined from ASHRAE Fundamentals, 2009). The air thermal capacity is also corrected by a hypothetical factor ($F_{f,i,c} = 2$), taking into account the capacity of ventilation ducts and water conduits placed inside the usually tight ceiling void (see Figure 4.2).

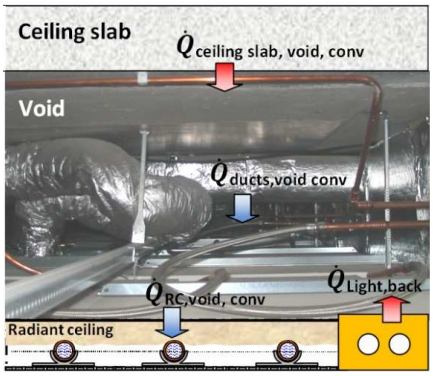

Figure 4.2: View of the ceiling void

4.2.3 Walls ceiling model

The heat flow passing through the room envelope is the sum of two contributions: the heat transmission trough windows (without energy storage) and opaque massive walls (with energy storage). A two-port R-C network model is used to simulate each surrounding wall (floor and ceiling slabs, external wall, inactive radiant ceiling and partition walls). The parameters of this wall R-C network are adjusted through a frequency characteristic analysis. This building zone model has been successfully validated by means of analytical, experimental and comparative validation tests (Bertagnolio *et al*., 2008).

In the present study, isothermal boundary conditions (Masy, 2008) are used for external and internal walls. The admittance matrix method is used to calculate the whole wall transmittance and admittance whose modulus are imposed to the 2R1C model in order to adjust its parameters.

The balances of the considered nodes are given here after. Solar gains and infrared losses are taken into account and injected or taken out of the outdoor surface node of the external wall (Figure 4.3).

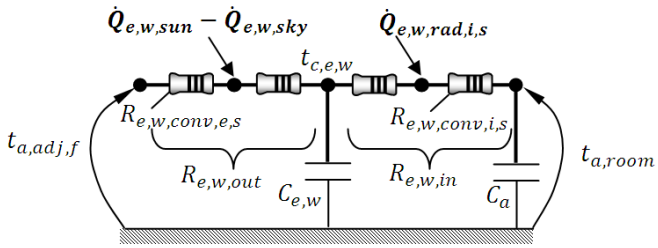

Figure 4.3: Equivalent R-C Two-port network for the room external wall

The (convective) thermal balance on the external wall can be expressed as:

$$\dot{U}_{e,w} = \dot{Q}_{out,e,w} - \dot{Q}_{in,e,w} \quad [W] \quad (4.16)$$

$$\Delta U_{e,w} = \int_{\tau_1}^{\tau_2} \dot{U}_{e,w}.d_{\tau} \quad [J] \quad (4.17)$$

$$\Delta U_{e,w} = C_{e,w}.\left(t_{c,e,w} - t_{c,e,w,1}\right) \quad [J] \quad (4.18)$$

$$C_{e,w} = \phi_{e,w}.m_{e,w}.c_{p,e,w} \quad [J\ K^{-1}] \quad (4.19)$$

The balance of the external side of the wall gives:

$$\dot{Q}_{e,w,out} = \dot{Q}_{e,w,conv,e,s} + \dot{Q}_{e,w,sun} - \dot{Q}_{e,w,sky} \quad [W] \quad (4.20)$$

where

$$\dot{Q}_{e,w,out} = \frac{t_{a,adj,f} - t_{e,w,e,s}}{R_{e,w,conv,e,s}} \quad [W] \quad (4.21)$$

$$R_{e,w,conv,e,s} = \frac{1}{A_{e,w}.h_{e,w,e,s}} \quad [K\ W^{-1}] \quad (4.22)$$

$$\dot{Q}_{e,w,out} = \frac{t_{e,w,e,s} - t_{c,e,w}}{R_{e,w,out} - R_{e,w,conv,e,s}} \quad [W] \quad (4.23)$$

$$R_{e,w,out} = (1 - \theta_{e,w}).R_{e,w,total} \quad [K\ W^{-1}] \quad (4.24)$$

$$R_{e,w,total} = \frac{1}{AU_{e,w}} \quad [K\ W^{-1}] \quad (4.25)$$

The $\theta_{e,w}$ and $\phi_{e,w}$ values are the accessibility and proportion parameters respectively (*R-C* network) of the considered wall. They are obtained using the methodology proposed by Masy, (2008).

The balance of the internal side of the external wall gives:

$$\dot{Q}_{e,w,in} + \dot{Q}_{e,w,i,load,rad} + \dot{Q}_{e,w,rad} - \dot{Q}_{e,w,conv,i,s} = 0 \quad [W] \quad (4.26)$$

with

$$\dot{Q}_{e,w,i,load,rad} = \dot{Q}_{i,load,rad}.\phi_{rad,i,w}.\frac{A_{e,w}}{A_{room,i,s,total}} \quad [W] \quad (4.27)$$

where

$$\phi_{rad,i,w} = 1 - \phi_{rad,RC} \quad [-] \quad (4.28)$$

The coefficient $\phi_{rad,RC}$ is the radiative fraction of the internal thermal load or gain to the radiant ceiling (from the view factors).

and

$$\dot{Q}_{i,load,rad} = \dot{Q}_{i,load}.\phi_{i,load,rad} + \dot{Q}_{sun,win} \quad [W] \quad (4.29)$$

with

$$\phi_{i,load,rad} = 1 - \phi_{i,load,conv} \quad [-] \quad (4.30)$$

The coefficient $\phi_{i,load,conv}$ is the convective fraction of the internal thermal load or gain (from ASRAE Fundamentals, 2009 information). The sun heat radiation though the window is considered here as an internal thermal load and distributed on each internal wall surface.

Finally, the conductive heat flux through the wall can be defined as follows:

$$\dot{Q}_{e,w,in} = \frac{t_{c,e,w} - t_{e,w,i,s}}{R_{e,w,in} - R_{e,w,conv,i,s}} \quad [W] \quad (4.31)$$

where

$$R_{e,w,in} = \theta_{e,w}.R_{e,w,total} \quad [K\ W^{-1}] \quad (4.32)$$

For the internal walls, the methodology is almost the same, obviously without the effect of the sun and infrared radiation with the sky considered in the external wall surface.

In order to analyze the internal surface radiant exchanges ($\dot{Q}_{w,rad}$) for a multi-surface case, each surface *i* of the enclosure can be characterized by its uniform radiosity and irradiation according to the methodology described in Chapter 1 and 3.

4.2.4 Solar gains and infrared losses

The equation used to compute solar gains and infrared losses through the external wall and window are taken from Masy, (2008) and Bertagnolio *et al*., (2008).

The absorbed solar radiation on external wall can be calculated as:

$$\dot{Q}_{sun,e,w} = \alpha_{e,w}.A_{e,w}.I_{sun,e,w} \quad [W] \quad (4.33)$$

where

$$I_{sun,e,w} = I_{direct,e,w} + 0.5.I_{glob}.albedo + 0.5I_{diff} \quad [W\ m^{-2}] \quad (4.34)$$

$$F_{e,w} = \frac{F_{e,w,S}.F_s + F_{e,w,W}.F_W + F_{e,w,E}.F_E + F_{e,w,N}.F_N + F_{e,w,Shadow}}{\sigma_{F_{e,w}}} \quad [-] \quad (4.35)$$

$$\sigma_{e,w} = F_{e,w,S} + F_{e,w,W} + F_{e,w,E} + F_{e,w,N} + F_{e,w,Shadow} \quad [-] \quad (4.36)$$

$$I_{direct,e,w} = (I_{glob} - I_{diff}).F_{e,w} \quad [W\ m^{-2}] \quad (4.37)$$

The infrared losses can be calculated as:

$$\dot{Q}_{ir,win,sky} = 0.5.\varepsilon_{ir,win}.A_{win}.I_{ir,h} \quad [W] \quad (4.38)$$

$$\dot{Q}_{ir,e,w,sky} = 0.5.\varepsilon_{ir,e,w}.A_{e,w}.I_{ir,h} \quad [W] \quad (4.39)$$

where

$\alpha_{e,w}$ is the external wall absorption factor, [-].

$I_{sun,e,w}$ is the equivalent radiation reaching the external wall, [W m^{-2}].

$I_{direct,e,w}$ is the direct radiation reaching vertically the external wall, [W m^{-2}].

I_{glob} is the global radiation reaching a horizontal surface, [W m^{-2}].

Albedo is the reflective factor of the ground,

I_{diff} is the diffused radiation reaching a horizontal surface, [W m^{-2}].

$\varepsilon_{ir,e,w}$ is the opaque frontages infrared emission factor.

$I_{ir,h}$ is the pre-computed infrared loss of an horizontal surface (obtained thanks to linear interpolation between 100 and 45 [W m^{-2}]. These extreme values correspond respectively to serene and cloudy sky (Davies, 2004)).

The $F_{e,w}$ factors are the fraction of the external wall surface in different orientations . *F* values are the projection factors for a vertical wall in the principal orientations. $F_{e,w,shadow}$ is the fraction of shadowed external wall surfaces. The factors 0.5 in Eq. 4.38 and 4.39 are added because a vertical wall faces only half of the sky. The global and diffuse radiations come directly from the meteorological data.

The solar gain directly injected in the zone through windows is composed of direct, diffuse and reflected radiation. For each orientation, the three contributions are included in the global solar radiation as:

$$\dot{Q}_{sun,win} = A_{win}\left|\frac{F_{win,S}.I_{sun,s} + F_{win,W}.I_{sun,W} + F_{win,N}.I_{sun,N} + F_{win,E}.I_{sun,E}}{\sigma_{F_{win}}}\right| \quad [W] \quad (4.40)$$

where the F_{win} factors are the fraction of the glazed surface in different orientations and I_{sun} is the equivalent global radiation for each orientation.

The σ_{Fwin} value is the sum of the F factors for the window.

$$\sigma_{F_{win}} = F_{win,S} + F_{win,W} + F_{win,E} + F_{win,N} + F_{win,Shadow} \quad [-] \quad (4.41)$$

where $F_{win\ shadow}$ is the fraction of shadowed glazed surface.

The three contributions are included in the global solar radiation for each orientation $I_{sun,S}$ etc, as:

$$I_{sun,S} = SF_{win,S}.I_{direct,S} + SF_{win,hemis}.(0.5.I_{glob}.albedo + 0.5.I_{diff}) \quad [W\ m^{-2}] \quad (4.42)$$

$$I_{direct,S} = (I_{glob} - I_{diff}).F_S \quad [W\ m^{-2}] \quad (4.43)$$

where $I_{direct,S}$ is the direct radiation reaching the vertical glazed surface South oriented. The coefficient $SF_{win,S}$ is the solar factor for the South oriented windows and $SF_{win,hemis}$ is the solar factor related to the hemispherical (reflected and diffuse) radiation.

The factors 0.5 in Eq. 4.42 are added because a vertical wall faces only half of the sky. The global and diffuse horizontal radiations come directly from meteorological data. The solar factors for direct radiation globalizes the reflection, absorption and transmission factors of the double glazing windows in one value and is computed as a function of the incidence angle of direct radiation and can be calculated for the South oriented window and related to a hypothetical hemisphere (reflected and diffuse) as:

$$SF_{win,S} = SF_{win,0}.\left[1 - \tan^{P}\left(\frac{\theta_s}{2}\right)\right] \quad [-] \quad (4.44)$$

$$SF_{win,hemis} = f_{hemis}.SF_{win,0} \quad [-] \quad (4.45)$$

where $SF_{win,0}$ is the normal solar factor of the window, p and f_{hemis} are correlation factors, Svendsen and Laustsen, (2002) suggest p =3 and f_{hemis}= 0.86 for a double glazing with low emittance coating. Finally θ is the Incidence angle.

4.2.5 Resultant temperature

The operation conditions and performance of a radiant ceiling system during the commissioning processes must be evaluated not only in terms of system capacity but also considering the comfort of the occupants. As the radiant ceiling can be correctly operating according to the design conditions (AS-BUILT files), its operation must be also related to its global behavior considering the interaction with the fenestration and ventilation system. The resultant temperature is therefore used in the model as comfort variable in order to evaluate the global system performance and can be calculated according to the methodology described in section 1.5.4 and the calculated values of air and surface temperatures.

4.3 DYNAMIC MODEL VALIDATION

The validation process is performed using the test bench type two (see section 2.3.2) for the radiant ceiling **T3** in cooling and heating mode.

The contact thermal resistance and heat transfer coefficient of this type of radiant ceiling are obtained in steady state conditions from experimental tests (Fonseca *et al*., 2009) and used in the dynamic model as parameters. The modifications considered here are the distance and velocity of the jet detachment defined from diffuser manufacturer's catalogue for the specific diffuser model (this parameters as well as the *R-C* network parameters are used to adjust the model as shown in Figure 4.1). The model outputs (air temperatures, water exhaust temperature and internal room surface temperatures) are compared directly with measurements performed during the regulation test (Aparecida C. *et al.,* 2000).

The tests used to validate the model simulate the actual conditions of a building office built to reproduce as accurately as possible the structure and functional characteristics of a large commercial building located in Brussels.

4.3.1 Heating mode validation

The test duration is nine and a half hours (measurements in time interval of 10 seconds). The main objective is to simulate the heating during the first hours in the morning, after a night cooling, without ventilation and without lighting.

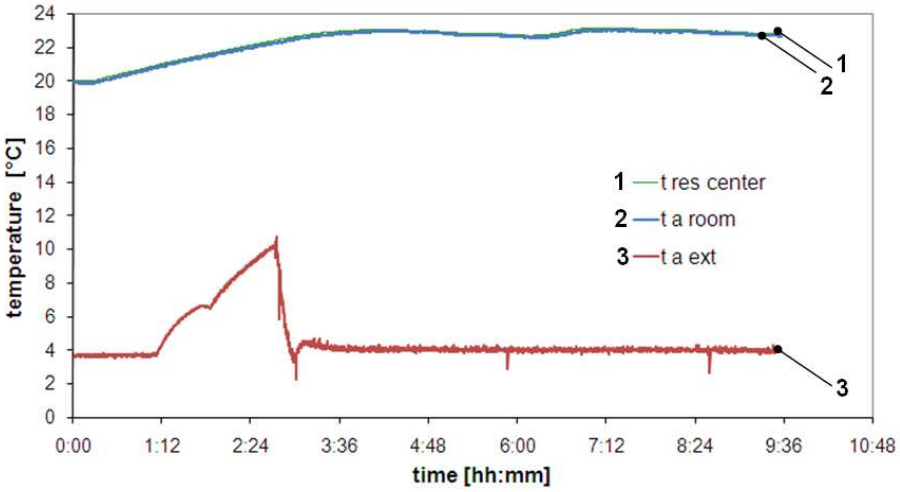

Figure 4.4 Air experimental conditions for heating mode validation.

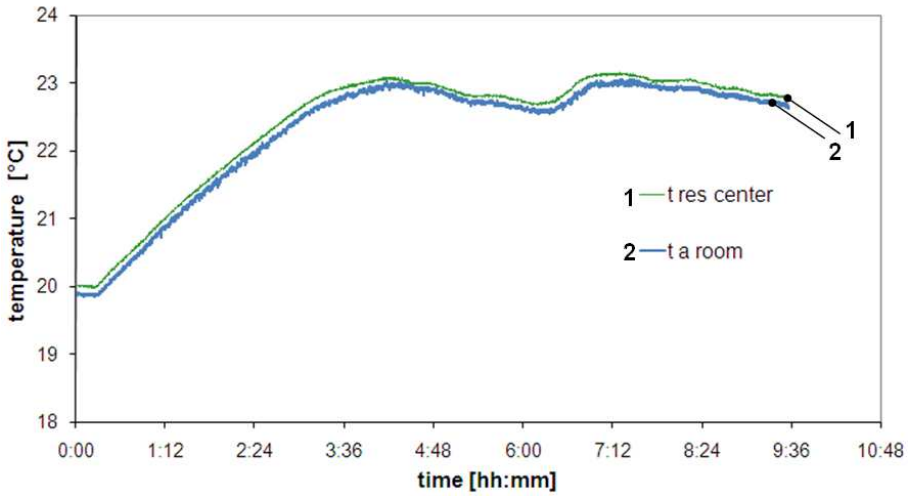

Figure 4.5 Detail on air experimental conditions for heating mode validation.

The experimental conditions of the external air (simulated in facade $t_{a,ext}$) and room air temperatures (resultant and air temperatures at the center of the office) are shown in Figure 4.4 and Figure 4.5.

In Figure 4.5 it is observed that during the test, the air temperature is systematically lower than the resultant temperature. This is due to the radiant ceiling operation (the water temperature is around 49 [℃]) and a limited convective effect in heating mo de.

The water temperature measurements are shown in Figure 4.6.

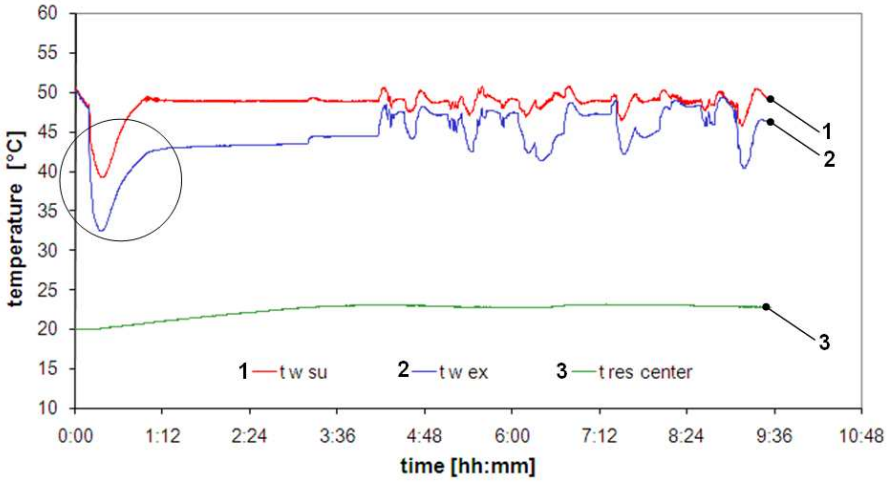

Figure 4.6 Water experimental conditions for heating mode validation.

The initial perturbation shown in Figure 4.6 is due to the fact that water exhaust of each panel block is mixed into the collector with the water previously stored in the system (panels and conduits) as a consequence of the by-pass effect (see section 2.3.2.1 and Figure 2.21).

In heating mode, only six panels placed close to the facade are operating. They are connected in three blocks, each one with two panels connected in series (see Figure 4.7). Figure 4.7 also shows the

time function intervals when each block of panels is operating, according to the activation signal of mass flow rate control valve (MF for cooling mode (inactive) and MC for heating mode (active) in Figure 4.7).

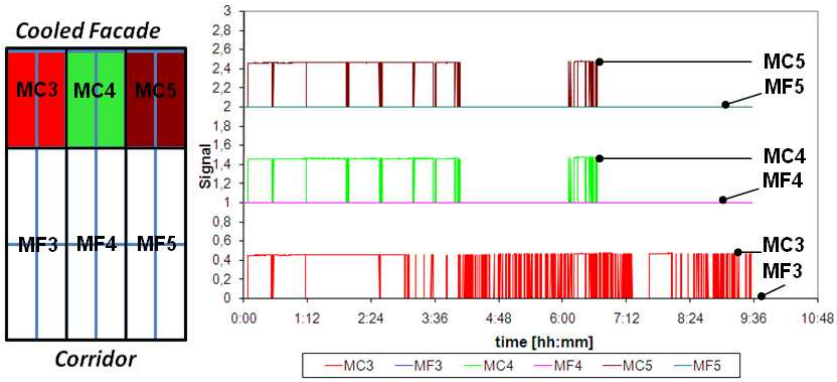

Figure 4.7: Panel's block water regulation in heating mode.

It is observed in Figure 4.7 that, at the beginning of the test (around 4 h), all of the three blocks of panels in heating mode close to the facade (MC) are active, after when the air temperature set point is reached, only one of them continues operating (MC3 in Figure 4.7) while the other two only operate sporadically. It is supposed that the hydraulic regulation system allows the mass flow rate to be perfectly equilibrated in the panels, however it is important to note that the regulation is made for nominal conditions (all the panel actives).

Results

Direct comparison between the model results and measured values of the internal wall and window surface temperature at the internal surface and water exhaust temperatures are shown in Figures 4.8, 4.9 and 4.10 respectively.

The error indicator *RMS* (root-mean-square) (Masy, 2008) is used to compare the measured and calculated values of the temperatures profiles of *n* measurements according to:

$$RMS = \sqrt{\frac{\sum_{i=1}^{n} \left(t_{meas} - t_{\mathrm{mod}\,el}\right)^2}{n}} \quad [\mathrm{K}] \qquad (4.46)$$

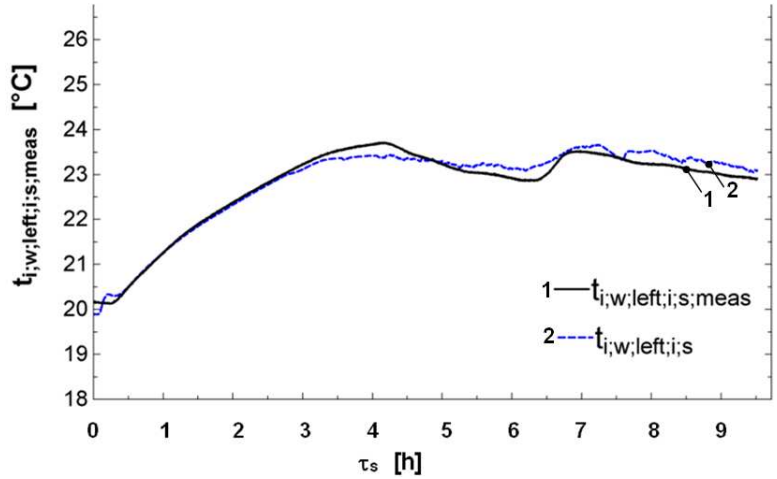

Figure 4.8: Comparison: Measured and calculated temperature of internal wall at the internal surface.

The initial perturbation in the wall surface temperature shown in Figure 4.8 (and also in other model outputs) is probably due to that the initial test conditions are not totally stabilized and could disturb the initial model response. An average error *RMS* value between simulated and measured values of internal surface temperature (left side) of ±0.23 [K] is observed, which is within the measurement uncertainty variation.

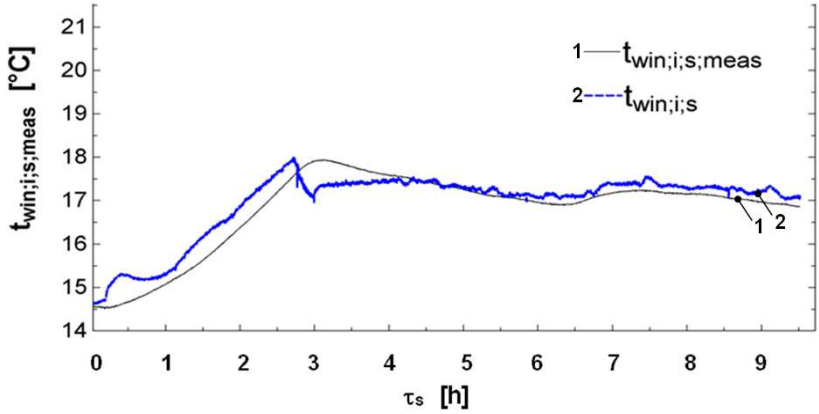

Figure 4.9: Comparison: Measured and calculated temperature of window internal surface.

In Figure 4.9 a *RMS* value of ±0.3 [K] between simulated and measured values is observed. However the model response for the window surface temperature presents an important variation with respect to the experimental values at 3 h time of the test. Due to the regulation, two out of three blocks of panels close to the facade are deactivated at this time and the model does not perfectly follow this perturbation due to the model assumptions related to the system regulation and actual valve time response.

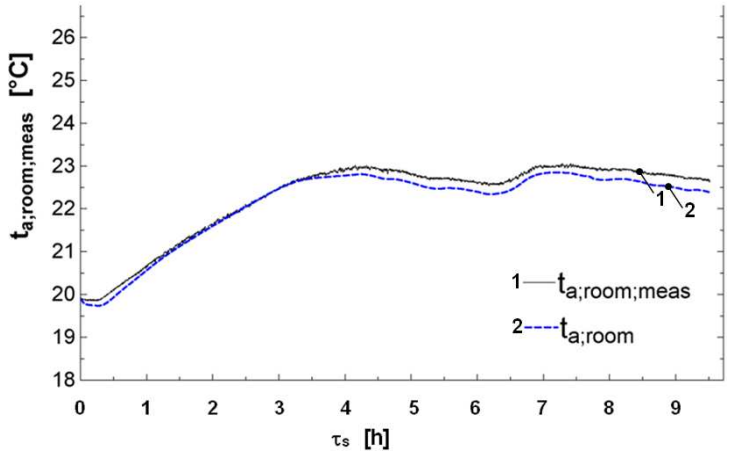

Figure 4.10: Comparison: Measured and calculated room air temperatures.

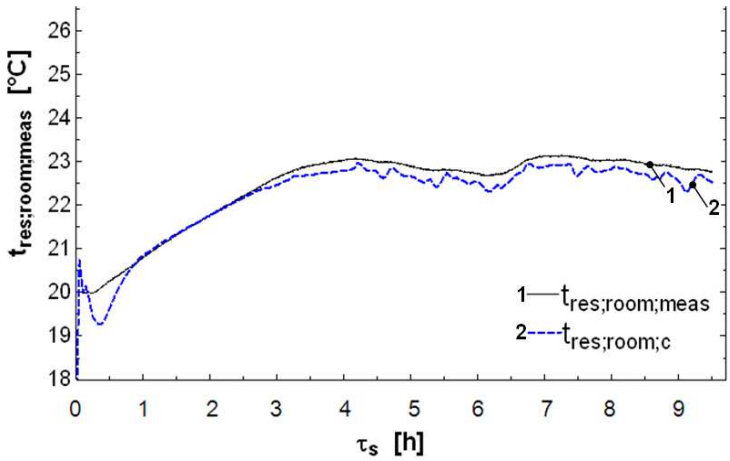

Figure 4.11: Comparison: Measured and calculated room resultant air temperatures.

For air and resultant room temperatures in Figure 4.10 and Figure 4.11, a *RMS* error between simulated and measured values of ±0.23 [K] is observed. It is also observed that the calculated value is systematically lower than the measured value. This is due to the fact that the comparison is based on the resultant and air temperatures ($t_{a,room}$ and $t_{res,room}$) measured at the center of the chamber and 75 [cm] above the floor, while the model considers homogeneous air conditions. Therefore the temperature stratification induced during the test in heating mode (see Chapter 2) is not considered and can explain an important part of the model error.

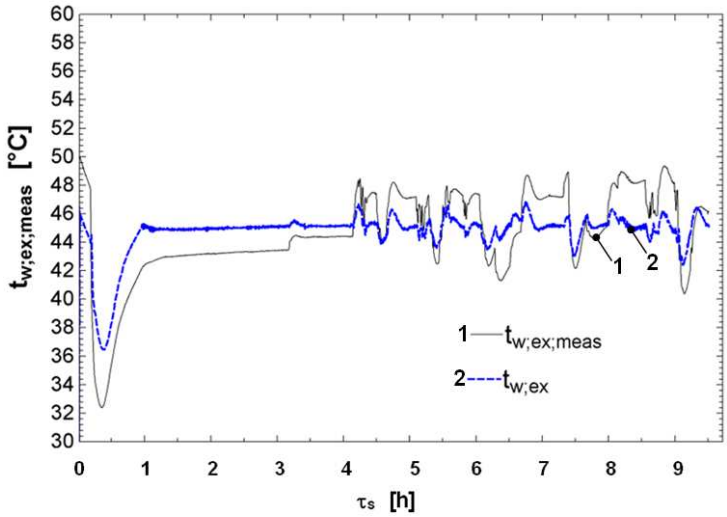

Figure 4.12: Comparison: Measured and calculated water exhaust temperature.

Figure 4.12 shows that the water exhaust temperature calculated by the model follows relatively well the average measured value. However the dynamic behavior is not well represented (*RMS* of ±2.32 [K]). It is basically due to the hydraulic circuit and the regulation system implemented (operation conditions of the control valve) (see Figure 2.21). In this circuit the measured water exhaust temperature corresponds to the mixing at the blocks exhaust and considers the by-pass effect. The by-pass makes it possible to operate in cooling (all the panels active) or in heating mode (panels active only close to the facade) in the configurations presented in Figure 4.13. However, it is important to note that in real buildings, the hydraulic circuit is simpler than considered here (as it is shown below for commissioning process in Chapter 5).

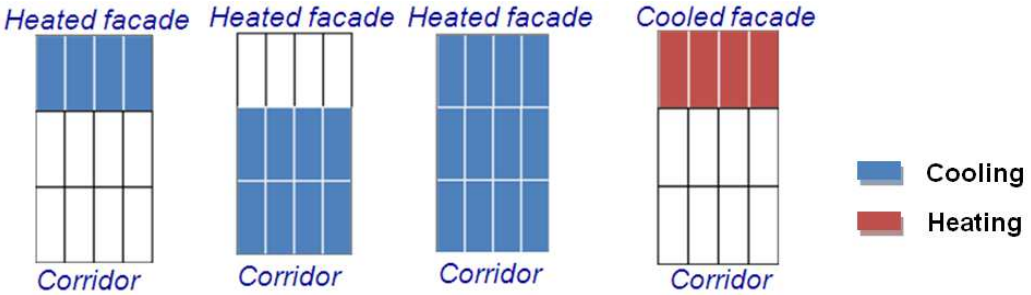

Figure 4.13: Operating conditions of the radiant ceiling system **T3**.

4.3.2 Cooling mode validation

The test duration is thirteen hours (measurements in time intervals of 10 seconds). The main objective of the test is to simulate the cooling mode operation of the system with ventilation (air renovation 105 m^3h^{-1}) and the injection of the internal thermal loads of 1196 [W] during the ceiling operation. The experimental conditions of external air (simulated in the facade $t_{a,ext}$) and room air temperatures (resultant and air temperatures at the center of the office) are shown in Figure 4.14.

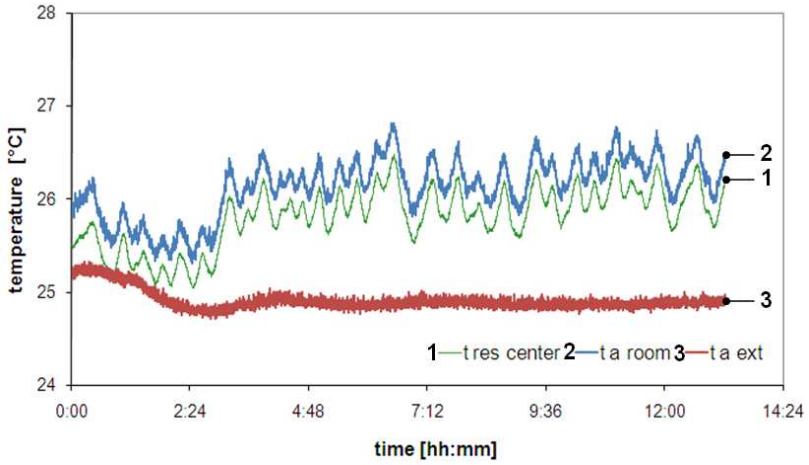

Figure 4.14 Air experimental conditions for cooling mode validation.

In Figure 4.14 can be observed that during the test, the air temperature is systematically higher than the resultant temperature. This is due to the radiant ceiling operation (the water temperature is around 14 [℃]).

The water temperature measurements are shown in Figure 4.15.

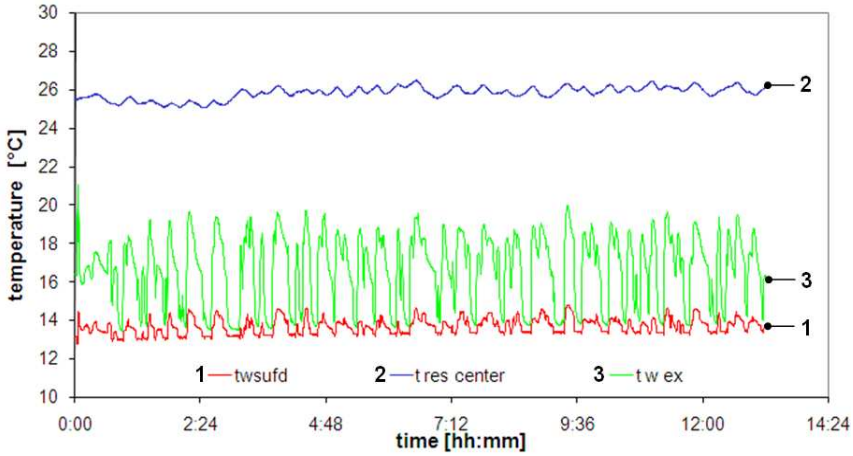

Figure 4.15: Water experimental conditions for cooling mode validation.

In Figure 4.15, the water exhaust temperature significantly varies due to the mixing in the collector.

In cooling mode, all the ceiling panels are operating. They are connected in three blocks, (see Figure 4.16) each one supplied by two parallel circuits. Figure 4.16 also shows the time function intervals when each block of panels are operating, according to the activation signal of mass flow rate control valve.

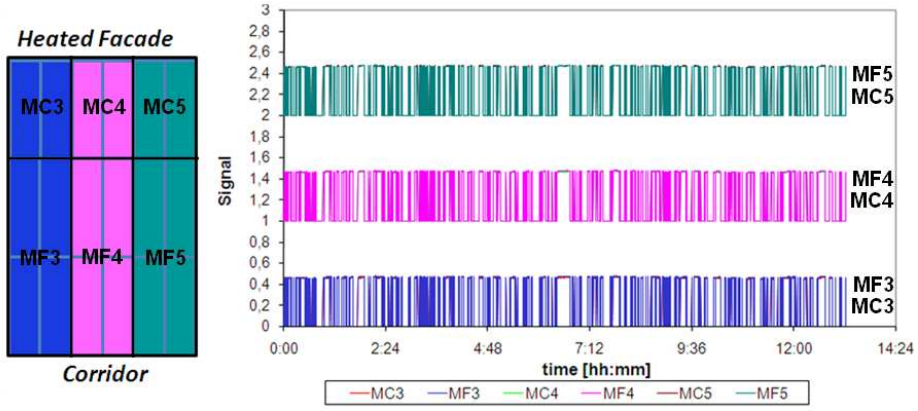

Figure 4.16: Panel's block water regulation in cooling mode.

It is observed in Figure 4.16 that most of the time, the blocks of panels are simultaneously operating in cooling mode (MF actives in Figure 4.16).

Results

The direct comparison between the model results and the measured values of the internal wall at the internal surface, window internal surface and water exhaust temperatures are shown in Figures 4.17, 4.18 and 4.19 respectively.

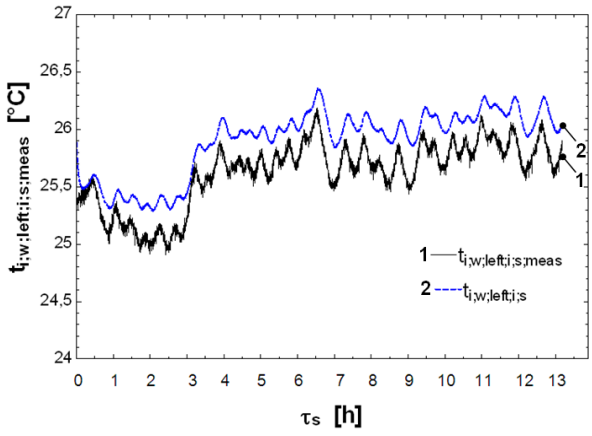

Figure 4.16: Comparison: Measured and calculated temperature of internal wall at the internal surface.

In Figure 4.16, a *RMS* value of ±0.4 [K] is observed, which is within the measurement uncertainty variation. The error also considers the temperature stratification induced experimentally during the test in cooling mode (see Chapter 2). It is assumed in the model that surface wall and windows temperatures are homogeneous, however the measured values consider the average temperature of five zones for each surface.

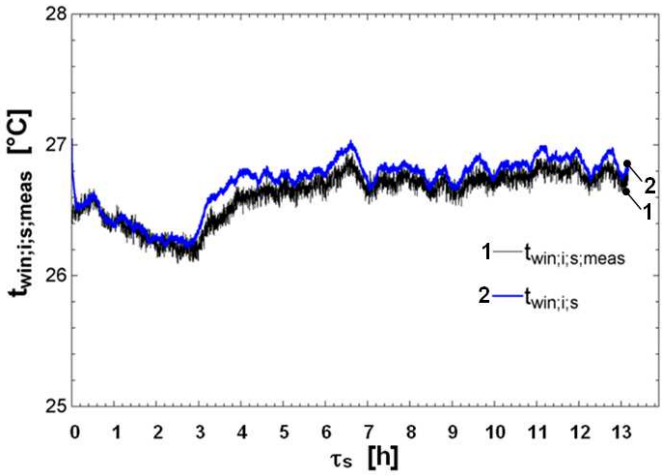

Figure 4.17: Comparison: Measured and calculated temperature of window internal surface.

In Figure 4.17, the model response of the window surface temperature does not show the perturbation observed during the heating mode validation. This is because during the considered test period in cooling mode, all the panels were active simultaneously. A *RMS* value of ±0.15 [K] is observed.

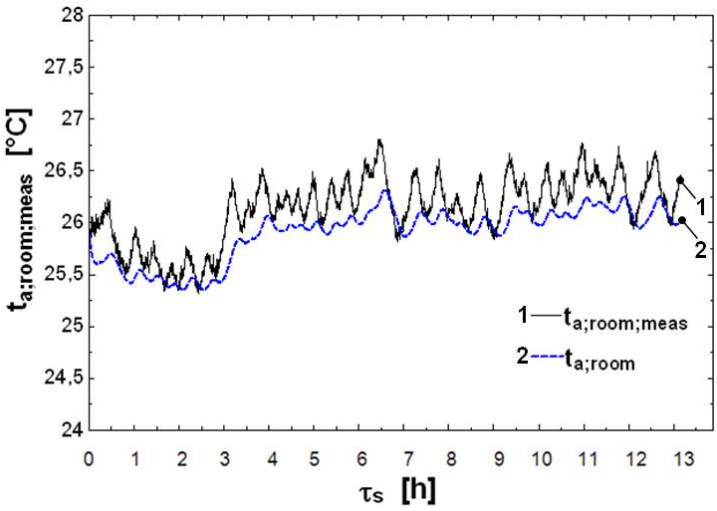

Figure 4.18: Comparison: Measured and calculated room air temperatures.

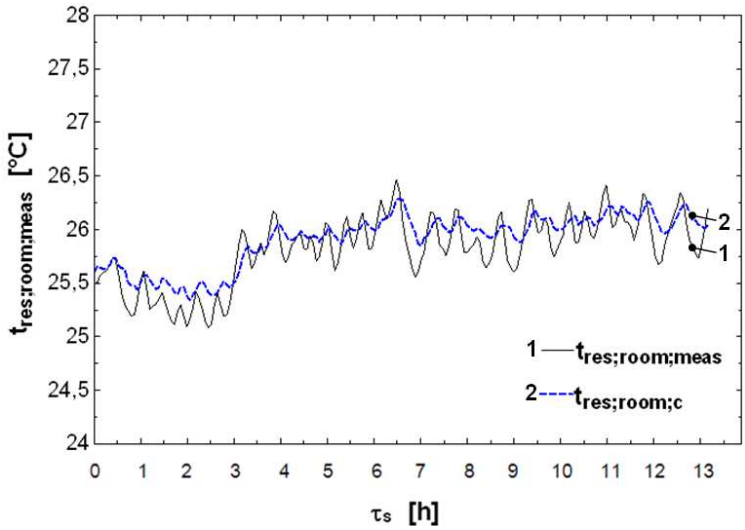

Figure 4.19: Comparison: Measured and calculated room resultant air temperatures.

For air and resultant room temperatures in Figure 4.18 and 4.19, *RMS* values of ±0.28 [K] and ±0.18 [K] respectively are observed. This can be explained by the fact that the air stratification is not taken into account by the model. Due to the lower temperature gradient between the ceiling surface and air and resultant temperatures, the air stratification is lower in cooling mode.

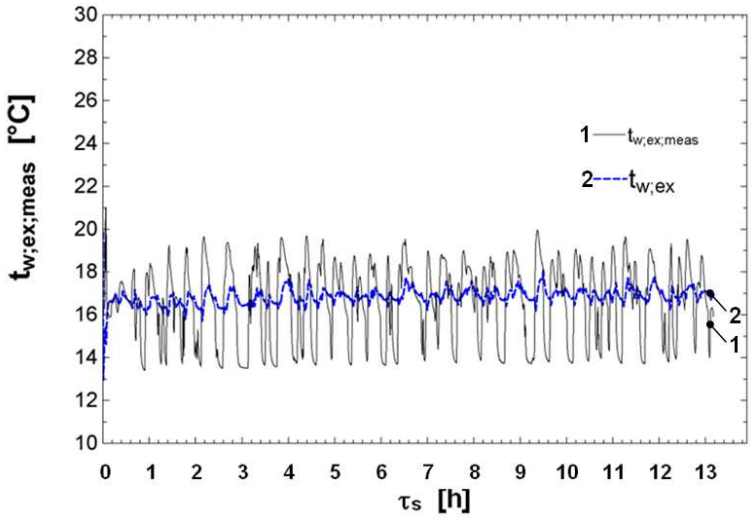

Figure 4.20: Comparison: Measured and calculated water exhaust temperature.

Figure 4.20 shows that the water exhaust temperature calculated by the model follows relatively well the measured average temperature. However, for the same reason as presented for heating mode, the dynamic behavior is not well represented (*RMS* value of ±1.78 [K]).

4.4 CONCLUSIONS

The dynamic model of the radiant ceiling systems and its environment is presented here as a part of the system study in cooling or heating modes. A good agreement is found between simulated and measured values. The results show that the average difference between simulated and measured air and surfaces temperatures is lower than ±0.5 [K]. However the simulated water exhaust temperature does not follow its dynamic behavior. This is due to the model assumptions and the particularities of hydraulic circuits implemented experimentally (more complex than the real case in a building).

The air and surfaces temperatures calculated as model outputs consider homogeneity conditions inside the room. The air stratification experimentally induced is not considered in the model and can partially explain the model error.

The dynamic model permits to support a global operation testing procedure of the system in the frame of commissioning procedure aiming at the verification of the radiant ceiling behavior coupled to the building, internal thermal loads, fenestration and ventilation systems and evaluation of the comfort conditions of the occupants. In this modeling the resultant temperature is calculated as a comfort indicator, as it depends strongly on the transient variation of the surface temperatures in the room. A dynamic simulation of the whole system must be included in the Functional Performance Testing (FPT) of this system in commissioning process (see Annex 1).

5. Model assisted commissioning of radiant ceiling systems

5.1 INTRODUCTION

As a part of a commissioning case study, the cooling ceiling system of a commercial building in Brussels is experimentally evaluated by means of a functional test procedure and the detailed static and dynamic thermal models of the system and its environment developed in this study. Due to the extended glazing surface of the building, overheating is noticed and the cooling capacity of the radiant system seems to be too limited in the zones exposed to solar gains. A representative office has been instrumented and data on the cooling ceiling system operating in real conditions have been collected.

The static model presented in Chapter 3 is used to evaluate the radiant ceiling performance: cooling power, exhaust water temperature, resultant temperature and average surface temperature. The behavior of the radiant ceiling system and the interactions with its environment (walls, ventilated facade, internal loads and ventilation system) were experimentally and numerically evaluated by the dynamic thermal model of the building and its HVAC system presented in Chapter 4. Commissioning test results show that the influence of surfaces temperatures inside the room, especially the facade, is considerable.

5.2 FUNCTIONAL PERFORMANCE TEST PROCEDURE (FPT)

From the precedent experimental and modeling results it was found that the radiant ceiling must be evaluated together with its designed environment and not as a separate HVAC equipment. Despite that the cooling or heating capacities can be within the design parameters according to the AS-BUILT files, it does not always mean that the occupant comfort is achieved.

Ventilation and fenestrations operating conditions and thermal load concentration can disturb the radiant ceiling operation, if they are not coupled to the radiant ceiling systems during the design and building construction phases or later in the building life cycle.

As shown in Chapter 1, the FPT is a commissioning tool that permits to verify that the equipment, subsystem and total system work with in harmony (including the stability and durability) in order to achieve the main objective of the building HVAC system.

According to the experience taken from experimental and modeling results (laboratory and commissioning), the testing procedure suggested can be subdivided into 6 steps:

1st Step: selection of a representative office.

Qualitative verification of thermal loads influence, solar radiation, equipment etc., for a representative analysis of the system inside the building.

2nd Step: visual inspection.

Verification of the active radiant ceiling surface, hydronic connections and insulation state. Considering that the temperature gradient into the metal ceiling panels is usually lower than 1 [K], a simple IR thermometer cannot be used in this case.

3rd Step: sub system definition.

Verification of subsystems related to the radiant ceiling operation: fenestration and ventilation systems.

4th Step: test in automatic stop.

Verification of the system state in automatic stop to prevent condensation risk.

5th Step: test of conformity operation (performance test).

Verification of the radiant ceiling performance by means of the static model of the radiant ceiling. The aim of this test procedure is to verify if the installation has been made according to the specification described in the “design documents”. In any case, this test verifies whether the specifications of the “design documents” are adapted to the actual needs of the building.

6th Step: test of global operation

Verification of radiant ceiling coupled to the building by means of a dynamic model of the radiant ceiling and its environment. The main goal of this test procedure is to verify that the global installation (radiant ceiling, ventilation and fenestration systems) fits the comfort requirements of the occupants.

Execution phase

Physical checking: visual comparison of the radiant ceiling parameters with information given in the AS-BUILT files (geometry, active surface, water mass flow rate etc.).

Condensation risk: a schematic diagram of the control system is shown in Figure 1.2. As long as the sensor registers condensation, either the flow to the ceiling is cut off by closing the control valve, or the supply temperature is raised. A steam generator can be used in order to check the control system. Periodical inspection and calibration of dew point sensors are required.

First parameter identification: the experimental data provided by the manufacturer can be used in order to identify the steady state model parameters (thermal contact resistance and the constant convective thermal coefficient).

Performance testing: the test includes the measuring of the variables defined as model inputs and calculation of the radiant ceiling capacity, ceiling and room surface average temperatures and water exhaust temperature by means of a static model of the radiant ceiling. The following experimental measurements must be taken:

One-time measurements:

$L_{p,} L_{room}$: panel and room length, [m].

W_p, W_{room} : panel and room width, [m].

$H_{room,} H_{void}$: room and void height, [m].

$\dot{M}_{w,c}$, $\dot{M}_{w}$: control and supply water mass flow rates (see Annex 1), [kg s^{-1}].

Continuous measurements:

$t_{w,c}$, $t_{w,su}$, $t_{w,ex}$: control, supply and exhaust water temperatures (see annex 1), [℃].

$t_{i,w,i,s}$, $t_{e,w,i,s}$ $t_{win,i,s}$: surface temperatures (walls, glazing, frame, inactive ceiling), [℃].

$\Delta_{T,w}$: difference between water supply and exhaust temperatures, [K].

$t_{res,room}$, $t_{a,room}$: resultant and air temperature, [℃].

$t_{a,void}$: ceiling void air temperature, [℃].

$t_{c,average}$: ceiling surface average temperature, [℃].

Global operation testing: the radiant ceiling behavior must be verified by coupling it to the corresponding structure of the building (walls, facade, internal loads and ventilation system). Therefore a simulation of the whole system must be performed by using a dynamic model. The model inputs must take into account the geometry and materials of the system and building, the supply and exhaust water temperatures, air and water mass flow rates and the following additional measurement:

One-time measurement:

$\Delta_{P,a}$: pressure differential for supply and return ventilation systems, [Pa].

Continuous measurements:

$t_{i,w,i,s}$, $t_{e,w,i,s}$ $t_{win,i,s}$: surface temperatures (walls, glazing, frame, inactive ceiling), [℃].

$t_{a,su}$, $t_{a,ex}$: ventilation supply and exhaust air temperature, [℃].

$t_{a,adj}$, $t_{a,ext}$: adjacent room and external air temperatures, [℃] .

$\dot{Q}_{i,load}$: internal thermal loads, [W].

I_{glob}, $I_{dir,e,w}$: solar radiation, [W m^{-2}].

Comfort test: air velocity, flow pattern from ventilation outlets and temperature pattern for the occupancy zone must be measured (the measurements must be vertically placed at 10 [cm] and 110 [cm] above the floor at the occupancy zones). A detailed FPT for radiant ceiling system is presented in Annex 1.

5.3 BUILDING AND RADIANT CEILING DESCRIPTION

The selected building for this study has a total of 38 floors with a floor area of 87200 [m^2]. The facade is composed of 6000 windows. The radiant ceiling consists of capillary tube mats on top of the perforated metallic panels with upward insulation. The internal walls are made of security glazing and isolated metallic panels. The floor and ceiling slabs are made of 130 [mm] concrete layer. The floor is composed of a carped placed on metal deck above an air space of 10 [cm]. Some details of facade, windows and internal walls are presented in Figure 5.1.

Figure 5.1: Building and radiant ceiling details.

The glazing is composed of an external double glazed unit and an internal single panel of clear glass. The cavity between the two skins is ventilated with return room air, which is extracted from the room at the base of the glazing and rejected to the ventilation system from the top. The principle is to position the shading devices between two layers of glazing, capturing the solar energy within the cavity. The energy can be expelled in periods with high gains and cooling demands or recovered in periods with heating demands (see Figure 5.2).

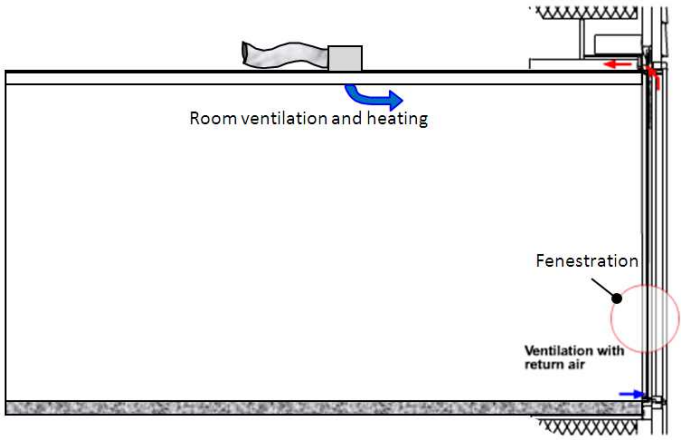

Figure 5.2: Fenestration system description.

The hydraulic circuit of the system is shown in Figure 5.3. Only 77 % of the ceiling surface is active. The capillary tube mats have a "**U**" configuration with glass-wood thermal and sound insulation above the mats.

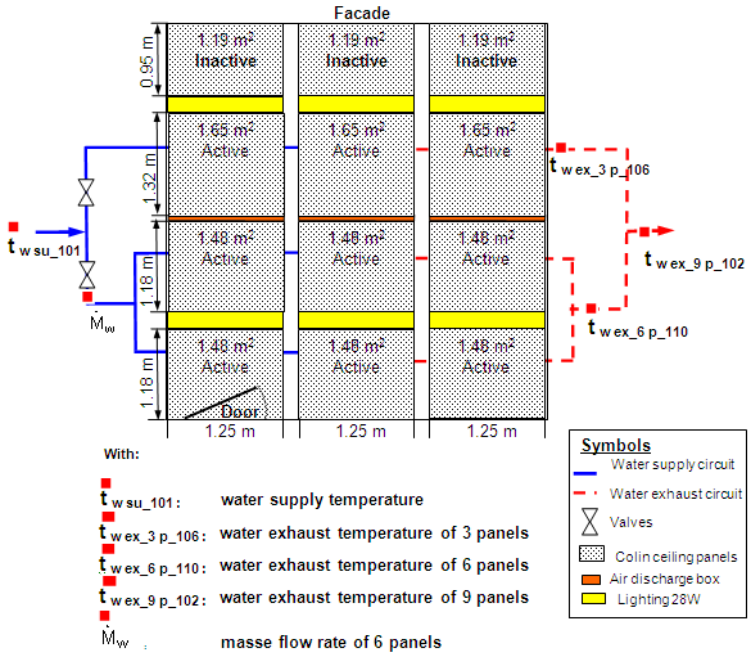

Figure 5.3: Commissioning study case: Hydraulic circuit

The radiant ceiling system operates only in cooling mode. During the winter time the heating is provided by the ventilation system. The air humidity control is performed directly at the Air-Handling Unit.

At the first visual inspection of the system, it was observed that the cooling ceiling panels close to the facade are inactive and 4 out of the 9 active panels were installed erroneously with shorter capillary

mats, which implies a reduction of the active cooling surface. Geometric and hydronic parameters for 9 active capillary tube mats (after correction of mats dimension) are presented in Table 5.1.

Table 5.1: Cooling ceiling configuration selected for commissioning processes

Characteristic	**6 panels back**	**3 panels front**
Radiant surface	Steel plate thickness: 0.8 [mm]	Steel plate thickness : 0.8 [mm]
Panel length (L_p):	1.25 [m].	1.25 [m].
Panel width (w_p):	1.18 [m].	1.32 [m].
Tube separation (w_t) :	10 [mm].	10 [mm].
Panel surface:	1.48 [m^2]	1.65 [m^2]
Perforated area ($\boldsymbol{\rho}$) :	16 %	16 %
N_s:	3	3
N_p:	2	1
Upward insulation:	20 [mm] mineral wool.	20 [mm] mineral wool.
Capillary tube union	directly placed on top of the metal ceiling panels	directly placed on top of the metal ceiling panels
D_e	3.4 [mm].	3.4 [mm].
D_i	2.3 [mm].	2.3 [mm].

5.4 COMMISSIONING RESULTS: RADIANT CEILING (performance test)

5.4.1 Measurements

The performance test is performed during the middle season (May 13 from 11 [h] to 13 [h]). The sensors positions are shown in Figures 5.4 and 5.3. In order to evaluate the fenestration and ventilation systems, the surface and air temperatures in different points of the room are measured.

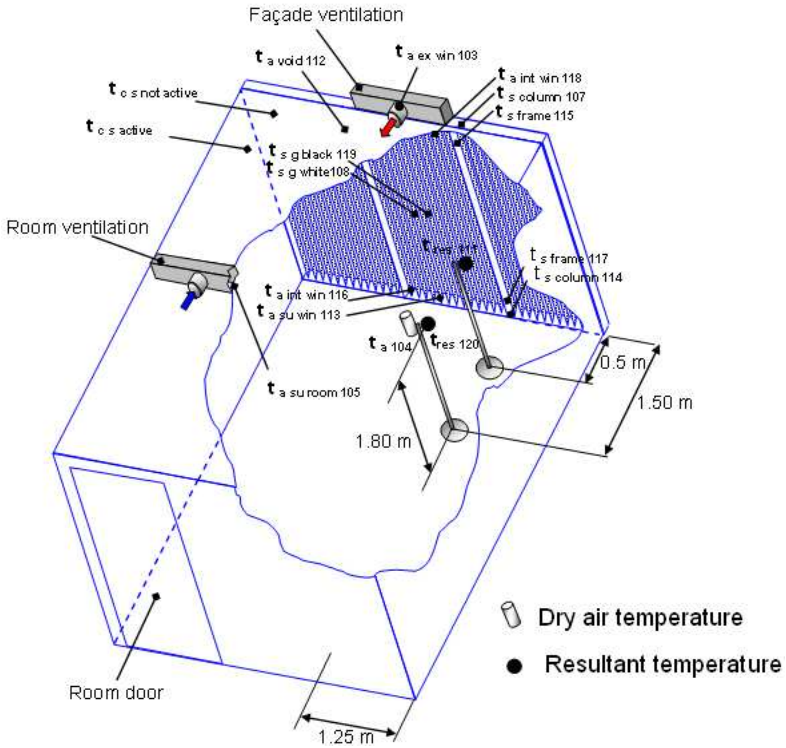

Figure 5.4: Sensors positions inside the room.

The results of measurements performed during one day (measurements in time interval of 5 minutes) are shown: in Figure 5.5 for water temperatures, Figure 5.6 for air temperatures and Figure 5.7 for window surface temperatures. The selected period for performance test is shown inside the vertical parallel lines. Figure 5.5 shows that the cooling ceiling is activated from 5:30 [h] to 18 [h] in the afternoon. It is observed also in Figure 5.6 that the air control temperature of the system (taken with the system probe) is systematically lower than the resultant temperatures (measured at 75 [cm] above the floor and 1.5 [m] and 0.5 [m] from the facade). This is due to the not representative position of the control sensor inside the room (close to the room door, see Figure 5.4) that does not consider the overheating close to the facade.

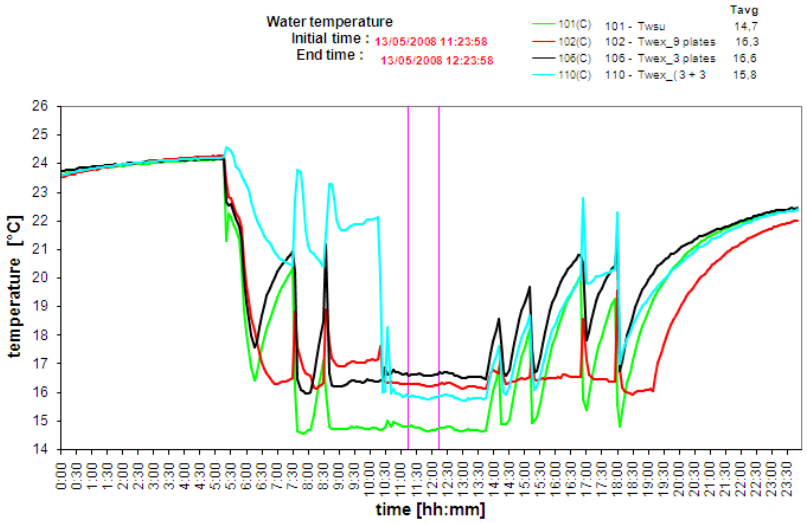

Figure 5.5: Commissioning: water temperatures measuring results

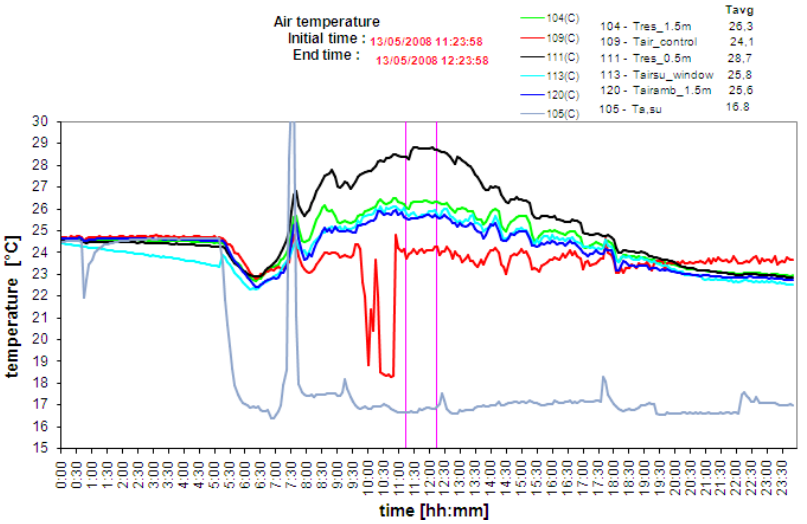

Figure 5.6: Commissioning: air temperatures measuring results

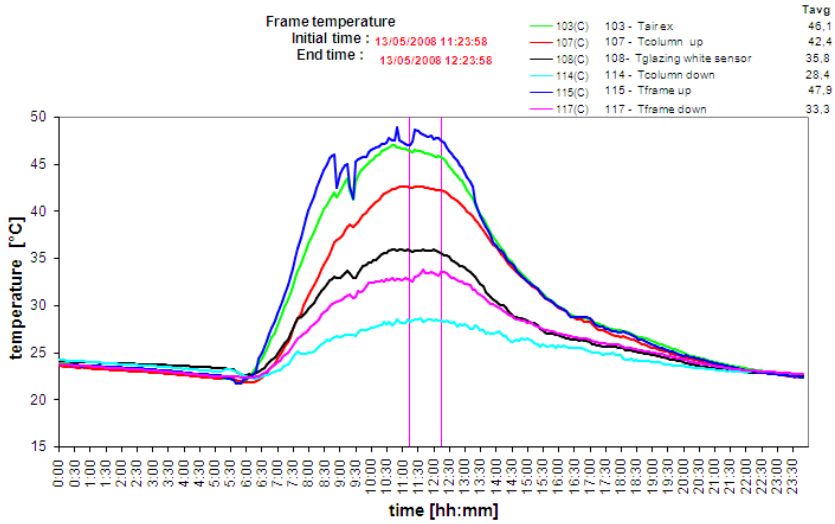

Figure 5.7: Commissioning: window surface temperatures measuring results

Table 5.2: Commissioning process: Cooling ceiling average results of measurements

Sub system	variable	result
Cooling ceiling 9 panels	$t_{w,su}$	14.7 [℃]
	$t_{w,ex}$	16.3 [℃]
	$\dot{M}_w$	0.189 [kg s^{-1}]
	$t_{res,room\ 120\ (1.5\ m)}$	26.3 [℃]
	$t_{res,room\ 111\ (0.5\ m)}$	28.7 [℃]
	$t_{a,room\ (1.5\ m)}$	25.6 [℃]
	$t_{a,void}$	25.2 [[℃]]
	$t_{c,average}$	18.7 [℃]
	L_p	1.25 [m]
	W_p	1.18 [m]
	L_{room}	5.15 [m]
	W_{room}	4 [m]
	H_{oom}	2.58 [m]

Table 5.3: Commissioning process: Facade and ventilation system average results of measurements

Sub system	variable	result
Facade	$t_{s\ ,column\ 107}$	41.7 [℃]
	$t_{s,frame\ 115}$	46.4 [℃]
	$t_{s,frame\ 117}$	32.9 [℃]
	$t_{s,\ column\ 114}$	28.2 [℃]
	$t_{a\ ,int\ win\ 118}$	**44.8 [℃]**
	$t_{a,int\ win\ 116}$	36.6 [℃]
	$t_{c,s,not\ active}$	28.9 [℃]
	$t_{s,g,black\ 119}$	**35.1 [℃]**
	$t_{s,g,\ white108}$	**35.5 [℃]**
	$t_{a,su,win\ 113}$	25.7 [℃]
	$t_{a,ex,win\ 103}$	**44.9 [℃]**
Ventilation system	$t_{a,su,room\ 105}$	16.8 [℃]
	Supply air overpressure principal duct	+13 [Pa]
	Return air depression principal duct	-64 [Pa]
	Return air depression window exhaust	-4 [Pa]

Average results of measurements for May 13th from 11 [h] to 13 [h] are summarized in Table 5.2 and 5.3 (Hannay *et al*., 2008). The average outdoor temperature and solar incident radiation intensity

taken on the glass facade during the time of the measurements presented in Table 5.2 and 5.3 are 21.5 [℃] and 600 [Wm $^{-2}$] (Lebrun J. *et al*., 2008).

In Figure 5.7 and Table 5.3 a strong overheating of the facade is observed (window air circulation, glazing and frame surfaces) considering that measurements were performed during middle season.

After measurements of pressure differentials at the supply and exhaust ventilation ducts and window, it was also found that the damper initially installed in the facade ventilation system does not correspond to the specifications of the AS-BUILT files and the regulation of pressure and mass flow rates must be corrected. Finally the nominal water mass flow rate and pressure drop for the operation conditions must be 0.053 [kg s^{-1}] and 0.6 [kPa] respectively (according to manufacturer documentation). However, the measured mass flow rate is around 3.15 times higher. This does not influence the cooling emission, nevertheless the pressure drop of the system increases to 1.65 [kPa].

The combination of these factors and the fact that the radiant ceiling surface was reduced and the control temperature is inappropriate makes that the sophisticated BEMS and measuring systems provided at the building cannot operate correctly.

5.4.2 Cooling ceiling performance test results

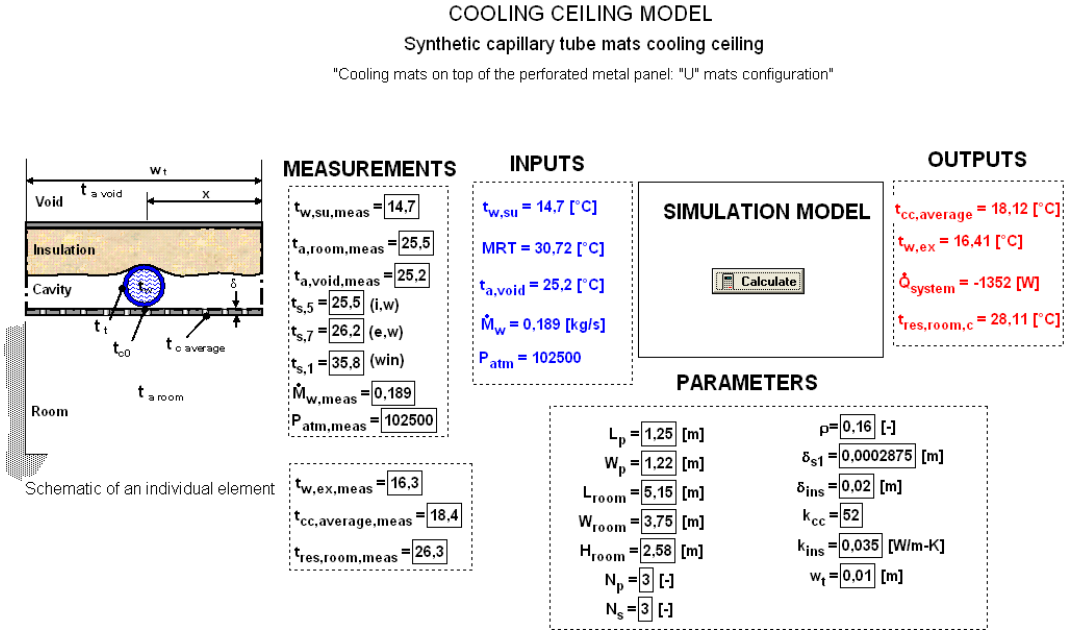

Figure 5.8: Block diagram of the cooling ceiling model (EES software): Commissioning results.

If the cooling ceiling model (described and validated in Chapter 3 for "U" mats configuration on top of perforated metallic panels with upward insulation) is used with the measurements results presented in Table 5.2 with air and resultant temperatures measurements at 1.5 [m] from the facade, the commissioning results can be observed in the model diagram (Figure 5.8).

Figure 5.8 shows that the resultant temperature measured at 1.5 m from the facade and 75 [cm] above the floor is lower that the calculated value. This is due to the possible experimental underestimating of the influence of short-wave radiation on the globe thermometer coming from the sunshine and overheated facade (*IR* radiation). The comparison between calculated and measured values selected for commissioning process is presented in Table 5.4.

Table 5.4 Results of cooling ceiling measurements and calculated values

Variable	Measured value	Model results
$t_{cc,avarege}$	18.4 [℃]± 0.5 [℃]	18.11 [℃]
$t_{w,ex}$	16.3 [℃]± 0.25 [℃]	16.4 [℃]
$\dot{Q}_{system}$	1266 W ± 270 [W] ($\dot{Q}_{no\,min\,al}$ 1221 [W])	1348 [W]

In Table 5.4, due to the high water flow rates imposed for this kind of systems (0.183 [kg s^{-1}]), the water temperature differences across the ceiling are small (1.2 [K]) thus a great uncertainty on direct cooling capacity is expected as the accuracy of the thermocouples is in the range of 0.2-0.3 [K] (Fissore and Fonseca, 2007). That makes it difficult to compare the experimental and calculated values. However it can be observed that the cooling emission of the system fits inside the expected range (according to the AS-BUILT files) for the case study presented here but the cooling ceiling capacity is insufficient to fulfill the comfort conditions expected by the occupants, this is due to the overheating of the facade and the very low thermal inertia of the building. Indeed, the comfort index *PMV* value was about 1.6, resulting in a *PPD* of about 57 %. (*PMV* and PPD indices are calculated by means of the classical Fanger's method described in ASHRAE, 2009). According to the experimental results (commissioning and laboratory test) an important influence of the facade on the cooling ceiling performance is observed. The possible solutions of the problem could be to consider the activation of the cooling ceiling panels close to the facade (regarding to the thermal load concentration in this zone) and also the use of an additional mobile shading device, transparent to visible light, but opaque to infra-red radiation, in order to reduce the overheating of the occupancy zone.

5.5 COMMISSIONING RESULTS: RADIANT CEILING COUPLED TO THE BUILDING (Test of global functioning)

5.5.1 Measurements

The dynamic test was performed during summer time (July 4 during one day and measurements in time interval of 5 minutes) in the same office described in section 5.3. The measurements results are shown in Figure 5.9 for water temperatures and Figure 5.10 for air temperatures. In Figure 5.9, the cooling ceiling is activated from around 5:30 [h] to 19:30 [h] in the afternoon.

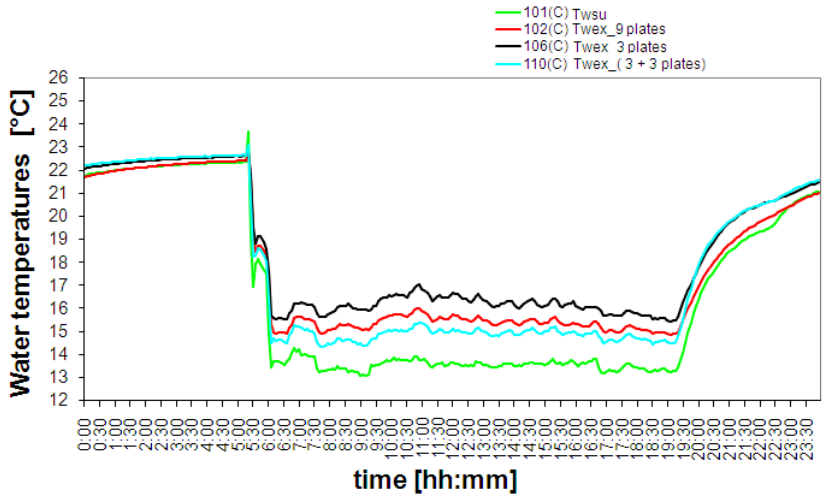

Figure 5.9: Commissioning: Water temperatures measuring results

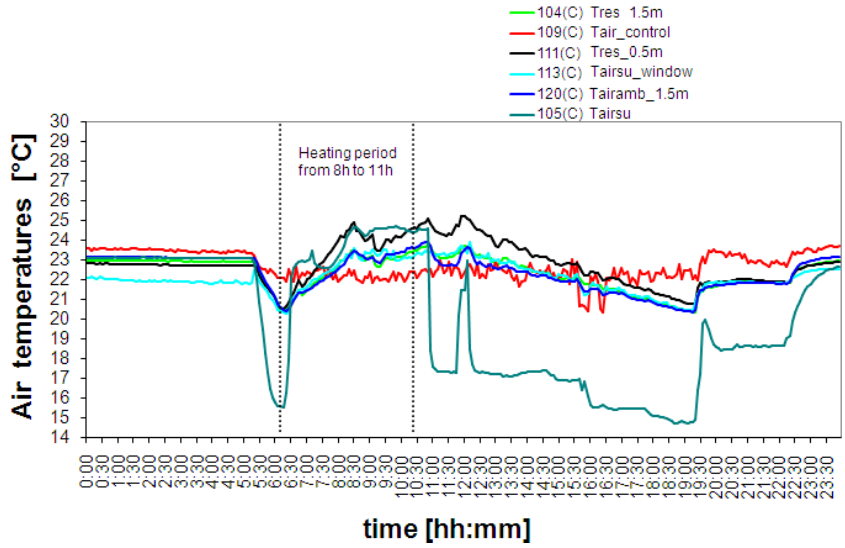

Figure 5.10: Commissioning: Air temperatures measuring results

The ventilation system is used to inject warm air as thermal load during the test (see Tairsu in Figure 5.10).

In Figure 5.10 it is also observed that the air control temperature of the system is systematically lower than the resultant temperatures (measured at 75 [cm] above the floor and 1.5 [m] and 0.5 [m] from the facade).

For the dynamic simulation, it is assumed that all the adjacent zones are at the same air temperature. The air ventilated cavity in the window is used here as adjacent zone of the facade in the absence of a detailed model of the fenestration system. The supply and exhaust air temperatures of the window's ventilation are measured and an average is considered as the adjacent temperature in this zone. The heat transfer coefficient in this zone is calculated using the procedure described in section 4.2, using the measured mass flow rate and air velocity considering forced convection on an external surface of the external wall.

5.5.2 Global functioning commissioning test results

The test consists of measuring the variables defined as model inputs (Figure 4.1) and calculating the radiant ceiling capacity, room air and resultant temperatures, room surface average temperatures and water exhaust temperature by means of a dynamic model of the radiant ceiling coupled to its environment.

The contact thermal resistance and heat transfer coefficient of this type of radiant ceiling are obtained in steady state conditions from experimental tests and model validation (Fonseca *et al.*, 2009) and used in the dynamic model as a parameter. The modifications considered here are the distance and velocity of air jet detachment considering that they are defined from diffuser manufacturer's catalogue for the specific diffuser model used in this case (this parameters as well as the *R*-*C* network parameters are used to adjust the model as shown in Figure 4.1).

The comparison between the model results and the measured values of the room air temperature, window surface and water exhaust temperature are shown in Figures 5.11, 5.12 and 5.18 respectively.

It is observed in Figures 5.11, 5.12 and 5.13 that the maximal variation between measured and calculated values varies between 0.25 [K] and 0.5 [K], which are within the measuring uncertainty. It is also important to remark that, the water exhaust temperature calculated by the model follows relatively

well the dynamic behavior of the system. Here, the hydraulic circuit is much simpler than the one used during the dynamic model validation and the selected model assumptions are close to the real behavior of the system.

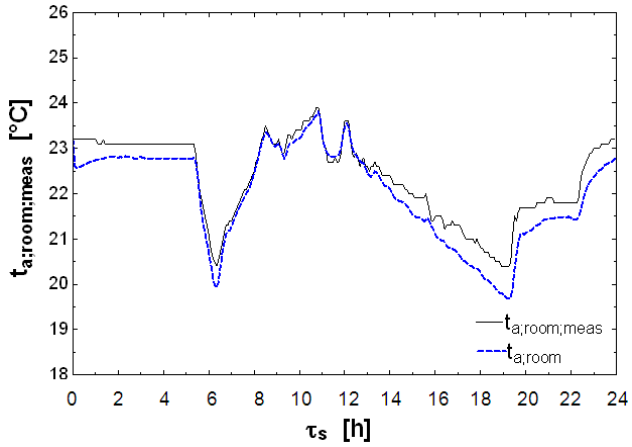

Figure 5.11: Comparison between measured and calculated air room temperatures

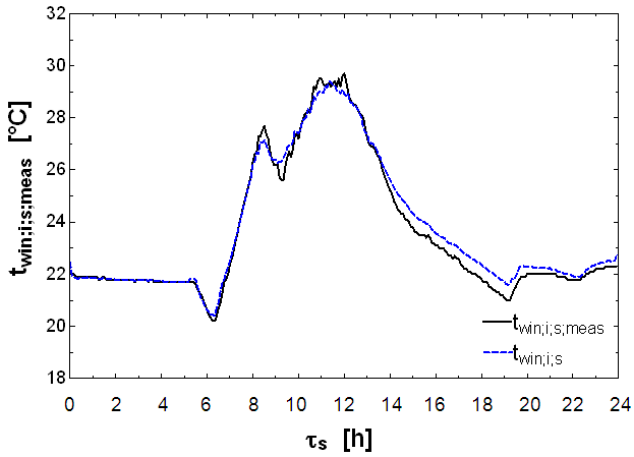

Figure 5.12: Comparison between measured and calculated window surface temperatures

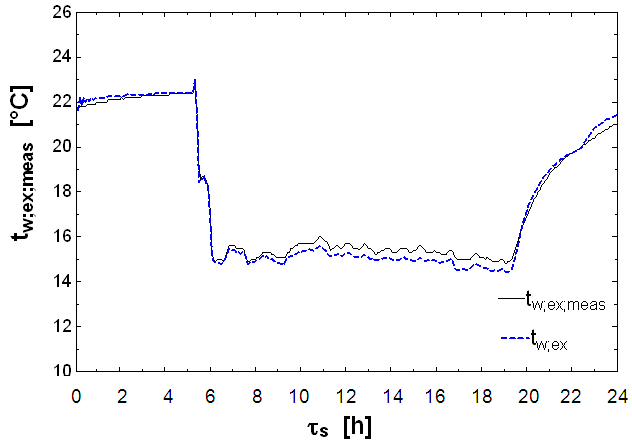

Figure 5.13: Comparison between measured and calculated water exhaust temperatures

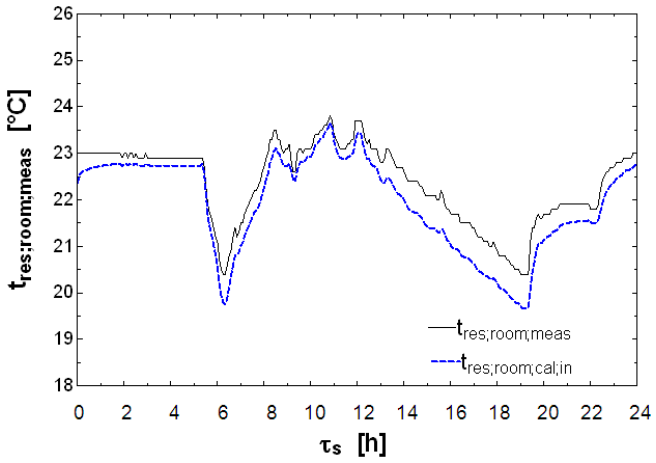

Figure 5.14: Comparison between measured and calculated resultant temperatures

The measured and calculated values of the resultant temperature at 75 [cm] above the floor and 1.5 [m] from the facade are shown in Figure 5.14. A maximal variation of 0.5 [K] is observed which is within the measuring uncertainty variation (see Chapter 1). In this case the influence of short-wave and *IR* radiations (sunshine and overheated facade) on the globe sensor seems to be reduced considering the climatic conditions during the test.

The *RMS* errors are given in Table 1 and are of the same order of magnitude as the measuring uncertainty (Fonseca *et al*., 2009a).

Table 1: RMS errors

Temperature	***RMS* value**
Air room	±0.39 [K].
Water exhaust	±0.43 [K].
Air resultant	±0.47 [K].

5.5.3 Sensitive analysis

As a part of the commissioning process, the dynamic model of the radiant ceiling system coupled to the room, allows for the evaluation of the possible measurements envisaged to improve indoor comfort.

As an example, in the present case (although the dynamic test conditions do not represent a facade overheating case), two modifications are possible to reduce the resultant temperature close to the facade. These are an increase of the active radiant ceiling area in the facade and a reduction of supply water temperature. If the panels close to the facade are activated (enhancement of 18 % effective radiant ceiling area) the effect of this modification (**m1**) with the other conditions unchanged,

on the resultant temperature calculated previously (condition initial (in)) can be observed in Figure 5.15. An average reduction of 0.35 [K] on the resultant temperature can be attained with **m1** modification.

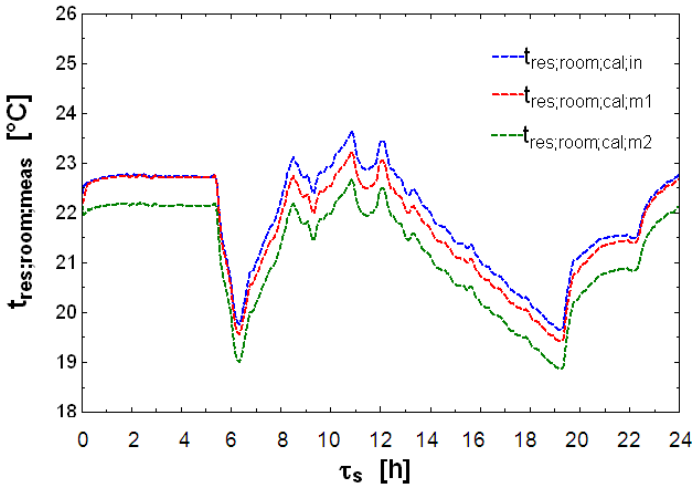

Figure 5.15: Comparison between modified and initial calculated resultant temperatures

In addition to the modification **m1**, if the water supply temperature is reduced by 1.5 [K] (in the limit of condensation risk) (modification **m2**) the result can be observed also in Figure 5.15.

As the results of the combination of **m1** and **m2** modifications, the resultant room temperature is reduced by around 1 [K]. According to the actual room and radiant ceiling conditions, the only way to reduce even more the room resultant temperature, is to perform some modifications of the facade shading devices.

5.6 CONCLUSIONS

It was found that when considering the reduced temperature differences (characteristic of the system), the measuring uncertainty has a significant influence on the commissioning test results. A Functional Performance Testing (FPT) for cooling ceiling commissioning is proposed (Annex 1).

It is important to note that in spite of the sophisticated BEMS and measurements system provided at the buildings, an inadequate installation, verification and management of the individual and global system performance (according to the AS-BUILT files) produce the deterioration of the components and global system conditions which implies an increase of the energy consumption.

Commissioning test results show that the influence of heat sources distribution and surfaces temperatures inside the room, especially the facade, are significant. Therefore the laboratory conditions should correspond to the site conditions (relation between commissioning and laboratory testing) and the cooling ceiling must be evaluated together with its designed environment and not as a separate HVAC equipment.

6. General conclusion and recommendations

This thesis has presented different experimental and modeling investigations that allow for a better understanding of radiant ceiling systems giving better bases the for modeling and/or verification of performance at the level of laboratory or *in situ* commissioning. The methodology used for laboratory or *in situ* verification permits to propose a testing procedure and the radiant ceiling modeling that can be used as a design or commissioning tool.

About the heat transfer mechanisms

The convective and radiative heat exchange on a radiant ceiling surface is a really complex process, considering specially the combined effect of ventilation and fenestration systems. In the convective part, a correlative method cannot describe completely the heat transfer processes, considering that in modern buildings there are too many configurations and possible combinations of these systems. In this study, one seeks to make an analysis of the radiant ceiling convection, considering that there are not enough tests to identify a correlation law for all the possible combinations which may occur in a real case.

Some empirical models have been presented to determine the convective heat transfer coefficients and radiation heat exchange. This analysis allowed for better understanding of the complexity of the choice among different correlations available in the literature, for radiant ceiling systems. The modeling proposed considers mixed convection, perforation effect and a detailed radiative heat exchange method for radiant ceiling systems (fifteen isothermal internal surfaces can be considered in the room). The radiosity method is also used to evaluate the mean radiant temperature (twenty-four isothermal internal surfaces can be considered in the room), considering a spherical point representing a person sitting in a spatial position inside the room in order to calculate the resultant temperature in any place inside the room and compare it with the measured value at the same position, for example during the commissioning process.

About the experimental analysis

For the tested radiant ceiling system, the water mass flow rate has a small influence on radiant ceiling capacity, but the corresponding pressure drop deserves to be carefully checked.

The resultant room temperature varies significantly close to the facade and depends also on the thermal load concentration. Therefore the radiant ceiling capacity evaluated at the center of the room could be insufficient to provide comfort to the occupants. The system must be evaluated together with its designed environment and not as separate HVAC equipment.

In the experimental domain considered and radiant ceiling types studied here, the influence of ventilation system coupled to the radiant ceiling plays a beneficial role in the heat exchange of the system. An increase of radiant ceiling capacity of 30 % and 6 % is observed in heating and cooling modes respectively.

The thermal contact resistance is also a key parameter of the radiant ceiling performance. A reduction of the radiant ceiling capacity for capillary tubes mats on the top of metallic plates is observed, related to the copper tube types at the same test conditions (in a similar way for capillary tubes mats on the top of the gypsum plaster board as a radiant surface).

About the static radiant ceiling modeling

With the regard to the previous studies the main difference is the detailed treatment of convection and radiation heat exchange (considering the influence of ventilation, facade and perforation effects) which is usually neglected or too simplified.

The static model was validated experimentally with four different radiant ceiling types. A good agreement was found between simulated and measured values.

The model can be used for commissioning process to verify if the installation is operating according to the specification described in the “design documents”. In any case, this model allows to verify if the specification of the “design documents” are adapted to the actual needs of the building.

About the dynamic modeling of the radiant ceiling and its environment.

The main differences with previous studies and the large building energy programs available publicly are the detailed convection and radiation treatment on the radiant ceiling surface and the theoretical approach used in order to enable the model application as a commissioning tool.

The dynamic model was validated experimentally in two cases (cooling and heating mode). Except for water exhaust temperature which depends on the complexity of hydraulic circuit related to the measuring position, a good agreement was found between simulated and measured values.

The definition of the radiant ceiling geometry and ventilation parameters allows for the use of the manufacturer technical information of radiant ceiling systems and diffusers in order to simplify the commissioning process. On the other hand the choice of the resultant temperature as a comfort indicator allows for a relatively easy verification of this variable in the room.

About the model assisted commissioning of radiant ceiling systems

Dynamic and static models applications of a radiant ceiling system and its environment are presented here as a part of a commissioning study. A good agreement is found between simulated and measured values. The results show that the *RMS* error between simulated and measured values is lower than ±0.5 [K]. The theoretical approach gives to the user an appropriate tool for preliminary calculation and commissioning processes.

The radiant ceiling behavior must be verified by coupling it to the corresponding structure of the building (facade, walls, internal loads and ventilation system), climate and functioning conditions. Therefore a simulation of the whole system must be performed by using a dynamic model and this procedure should be included in the Functional Performance Testing (FPT) of this system for the commissioning procedure.

Commissioning test results show that the influence of heat sources distribution and surfaces temperatures inside the room, especially the facade, is significant.

The static and dynamic models specially allow to evaluate the radiant ceiling performance and its global operating conditions respectively but also to perform a sensitivity analysis that could be helpful

during commissioning process in order to estimate the possible alternatives to improve its operation and performance.

It is also important to note that despite of the sophisticated BEMS and measuring system provided at the buildings, in the case of radiant ceiling systems, an inadequate installation, verification and management of the individual and global system performance (according to the AS-BUILT files) produces the deterioration of the comfort level, components and global system conditions which implies an increase of energy consumption.

Recommendations

The simulation reliability could be improved by:

- Creating a database of different parameters of the models for different types of radiant ceilings available on the market (cooling and heating mode experimental validation) that could simplify the model application (characterize the thermal contact resistance and heat transfer coefficients in the most representative cases).
- Improving the average water temperature calculation considering a log mean temperature difference for each individual panel.
- Providing a detailed hydraulic calculation to reduce the effect of the complexity of the hydraulic circuit on the accuracy of water exhaust temperature calculated by the model.
- Improving the dynamic modeling by coupling it to a detailed model of the fenestration system.

References

ANSI/ASHRAE *Standar* 41.1-1986 (RA 91). 1991. *Standard Method for Laboratory Airflow Measurement.* Atlanta: American Society of Heating, Air-Conditioning and Refrigeration Engineers, Inc.

ANSI/ASHRAE *Standar* 41.2-1987 (RA 92).1992. *Standard Method for temperature Measurement.* Atlanta: American Society of Heating, Air-Conditioning and Refrigeration Engineers, Inc.

ANSI/ASHRAE *Standar* 41.3 – 1989. *Standard Method for Pressure Measurement.* Atlanta: American Society of Heating, Air-Conditioning and Refrigeration Engineers, Inc.

Aparecida C.,Cuevas C. and Hannay J. 2000. Radiant ceiling system: regulation test report. University of Liege. Liege Belgium.

ASHRAE HANDBOOK-HVAC Systems and Equipment. 2004. Chapter 6. Atlanta: American Society of Heating, Air-Conditioning and Refrigeration Engineers, Inc.

ASHRAE Guideline 2-2005. Engineering analysis of experimental data. American Society of Heating, Refrigerating, and Air-Conditioning Engineers, Inc., Atlanta, USA.

ASHRAE HANDBOOK. 2009. Fundamentals Atlanta: American Society of Heating, Air-Conditioning and Refrigeration Engineers, Inc.

ASHRAE. Experimental methods for engineers. Guideline; Atlanta: American Society of Heating, Refrigeration and Air-conditioning Engineers. Inc., 1986.

Alamdari F. and Hammond P. 1983. Improved data correlations for bouyancy-driven convection in rooms. Building Services Engineering research and Techonology. Vol 4. N°3; pp.106-112.

Antonopoulos A. Vrachopoulos M. Tzivanidis C. 1997. Experimental and theoretical studies of space cooling using ceiling embeddes piping.Applied Thermal Engineering. Vol 17 No4 pp. 351-367.

AuditAC 2006. Successful case Studies in AuditAC. Technical Guides for owner/manager of HVAC systems. Vol 10.

Awbi H. and Hatton A. 2000. Mixed convection from heated room surfaces. Energy and Buildings. Vol 32; pp. 153-166.

Bar J. and Hanjalic K. 2003. Estimation of shape factors for transient conduction. International Journal of Refrigeration. Vol 26; pp. 360-367.

Behne M. 1996. Is there a risk of draft in rooms with cooled ceilings. Measurement of air velocities and turbulences ; ASHRAE Transactions: Symposia – SD 96-4-5; pp. 744-751.

Behne M. 1999. Indoor air quality in rooms with cooled ceiling. Mixing ventilation or rather displacement ventilation?. Energy and Building. Vol 30; pp. 155-166.

Bertagnolio S, Masy G, Lebrun J, André P (2008). Building and HVAC System simulation with the help of an engineering equation solver. Proceedings of the Simbuild 2008 Conference, Berkeley, USA.

Bourdouxhe J., Georges B., Lebrun J. 1998 a. Rapport No.1, Etude expérimentale du plafond rayonnant chauffant et rafraîchissant. Laboratoire de thermodynamique applique Université de Liège. Belgium.

Bourdouxhe J., Georges B.,Ternoveanu A., Lebrun J. 1998 b. Rapport No.4, Etude expérimentale des plafonds rayonnants chauffants et rafraîchissants. Laboratoire de thermodynamique applique Université de Liège. Belgium.

Bruce E. Birdsall, W. F. Buhl, K. L. Ellington, A. E. Erdem, F. C. Winkelmann, J. J. Hirsch, and S. D. Gates. 1994. DOE-2 Basics. Rep. LBNL-35520.

Celata P., Cumo M and McPhail J., G Zummo. 2007. Single-phase laminar and turbulent heat transfer in smooth and rough microtubes. Microfluid Nanofluids.Vol 3; pp. 697-707.

Conroy C. and Mumma S. 2005. Ceiling Radiant Cooling Panels as a viable distributed Parallel Sensible Cooling Technology integrated with dedicated Outdoor air Systems. ASHRAE tarnsactions, 107. Part 1 AT-01-7-5.

Cuevas C. and Lebrun J. 2002. Re-commissioning of a cooling plant. Faculty of Applied Sciences. University of Liege, Belgium.

Cuevas C.2006. Contribution to the modelling of refrigeration systems. Ph.D Thesis. University of Liege. Liege Belgium.

Davies M. 2004. Building heat transfer. John Wiley and Sons, Ltd Editors. University of Liverpool.UK.Chapter 4-6.

DIN 4715-1 1993. Entwurf, Raumkühlflächen; Leistungmessung bei freier Strömung; Prüfregeln, Beuth Verlag GmbH, Berlin.

EnergyPlus Engineering Document – The Reference to EnergyPlus Calculations, The Ernest Orlando Lawrence Berkeley Laboratory, USA. April 2008.

Feustel H. and Stetiu C. 1995. Hydronic radiant cooling- preliminary assessment. Energy and Building.Vol 22; pp. 193-205.

Fissore A. and Fonseca N. 2007. Experimental study of the thermal balance of a window, design description. Buildong and Environment. Vol. 47; pp. 3309-3321.

Fonseca N. 2009. Methodology for uncertainty calculation of net total cooling effect estimation for rating room air conditioners and packaged terminal air conditioners. International Journal of Refrigeration. Vol 32. Issue 6; pp. 1472-1477.

Fonseca N., Lebrun J. André P. 2009 a. Experimental study and modeling of cooling ceiling systems using steady- state analysis. International Journal of Refrigeration. Accepted revision. September.

Fonseca N., André P., Cuevas C. 2009 b. Commissioning case study of a cooling ceiling system. Building Simulation 2009. Eleventh International IBPSA Conference. Glasgow, Scotland. pp. 1997-2004.

Fonseca N., Bertagnolio S., André P. 2009 c. Dynamic thermal modeling of a radiant panels system and its environment for commissioning: application to case study. The 9th International Conference for Enhanced Building Operations. November 17-18, 2009, Austin, Texas. USA.

FTZ Forschungs-und Transferzentrum e.V and der Westsächsischen Hochschule Zwickau (FH).2003. Prüfbericht über die Ermittung der Kühlleistung einer Raumkühfläche nach DIN 4715-1. Prüfberich Nr.:FTZ_2003_KF1022.

FTZ Forschungs-und Transferzentrum e.V and der Westsächsischen Hochschule Zwickau (FH).2002. Prüfbericht über die Ermittung der Kühlleistung einer Raumkühfläche Messung analog DIN 4715-1.

Fredriksson J., Sandberg M., Moshfegh B.2001. Experimental investigation of the velocity fiel and airflow pattern generated by cooling ceiling beams. Building and Environment. Vol 36. pp. 891-899.

Gerhard Zweifel, Simulation of displacement ventilation and radiative cooling with DOE-2. ASHRAE Trans., (99) (2) 1993.

Hannay J. and Fonseca N. 2003. Etude en chambre climatique rapport d'essais. Laboratoire de thermodynamique applique Université de Liège.

Hannay J. Aparecida C. 2008. Building Commissioning results rapport. Laboratoire de thermodynamique applique Université de Liège.

Hauser G. Kempkes C. Olsen B. 2000. Computer Simulation of hydronic heating/cooling system with embedded pipes. ASHRAE Transaction 2000. Vol. 106. Pt.

HLK Heizung Lüftung Klimatechnik Prüfstelle. University of Stuttgar. 1995. Prüfbericht über die Ermittung der Kühlleistung einer Raumkühfläche nach DIN 4715-1. Prüfberich Nr.:VR95 K29. 1134.

International Energy Agency (IEA). 2003. Commissioning of Building and HVAC systems for improve energy performance. Annex 40 Final report.

ISO 5167-1.1991. Measurement of fluid flow by means of pressure differential devices Part 1: Orifice plates, nozzles and venturi tubes inserted in circular cross-section conduits running full. Geneva: International Organization for Standardization.

ISO GUM. Guide to the Expression of Uncertainty Measurement, Fists edition, 1993, corrected and reprinted International Organization for Standardization, Geneva Switzerland, 1995.

Incropera F. and DeWitt D. 1996. Fundamentals of Heat and Mass Transfer. Fourth Edition. School of Mechanical Engineering Purdue University.

Jae-Weon Jeon and Mumma S. 2004. Simplified cooling capacity estimation model for top insulated metal ceiling radiant cooling panels. Applied Thermal Engineering. Vol.24; pp. 2055-2072.

Kulpmann R. 1993 Thermal comfort and air quality in rooms with cooled ceilings – results of scientific investigations; ASHRAE Transactions: Symposia – DE 93 – 2 – 2; pp. 488-502.

Kilkis B. 1995. Coolp: A computed program for the design and analysis of ceiling cooling panles. ASHRAE Transaction: Symposia. SD 95-4-4. pp. 705-710.

Kreith F. Bohn M. 1986 Principles of heat Transfer. Revised Fourth Edition. Harper International edition. New York.

Klein, S.A., Alvarado. F. 2008. Engineering Equation Solver. F-chart software.

Kochendörfer C. 1996. Standard testing of cooling panels and their use in system planning. ASHRAE Transactions 102 (1) pp. 651-658.

Koschenz.M., and Dorer V. 1996. Design of air systems with concrete slab cooling. Proc. 5th Int. Conf. Air Distribution in Rooms, Yokohama, Japan.

Lebrun J. 2006. Climatisation: Transferts de Chaleur et de Masse. Notes de curs. Laboratoire de thermodynamique applique Université de Liège.Belgium.

Lebrun J., Hannay J. and Aparecida C. 2008. Building Commissioning results rapport: Study and modelization of double glazed façade. Laboratoire de thermodynamique applique Université de Liège.

Masy G. 2008. Definition and validation of a Simplified multizone dynamic building model connected to heating system and HVAC unit. PhD Thesis. University of Liege. Liege Belgium.

Min T., Schutrum L., Parmelee G. and Vouris J. 1956. Natural convection and radiation in a panel heated room. ASHRAE Transaction: 62:337.

Mc Adams H. 1954.Heat Transmission, 3rd ed., Mc Graw-Hill, New York. Chap 7.

Miriel J., Serres L. and Trombe A. 2002. Radiant ceiling panel heating-cooling systems: experimental and simulated study of the performances, thermal comfort and energy consumptions. Applied Thermal Engineering, Vol. 22; pp. 1861-1873.

Nickel, J. 2007. Cooling and Heating systems with ceiling, Special Publication from the TAB Nº 05/07, pag. 41-48. Aachen - Germany.

Niu J., and van der Kooi J.1994. Indoor climate in rooms with cooled ceiling systems. Building and Environment, (29) (3).

Novoselac A., Burley B., and Srebric J. 2006. New convection correlation for cooled ceiling panles in room with mexed and stratified airflow.HVAC/R Reseach. Vol 12. Number 2; pp. 279 -294.

Rao C and Rahmman M. 2006. Transient conjugate heat transfer model for circular tubes inside a rectangular substrate. Journal of Thermophysics and Heat Transfer. Vol 20; pp. 122-134.

Spitler J., Pedersen C. and Fisher D. Interior convective heat transfer in buildings with large ventilative flow rates. ASHRAE Transsactions 97 (1): 505-515.

Svendsen S and Laustsen J. 2002. Calculation tool for determining the net energy gain trough windows. Building Physics, 6th Nordic Symposium.

Klein, et. al., TRNSYS – A Transient System Simulation Program User Manual, The Solar Energy Laboratory, University of Wisconsin – Madison., 2009.

Ternoveanu A, Hannay, C, Qingping, W. 1999. Preliminary Analysis on a Research Project for Cooling Ceilings- synthesis of available information. Laboratoire de thermodynamique applique Université de Liège.

Tadeu A. Simoes N. 2001. Transient conduction and convection phenomena across a solid layer structure with thermal heterogeneities. Journal of computer modeling in Engineering and Sciences. CMES 2 pp. 477-495.

Udagawa M. 1998. Simulation of panle cooling systems with linear subsystem model. ASHRAE Transaction: Symposia. DE 98-3-2. pp. 534-547.

Yuge T. 1960. Experiments on heat transfer from spheres including combined natural and forced convection. Trans. ASME Journal of Heat Transfer 82 (1960)3 pp. 214-220.

Walton G.1980. A new algorithm for radiant interchange in room loads calculations. ASHRAE Transaction: 86 (2) 190-208.

Annex 1

A.1 RADIANT CEILING FUNCTIONAL PERFORMANCE TESTING GUIDE

The functional performance testing guide (FPT) is devoted to the detection of a possible malfunction and to its diagnosis. The test can be "active" or "passive", according to the way of analyzing the component behavior: with or without artificial perturbation. Active tests are mostly applied in initial commissioning, i.e. at the end of the building construction phase. Later in the Building Life Cycle, i.e. in re-, retro- and on-going commissioning, a “passive” approach is usually preferred, in order to preserve health and comfort conditions inside all the building occupancy zones (EIA, 2003).

The FPT is just one part of the whole Commissioning process. It has only to be started on the basis of a strict specification, given in the design Documents; the test results and interpretation must be incorporated into the AS-BUILT Records. Information and testing procedures are viewed from a system perspective, rather than a component perspective. This is especially critical for functional performance testing and for the overall success of the system. The performance of the system depends on three areas of interaction:

- The individual components in the system
- The components with each other as a subsystem
- The subsystem with other subsystems in the building

The FPT of HVAC system means to verify that the equipment, subsystem and total system work in harmony (including the stability and durability) to show the final function of the building air-conditioning.

A.2 FUNCTIONAL PERFORMANCE TEST PRESENTATION

Operating principles

Basic and working principle:

Presented in Chapter 1.

Expected performance:

- The radiant ceiling power must be sufficient to maintain the setpoint for the room temperature which is the comfort temperature corresponding to the activity and clothing level of the occupants. Depending on the type of ceiling/assembly configuration, cooling or heating capacities from 75 to 110 W/m² can be attained
- The water temperature should be the minimum to avoid condensation condition (0.5 [K] above the indoor dew point is usually implemented). The indoor dew point must be controlled by an air conditioning system. If the windows are opening, they must be equipped with automatic cut-off of the water pumps.
- The mean temperature difference between water and air room (resultant) temperatures should vary between 6-12 [K], with absolute values of 13 -18 [℃] and 37- 49 [℃] for water and 24-26 [℃] and 21-23[℃] for air in cooling and heating m ode respectively. The lower limit corresponds to a minimal cooling or heating power available while the upper limit corresponds to maximal acceptable room air velocity and temperature and the surface temperature to avoid condensation risk or asymmetric radiation.
- The water flow rate should be the lowest value still sufficient to maintain a turbulent flow on the water side and a reasonable water temperature drop across the ceiling (2- 3 [K]).
- The water circuit should be designed to favor parallel flow and minimize pressure drops. A special attention has to be paid to the installation phase of pipes connections and bends in order to allow for an equal flow rate in parallel circuits and avoid exaggerated local pressure drops.
- The slot diffuser should be located between the ceiling panels and above the occupancy zone. The air flow should be blown horizontally along the ceiling surface in order to increase the

heat transfer coefficient and to avoid jet fall in occupancy zone due to “Coanda effect” (Behhe M. 1999).

- The contact quality (bonds between water pipes and ceiling panels) is crucial for radiant ceiling effectiveness. It is proved that identical ceiling modules (as designed) can provide completely different results only due to a bad contact quality.
- The thermal and sound insulation of the room ceiling void is recommended (in some cases required) and direct contact between ceiling elements and room surfaces is prohibited (cold bridges) (Ternoveanu *et al*., 1999).
- The free air circulation between rooms ceiling voids is allowed only if both rooms are equipped with the same radiant ceiling system and have identical destination (for example as offices).
- The ventilation system should ensure an over pressure for the rooms equipped with radiant ceilings in order to guarantee the air tightness (parasitic air flow from adjacent enclosures may disturb indoor convective flow).
- The air velocity pattern at the occupancy zone must fulfill the comfort requirements. This means a maximal accepted average velocity in the range of 0.15-0.2 [m s^{-1}] with peak values limited at 0.25-0.3 [m s^{-1}] and a maximal allowed vertical temperature gradient of 2-3 [K] on the total height of the room.

Calculation methods and simulation models (used in the design and commissioning):

The thermal model presented here after (Chapter 3) allows to calculate the radiant ceiling capacity, ceiling surface average temperature, air room resultant temperature and water exhaust temperature. Also a general and limited evaluation of radiant ceiling performance can be achieved by the empirical equation giving the relationship between cooling or heating power and temperature difference:

$$\dot{q} = C\Delta T^{n} \qquad [\text{W m}^{-2}] \qquad \text{(A.1)}$$

where

$\Delta T = t_{res\ room} - t_{w\ average}$

C and *n* for a particular system may be either experimentally determined or calculated from design material given in the literature (ASHRAE, 2004). In either case, sufficient data or calculation points

must be gathered to cover the entire operational design range. It is important to note that the base of this information is usually the standard test (without ventilation or facade asymmetry effects).

Interaction with other (sub) systems:

The radiant ceiling systems must be evaluated in parallel with the ventilation and fenestration systems and the building structure by a dynamic model of the whole system.

Manufacturers Data

Radiant ceiling manufacturers publish technical sheets and performance data sheets, including showed curves of the radiant ceiling (relationships among the different variables of the systems: cooling or heating capacity, pressure drop, surface temperature) and also maintenance information. These sheets are also supposed to be available in the As-Built Records. A typical example of data sheet is presented in Figure FA.1.It is important to note that the base of this information is usually the standard test (without ventilation or facade asymmetry effects)

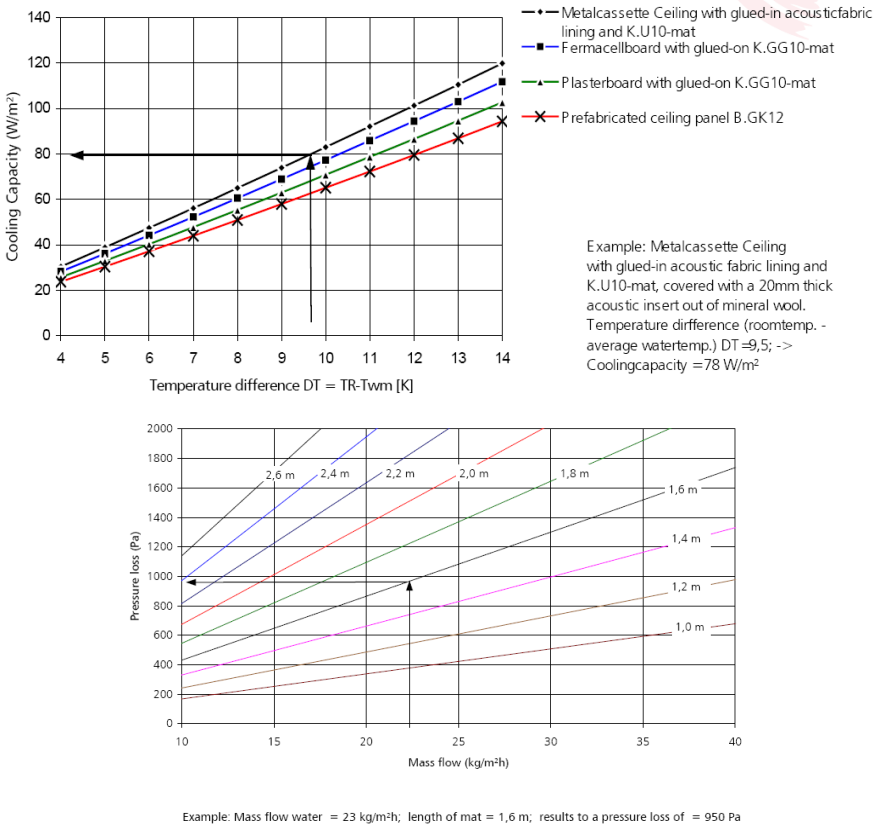

Figure FA1: Example of manufacturer data sheets

Problems to be considered

- The condensation risk: this is occurring on ceiling surface in cooling mode in case of windows opening or accidental reduction of water supply temperature. The indoor dew point temperature must be permanently controlled during the functioning of cooling ceilings. Therefore the ventilation system must be started before the cooling ceiling is set on (the delay can be calculated as a function of system parameters) so the temperature constraint is given by the indoor dew point corresponding to ventilation steady-state regime.
- Pressure drop: the choice of the water flow rate is practically defined by the turbulent flow condition and geometry of the radiant elements. In order to minimize the pumping energy consumption, the water velocity inside the pipes should correspond to the Reynolds value for turbulent regime (Re_{cr}>10000).
- Noise problems: the noise level provided by radiant ceilings is practically negligible in comparison with other sources as ventilation outlets and computers. The values of the water velocity imposed by the pressure drop limitation cannot generate noise due to the flow. However in office buildings, where the same radiant ceiling system is supplies two or more rooms in parallel, one should check the noise propagation between rooms.
- Contact thermal resistance: the contact conductance is practically depending on the quality of bonds between water pipes and the radiant ceiling surface. A poor quality of contact (due to manufacturing or installation) is directly influencing the heat transfer and the system performance.
- Ventilation system: the ventilation contribution is usually limited to cover only hygienic requirements, which corresponds to small flow rates. However in some cases the ventilation is also used to provide or remove some part of the thermal loads or heat gains especially in buildings with a big fenestration surface. Therefore, its influence can be significant and the regulation of pressure and mass flow rates needs to be carefully checked.
- Surfaces temperatures: the radiant temperature asymmetry between radiant ceiling system and room surfaces (especially with facade) must remain between the allowed values for thermal comfort requirements.

- Insulation level of the void (towards upper floor): the fraction of the total cooling or heating power lost through the ceiling towards roof or rooms located on the next floor can be considered as useful if the upper floor is occupied but the cooling or heating energy is not available instantaneously. However it can be accumulated and released progressively from the ceiling thermal storage.

A.3 TEST SPECIFICATIONS

Objectives and sequence of the test

The aim of this test is to verify if the installation is in accordance to the specifications described in the "design documents". In any case, this test verifies if the specifications of the "design documents" are adapted to the actual needs of the building. The testing procedure is subdivided into 6 steps, each one aiming at checking some specific performance:

1st Step: selection of a representative office.

Qualitative verification of thermal loads influence, solar radiation, equipment etc., for a representative analysis of the system inside the building.

2nd Step: visual inspection.

Verification of the active radiant ceiling surface, hydronic connections and insulation state. Considering that the temperature gradient inside the metal ceiling panels is usually lower than 1 [K], a simple IR thermometer cannot be used in this case.

3rd Step: sub system definition.

Verification of subsystems related to the radiant ceiling operation: fenestration and ventilation systems.

4th Step: test in automatic stop.

Verification of the system state in automatic stop to prevent condensation risk.

5th Step: test of conformity operation (performance test).

Verification of the radiant ceiling performance by means of the static model of the radiant ceiling. The aim of this test procedure is to verify if the installation has been made according to the specification described in the "design documents". In any case, this test verifies whether the specifications of the "design documents" are adapted to the actual needs of the building.

6th Step: test of global operation

Verification of radiant ceiling coupled to the building by means of the dynamic model of the radiant ceiling and its environment. The main goal of this test procedure is to verify that the global installation (radiant ceiling, ventilation and fenestration systems) fits the comfort requirements of the occupants.

Required material

- Temperature sensor (air, resultant and surface temperature measurements)
- Water flow counter.
- Portable humidity sensor.
- Portable air velocity sensor.
- Portable steam generator.
- Portable data acquisition system.
- Portable differential manometer.
- Thermal imaging system.

Time required for the test execution

It depends on the accuracy and also on the characteristics of the components involved in the test and on the control possibilities. If the building BEMS can be used, the system might be monitored and studied in real time (using the remote access by internet) reducing significantly the required time for the test. The control system can serve as a commissioning tool by making use of its ability to manipulate energy systems through interfaces such as actuators and switches.

Pre-requirements

In order to make this test, it is necessary that:

- The design documents are available
- The availability of measuring points in order to place the sensor.
- Calibrated sensors must be used.

Preparation phase

1. Technical information from manufactures should be available. Before applying the method described hereafter, a certain number of preliminary studies from documentation must be made:

- Geometric and characteristic data of the radiant ceiling system.
- Evaluation of expected performance.

2. Measuring instruments have to be installed. As already shown, the position and the way in which measurements are taken and their individual accuracies play a significant role in radiant ceiling commissioning (see Chapter 5).

The accuracy of the enthalpy flow rate definition (used for experimental verification of radiant ceiling performance) can be increased by measuring directly the water temperature difference and by using, during the functional test, a water loop as shown in Figure FA.2. This method allows to increase the accuracy on enthalpy flow rate as the total flow rate across the ceiling is maintained constant. The water supply temperature is adjusted using the by-pass valve. Consequently the radiant capacity can be defined from a heat balance on the whole loop (water pump included) by using this time higher temperature differences (2 to 3 times) as the water flow rate is lower.

$$\dot{Q}_{system} = \dot{M}_{w\_c} c_{pw} \left(t_{wex} - t_{wc}\right) - \dot{Q}_p \qquad [W] \qquad (A.2)$$

where

$\dot{Q}_p$ Electrical power dissipated by the water pump. [W]

The value of the water supply temperature in the ceiling can be recalculated by taking as reference Eq. A.3.

$$t^*_{w\_su} = \left(1 - \frac{\dot{M}_{wc}}{\dot{M}_{wsu}}\right) t_{w\_ex} + \frac{\dot{M}_{wc}}{\dot{M}_{wsu}} t_{wc} + \frac{\dot{Q}_p}{\dot{M}_{wsu} c_{pw}} \quad [℃] \qquad (A.3)$$

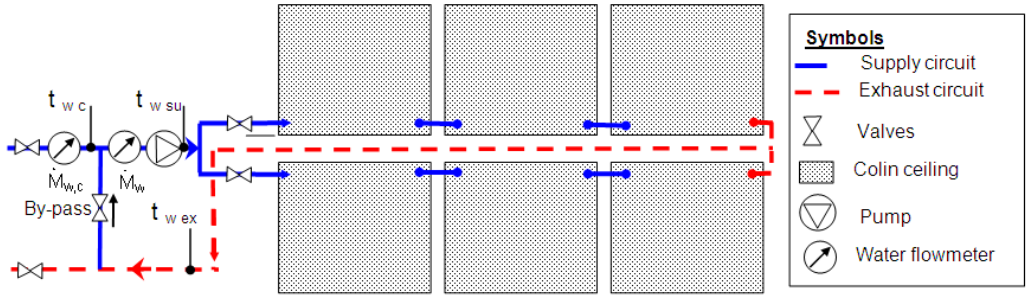

Figure FA.2: Water loop for radiant ceiling power measuring.

Execution phase

- Physical checking: visual comparison of the radiant ceiling parameters with the information given in the as-build files (geometry, active surface, water mass flow rate etc.)
- Condensation risk: a schematic diagram of the control system is shown in Figure FA.3. As long as the sensor is registering condensation, either the flow to the ceiling is cut off by closing the control valve, or the supply temperature is raised. A steam generator can be used in order to check the control system. Periodical inspection and calibration of dew point sensors are required.

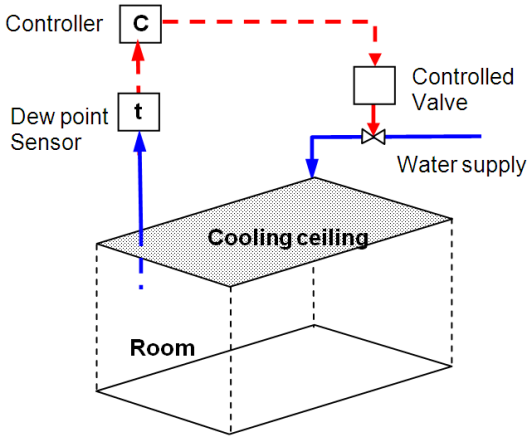

Figure FA.3: Simplified scheme of ceilings control system.

- First parameter identification: the experimental data provided by the manufacturer can be used in order to identify the model parameters (thermal contact resistance and the constant convective thermal coefficient).
- Performance testing: the test consists of measuring the variables defined as model inputs and calculates the radiant ceiling capacity, ceiling and room surface average temperatures and

water exhaust temperature by means of a static model of the radiant ceiling. The following experimental measurements must be taken:

$L_{p,}$ L_{room} : panel and room length, [m]

W_{p}, W_{room} : panel and room width, [m]

$H_{room,}$ H_{void} : room and void height, [m]

t_{wc}, $t_{w,su}$, $t_{w,ex}$: control, supply and exhaust water temperatures (see annex 1), [℃].

$t_{i,w,i,s}$, $t_{e,w,i,s}$ $t_{win,i,s}$: surface temperatures (walls, glazing, frame, inactive ceiling) [℃].

$\Delta_{T,w}$: difference between water supply and exhaust temperatures, [K].

$\dot{M}_{w,c}$ $\dot{M}_{w}$: control and supply water mass flow rates (see annex 1), [kg s^{-1}].

$t_{res,room}$, $t_{a,room}$: resultant and air temperature, [℃].

$t_{a,void}$: ceiling void air temperature, [℃].

$t_{c\ average}$: ceiling surface average temperature [℃].

- **Global function testing**: The radiant ceiling behavior must be verified by coupling it to the corresponding structure of building (walls, facade, internal loads and ventilation system). Therefore a simulation of the whole system must be performed by using a dynamic model. The model inputs must consider the geometry and materials of the system and building, the supply and exhaust water temperatures, mass flow rate and the following additional measurements:

  $\Delta_{P,a}$: Pressure differential for supply and return ventilation systems, [Pa].

  $t_{i,w,i,s}$, $t_{e,w,i,s}$ $t_{win,i,s}$: Surface temperatures (walls, glazing, frame, inactive ceiling) [℃].

  $t_{a\ su}$, $t_{a\ ex}$: Ventilation supply and exhaust air temperature, [℃].

  $t_{a,adj}$, $t_{a\ ext}$: Adjacent room and external air temperatures, [℃] .

  $\dot{Q}_{i,load}$: Internal thermal loads, [W].

  I_{glob}, $I_{dir,e,w}$ **:** Solar radiation, [W/m^2].

- Comfort test: air velocity and pattern from ventilation outlets and representative air velocity and temperature pattern for the occupancy zone must be measured (the measurements must be vertically placed at 10 cm and 110 cm above the floor at the occupancy zones).